UNIVERSIDADE FEDERAL DE MINAS GERAIS
FACULDADE DE FARMÁCIA
PROGRAMA DE PÓS-GRADUAÇÃO EM CIÊNCIAS FARMACÊUTICAS

CAROLINE MARI RAMOS ODA

MICELAS POLIMÉRICAS CARREADORAS DE PACLITAXEL: POTENCIAL NANOPLATAFORMA TERANÓSTICA ANTICANCER

Belo Horizonte - MG
2019

CAROLINE MARI RAMOS ODA

MICELAS POLIMÉRICAS CARREADORAS DE PACLITAXEL: POTENCIAL NANOPLATAFORMA TERANÓSTICA ANTICANCER

Tese apresentada como requisito parcial para obtenção do título de Doutor no Programa de Pós-Graduação em Ciências Farmacêuticas da Faculdade de Farmácia da Universidade Federal de Minas Gerais.

Orientadora: Prof. Elaine Amaral Leite

Coorientador: Prof. André Luís Branco de Barros

Belo Horizonte - MG
2019

Oda, Caroline Mari Ramos.
O22m Micelas poliméricas carreadoras de paclitaxel: potencial nanoplataforma teranóstica anticancer / Caroline Mari Ramos Oda. – 2019.
130 f. : il.

Orientadora: Elaine Amaral Leite.
Coorientador: André Luís Branco de Barros.

Tese (doutorado) – Universidade Federal de Minas Gerais, Faculdade de Farmácia, Doutorado em Ciências Farmacêuticas.

1. Câncer – Teses. 2. Micelas poliméricas – Teses. 3. Paclitaxel – Teses. 4. Nanomedicina teranóstica – Teses. 5. Neuropatia periférica – Teses. 6. Atividade antitumoral – Teses. I. Leite, Elaine Amaral. II. Barros, André Luís Branco de. III. Universidade Federal de Minas Gerais. Faculdade de Farmácia. IV. Título.

CDD: 616.994

Elaborado por Darlene Teresinha Schuler – CRB-6/1759

UNIVERSIDADE FEDERAL DE MINAS GERAIS

PROGRAMA DE PÓS-GRADUAÇÃO EM CIÊNCIAS FARMACÊUTICAS

FOLHA DE APROVAÇÃO

MICELAS POLIMÉRICAS CARREADORAS DE PACLITAXEL: POTENCIAL NANOPLATAFORMA TERANÓSTICA ANTICANCER

CAROLINE MARI RAMOS ODA

Tese submetida à Banca Examinadora designada pelo Colegiado do Programa de Pós-Graduação em CIÊNCIAS FARMACÊUTICAS, como requisito para obtenção do grau de Doutor em CIÊNCIAS FARMACÊUTICAS, área de concentração CIÊNCIAS FARMACÊUTICAS.

Aprovada em 04 de outubro de 2019, pela banca constituída pelos membros:

Profa. Elaine Amaral Leite - Orientadora
UFMG

Prof. André Luis Branco de Barros - Coorientador
UFMG

Prof. Daniel Cristian Ferreira Soares
UNIFEI

Dra. Carla Cristina Pólo
Laboratório Nacional de Luz Sincroton

Profa. Mônica Cristina de Oliveira
UFMG

Prof. Lucas Antônio Miranda Ferreira
UFMG

Belo Horizonte, 4 de outubro de 2019.

COLABORADORES

Prof. Ângelo Malachias (Departamento de Física, Instituto de Ciências Exatas, UFMG)

Dr. Antônio Augusto M. Gasperini (Laboratório Nacional de Luz Síncroton, CNPEN)

Dra. Gwenaelle Pound-Lana (Laboratório de Desenvolvimento Galênico e Nanotecnologia, UFOP)

Prof. Vanessa Carla Furtado Mosqueira (Laboratório de Desenvolvimento Galênico e Nanotecnologia, UFOP)

Prof. Renes de Resende Machado (Departamento de Produtos Farmacêuticos, Faculdade de Farmácia, UFMG)

Prof. Geovanni Dantas Cassali (Instituto de Ciências Biológicas, UFMG)

Prof. Mônica Cristina de Oliveira (Departamento de Produtos Farmacêuticos, Faculdade de Farmácia, UFMG)

Prof. Valbert Nascimento Cardoso (Departamento de Análises Clínicas e Toxicológicas, Faculdade de Farmácia, UFMG)

MSc. Renata Salgado Fernandes

MSc. Juliana de Oliveira Silva

MSc. Alysson Vinícius Braga

Marina Xavier Teixeira

Dedico este trabalho às três pessoas que foram fundamentais para que eu chegasse até aqui: papai, mamãe e Fabrício.

AGRADECIMENTOS

Acima de tudo agradeço sempre a Deus, que nos dá o dom da vida, a sabedoria e fé para fazer o que fazemos.

Agradeço aos meus pais, Arnaldo e Betânia, que me ensinaram que somente uma educação de qualidade pode mudar o mundo e sempre me deram todo suporte e apoio para seguir até aqui. Eles são os melhores pais que eu poderia ter.

Agradeço ao Fa, meu companheiro para todas as situações, meu porto seguro. Obrigada por me fazer acreditar sempre e não perder a fé que tudo vai dar certo e por cuidar tão bem de mim.

Às minhas irmãs, Dani, Tati e Lelê, que são as pessoas que sei que posso contar sempre e em todas as situações.

À Elaine, que é a melhor orientadora que alguém pode ter e a melhor pessoa que alguém pode ter como aliada. Obrigada por todo apoio e confiança. Espero algum dia conseguir compensar ao menos um pouco do tanto que você tem feito por mim nesses últimos nove anos.

Ao André, que começou como meu orientador, e terminou como um dos melhores amigos que a vida poderia ter me dado. Para mim você é um grande exemplo de profissional e (sei que vou arrepender de dizer isso) saiba que te admiro muito. O doutorado teria sido muito menos divertido sem você.

Às Andrezetes, Renata, Ju, Lizi e Pequena. Sempre ali, para me ajudar na vida e no trabalho, para ouvir minhas lamentações e pra dar risadas, pelas companhia nos almoços intermináveis, nas nossas viagens e nas nossas ‘baladas’ não-jovens. Sem vocês minha vida nesses últimos anos teria sido menos feliz.

À Lizi (mais uma vez), minha irmã de bancada, que virou uma das minhas melhores amigas. Obrigada por ter me acolhido tão bem no LTF desde o meu primeiro dia.

Aos professores Mônica, Lucas, Gilson (*in memorian*) e Valbert, obrigada por terem construído o LTF e o Laboratório de radioisótopos e por nos disponibilizá-los e, principalmente, por nos inspirar a amar a pesquisa científica.

Aos outros professores do LTF, Marta, Gisele e Diego; muito obrigada por toda ajuda e disponibilidade quando precisei.

Ao professor Angelo Malachias, que tanto nos ajudou e ensinou sobre SAXS durante esses anos.

Ao professor Renes e ao Alysson, por toda ajuda prestada com a avaliação da neuropatia periférica.

Ao professor Ricardo, sempre tão solícito e disposto a ajudar.

Ao doutor Antônio Gasperini, que mesmo antes de nos conhecer, aceitou a nos ajudar em uma área completamente desconhecida por nós.

À doutora Gwen, também sempre muito solícita, obrigada pela sua ajuda com as análises de AF4.

Ao professor Geovanni Cassali e ao doutor Diego, pela ajuda com a avaliação histopatológica.

À Marina Xavier, por toda ajuda durante esses últimos anos, sempre com muita doçura e simpatia.

À Adelaide e ao Batista, muito obrigada por toda ajuda prestada com os animais.

Aos amigos e colegas do LTF, por todas as conversas com ou sem café no laboratório.

Aos amigos do laboratório de radioisótopos, Nara, Sued, Jana, Fernanda e Vanderli, que sempre me ajudaram quando precisei.

Aos meus familiares, especialmente minha tia Célia, por todo apoio e carinho.

Aos meus amigos da vida (Gui, Rê, Rick, amigos da BePro e alguns outros), pelo carinho, pelo apoio e pela torcida.

Enfim, a todos que de alguma forma colaboraram para que eu alcançasse esse sonho, meu muito obrigada.

RESUMO

Micelas poliméricas (MP) são carreadores nanoestruturados utilizados para a entrega de fármacos hidrofóbicos e/ou agentes de imagem por direcionamento passivo para tumores sólidos, permitindo criar uma plataforma teranóstica anticancer. A partir desse pressuposto, nosso grupo de pesquisa desenvolveu MP carreadoras de paclitaxel (PTX) radiomarcadas com tecnécio-99m (MP-DTPA-^{99m}Tc/PTX), a qual apresentou uma captação elevada na região tumoral em modelo de tumor de mama murino, indicando que esta é uma estratégia promissora para potencializar o tratamento e diagnóstico do câncer. Nesse contexto, o objetivo do presente estudo foi avaliar a organização estrutural desse nanossistema, propor uma estratégia para aumentar sua estabilidade e, realizar estudos pré-clínicos para avaliar a atividade antitumoral e toxicidade das MP carreadoras de PTX (MP/PTX). A avaliação estrutural realizada pela técnica de SAXS mostrou que a adição do fármaco promoveu um aumento no raio do núcleo micelar o qual foi compensado pela redução do raio de PEG (R_{PEG}), refletindo em um diâmetro constante. Essas variações de raio foram proporcionais à concentração de PTX até um máximo próximo a 0,6 mg/mL. Possivelmente, a redução do R_{PEG} é devido à mudança na conformação desse polímero de escova para cogumelo, o que refletiu diretamente nos estudos *in vivo* de depuração sanguínea que mostraram um tempo maior de circulação das MP brancas em relação a MP/PTX. Um kit liofilizado de radiofármaco para a reconstituição com $Na^{99m}TcO_4$ foi desenvolvido e sua estabilidade de armazenamento foi avaliada. Nenhuma alteração dos parâmetros físico-químicos (diâmetro, potencial zeta, teor de PTX) ou biológicos (perfil de biodistribuição e acúmulo na região tumoral), bem como na radiomarcação do sistema foi observada durante 180 dias de análise. Estudos *in vitro* de captação celular mostraram maior capacidade das MP em carrear o PTX (5,8%) para células 4T1 quando comparado ao PTX preparado com cremophor (CrEL/EtOH/PTX) (2,7%) após 2 horas. Nos estudos *in vivo* de toxicidade, camundongos que receberam MP/PTX em dose única ou mesmo repetida (7 doses) não apresentaram sinais de neuropatia periférica, a qual foi observada no grupo CrEL/EtOH/PTX. Além disso, as MP/PTX apresentaram uma melhor atividade antitumoral, com uma razão de inibição do tumor 1,5 vezes maior que CrEL/EtOH/PTX. Os dados obtidos sugerem a potencialidade das MP a para a entrega eficaz e segura do PTX, bem como do agente de imagem ^{99m}Tc, para tumores sólidos.

Palavras-chave: câncer; micelas poliméricas; DSPE-PEG; paclitaxel; teranóstico; SAXS; neuropatia periférica; atividade antitumoral.

ABSTRACT

Polymeric micelles (PM) are nanostructured carriers used in the delivery of hydrophobic drugs and/or imaging agents to solid tumors by passive targeting, enabling an anti-cancer theranostic platform. From this, our research group developed a ^{99m}Tc-radiolabeled PM carrying PTX (PM-DTPA-^{99m}Tc/PTX), which showed high tumor uptake in a murine breast tumor model, being a promising strategy for improving cancer treatment and diagnosis. In this context, the purpose of this study was to evaluate the structural organization of this nanosystem, to propose a strategy to increase its stability and to conduct preclinical studies to evaluate toxicity and antitumor activity of PM carrying PTX (PM/PTX). The structural evaluation performed by SAXS showed that the drug leads to an increase in the micelle core radius, which was compensated by a reduction of the PEG radius (R_{PEG}) and resulted in no change in PM diameter. These radius variations were proportional to the PTX concentration to a maximum close to 0.6 mg/mL. Possibly, the reduction in R_{PEG} is due to the change in brush-to-mushroom conformation of this polymer and was reflected in *in vivo* blood clearance studies that showed a longer circulation time for blank PM compared to PM/PTX. A radiopharmaceutical lyophilized kit for reconstitution with $Na^{99m}TcO_4$ was developed and its storage stability was evaluated. No changes in physicochemical (diameter, zeta potential, PTX content) or biological (biodistribution profile and accumulation in the tumor region) parameters after 180 days of storage were observed. *In vitro* cell uptake studies showed that PM had greater ability (5.8%) in delivery PTX to 4T1 cells after 2 hours of incubation when compared to cremophor-prepared PTX (CrEL/EtOH/PTX) (2.7%). In the *in vivo* toxicity studies, after receiving PM/PTX in single or repeated doses (7 doses) mice did not show signs of peripheral neuropathy, which was observed in the CrEL/EtOH/PTX group. In addition, PM/PTX presented higher antitumor activity, with a tumor inhibition ratio 50% higher than CrEL/EtOH/PTX. Data from this study suggest the potentiality of PM as an effective and safe delivery system for PTX and ^{99m}Tc for solid tumors.

Keywords: cancer; polymeric micelles; DSPE-PEG; paclitaxel; theranostic; SAXS; peripheral neuropathy; antitumor activity.

LISTA DE FIGURAS

LISTA DE TABELAS

LISTA DE ABREVIATURAS E SIGLAS

%ID/g	Percentual de dose injetada por grama
AF4	*Assymmetrical Flow Field-Flow Fractionation*/ Fracionamento em campo de fluxo assimétrico
ASC	Área Sob a Curva
ASTM	*American Society for Testing and Materials*
ATCC	*American Type Culture Colection*
CCD	Cromatografia em Camada Delgada
CEUA	Comissão de Ética em Uso de Animais
CLAE	Cromatografia Líquida de Alta Eficiência
CMC	Concentração Micelar Crítica
CrEL	Cremophor EL
^{64}Cu	Cobre-64
DLS	*Dynamic Light Scattering*/ Espalhamento Dinâmico de Luz
DM	Diâmetro Médio
DMEM	Meio Eagle Modificado por Dulbecco
DOTA	Ácido tetraazociclododecanotetraacético
DSC	Calorimetria Exploratória Diferencial
DSPE-PEG$_{2000}$	Distearoilfosfatidiletanolamina-*N*-(polietilenoglicol)2000
DTPA	Ácido dietilenotriaminopentacético
EDTA	Ácido etilenodiaminotetracético
ELS	*Eletrophoretic Light Scattering/*Espalhamento de Luz Eletroforético
EPR	*Enhanced Permeability and Retention/* Aumento da Permeabilidade e Retenção
EtOH	Etanol
^{18}F	Fluor-18
FFF	*Flow-Field Fractionation*/Fracionamento em Campo de Fluxo
^{67}Ga	Gálio-67
^{131}I	Iodo-131
^{125}I	Iodo-125
INCA	Instituto Nacional do Câncer
^{111}In	Indio-111
IV	Via Intravenosa

LNLS	Laboratório Nacional de Luz Síncroton
MALLS	*Multi Angle Light Laser Scattering/* Espalhamento de Luz Laser Multi Angulo
MET	Microscopia Eletrônica de Transmissão
MP-DTPA	Micelas Poliméricas de DSPE-PEG funcionalizadas com DTPA
MP-DTPA/PTX	Micelas Poliméricas de DSPE-PEG funcionalizadas com DTPA carreadoras de PTX
OMS	Organização Mundial da Saúde
PE	Fosfatidiletanolamina
PEG	Polietilenoglicol
PTX	Paclitaxel
PET	*Positron Emission Tomography*
RM	Ressonância Magnética
ROI	*Region of Interest*/Região de Interesse
R_{PEG}	Raio da camada externa de PEG
SAXS	*Small Angle X-ray Scattering*/ Espalhamento de raios-X a baixo ângulo
SFB	Soro Fetal Bovino
SFM	Sistema Fagocitário Mononuclear
SLS	*Static Light Scattering*/ Espalhamento de luz estático
$SnCl_2$	Cloreto Estanoso
SPECT	*Single PhotonEmissionComputedTomography*
TC	Tomografia Computadorizada
^{99m}Tc	Tecnécio-99 metaestável
TE	Teor de Encapsulação
WAXS	*Wide Angle X-ray Scattering/* Espalhamento de raios-X em alto ângulo

SUMÁRIO

1 INTRODUÇÃO

O câncer de mama é o segundo tipo de câncer de maior incidência no mundo (WHO, 2019). Por ser uma doença de difícil diagnóstico, o qual, frequentemente, ocorre em estágios avançados, a busca por novas alternativas de diagnóstico e tratamento tem crescido consideravelmente.

Entre os antineoplásicos utilizados no tratamento do câncer de mama, o paclitaxel (PTX) apresenta elevada eficácia, inclusive na sua forma metastática (SURAPANENI; DAS; DAS, 2012). No entanto, a formulação comercialmente disponível mais utilizada, o Taxol®, apresenta uma série de efeitos adversos, o que tem sido associado à presença do solvente Cremophor®EL (CrEL), além de apresentar baixa estabilidade após diluição para administração (OOSTENDORP; BUCKLE; LAMBERT, 2011). A fim de contornar esses inconvenientes, formulações nanoestruturadas contendo PTX têm sido desenvolvidas (PILLAI, 2014; ZHANG; ZHANG, 2013). Um grande exemplo é o Abraxane®, uma nanopartícula de albumina ligada ao PTX, que já teve o uso aprovado para tratamento de câncer de mama metastático pela *Food and Drug Administration* (FDA) e pela *European Medicines Agency* (EMA) e tem ganhado boa parte do mercado de PTX (SOFIAS et al., 2017). O Abraxane apresenta ganhos principalmente em relação à dose máxima tolerada (DMT) em relação ao Taxol®, entretanto, a toxicidade ainda representa uma grande preocupação. No entanto, como o PTX é um dos três quimioterápicos mais utilizado no mundo, a busca por formas mais eficazes e seguras é intensa, representada pelo fato de atualmente haver ao menos 18 companhias farmacêuticas investindo em pesquisas relacionadas à novas formulações de PTX.

Recentemente, nosso grupo de pesquisa desenvolveu um nanossistema de micelas poliméricas carreadoras de PTX e radiomarcadas com tecnécio-99m (^{99m}Tc-DTPA-MP/PTX), o qual apresentou características físico-químicas e biológicas promissoras para uma plataforma teranóstica antitumoral, com um grande potencial para acumular no tecido tumoral. No entanto, embora o procedimento de radiomarcação tenha sido rápido e eficiente, a quantidade e a estabilidade do fármaco encapsulado não foi satisfatória, indicando a necessidade de otimização desse sistema. Além disso, estudos físico-químicos e biológicos mais aprofundados que possibilitassem um maior entendimento do sistema desenvolvido tornou-se necessário.

Dessa maneira, a abordagem inicial desse trabalho compreendeu um estudo da organização estrutural das partículas isoladamente e no meio dispersante, ao nível molecular e supramolecular, permitindo-nos obter parâmetros que favorecessem a otimização do sistema bem como avaliar a influência desses no comportamento *in vivo.* Em seguida, considerando que

uma estratégia para contornar problemas relacionados à estabilidade de um sistema é a remoção de água (FONTE et al., 2014) e tendo em vista os parâmetros físico-químicos promissores obtidos, foi desenvolvido um kit da formulação liofilizada para radiomarcação com potencial utilização como teranóstico em tumores. Por fim, no intuito de verificar o potencial terapêutico desse novo sistema no tratamento de câncer de mama, estudos pré-clínicos (*in vitro* e *in vivo)* em modelo experimental de tumor de mama murino bem como estudos de toxicidade foram conduzidos.

2 REVISÃO BIBLIOGRÁFICA

2.1 Câncer

Câncer é um termo genérico utilizado para um grupo de doenças que se caracterizam por alterações celulares que levam ao crescimento e divisão anormal e descontrolada de células, as quais podem invadir partes adjacentes do corpo e/ou se espalhar para outros órgãos (WHO, 2019). É a segunda principal causa de morte em todo o mundo e estima-se que em 2018, cerca de 9,6 milhões de pessoas morreram em decorrência de algum tipo de câncer, sendo, portanto, um preocupante problema de saúde mundial (GLOBOCAN, 2019). Nos países em desenvolvimento sua incidência tem aumentado em decorrência do envelhecimento populacional, bem como da mudança no estilo de vida da população, com aumento no consumo de álcool, fumo e alimentos industrializados, além do sedentarismo (AHMEDIN JEMAL; ELIZABETH WARD; DAVID FORMAN, 2011).

Existem vários tipos de câncer, que podem ser agrupados em diferentes categorias de acordo com seu tecido de origem, sendo eles: carcinoma, sarcoma, leucemias, linfomas e mielomas e os tumores do sistema nervoso central. A maioria resulta em tumores visíveis, chamados de tumores sólidos, enquanto outros, como as leucemias, não (NCI, 2019). Os tipos mais incidentes de câncer são pulmão, mama, colo retal, próstata, pele não-melanoma e estômago, nesta ordem. Enquanto os mais letais incluem pulmão, colo retal, estômago, fígado e mama. De acordo com o sexo, os tipos mais comuns nos homens são pulmão, próstata, colo retal, estômago e fígado, enquanto nas mulheres destacam-se os cânceres de mama, colo retal, pulmão, colo do útero e tireoide (WHO, 2019).

O câncer de mama é o segundo tipo de câncer mais frequente no mundo e o tipo mais incidente e com maior taxa de mortalidade entre as mulheres. Segundo a Organização Mundial de Saúde (OMS), em 2018, uma incidência de 2,09 milhões de casos e cerca de 627.000 mortes em decorrência do câncer de mama foi estimada em todo o mundo (GLOBOCAN, 2019). Desses, aproximadamente 13.225 casos foram em mulheres brasileiras, e a estimativa de novos casos para o ano de 2018 foi de 59.700 de mulheres com câncer de mama (INCA, 2019).

O câncer de mama é uma doença heterogênea com vários subtipos e pode ser classificado de acordo com o grau de agressividade, em carcinoma *in situ* ou invasivo; de acordo com a sua histopatologia, em carcinoma tubular, medular e ductal. A classificação baseada no perfil molecular, considera a expressão dos receptores de estrogênio (ER), de progesterona (PR) e do fator de crescimento epidérmico humano 2 (HER-2). A ausência de expressão de ER, PR e

HER-2 caracteriza o câncer de mama triplo negativo (TNBC), o qual apresenta elevada agressividade e tende a gerar metástases. Por fim, existe uma classificação baseada no progresso da doença, sendo que no estágio 1, o tumor está na mama, no estágio 2–3, já ocorreu disseminação para tecidos e gânglios próximos enquanto no estágio 4 já houve disseminação para órgãos distantes como pulmão, osso e cérebro (FRAGUAS-SÁNCHEZ et al., 2019; SHARMA; JAIN; SAREEN, 2013).

Dessa forma, as estratégias de tratamento dependem do subtipo de câncer. As principais modalidades incluem a cirurgia, a radioterapia, a terapia hormonal, a terapia baseada em anticorpos e a quimioterapia. Essa última é usada em casos de tumores avançados e agressivos, como em casos de TNBC, para reduzir a carga tumoral e controlar e erradicar a metástase. Embora nem todos os carcinomas de mama precisem efetivamente do uso da quimioterapia, ela muitas vezes é usada como um tratamento neoadjuvante, antes da cirurgia, e/ou como um tratamento adjuvante após a cirurgia. Os antitumorais são escolhidos dependendo do estágio e do subtipo do câncer, entretanto, a maioria dos esquemas terapêuticos inclui a doxorrubicina, a ciclofosfamida, o 5-fuourouracil e o paclitaxel (PTX), administrados sozinhos ou em combinação. Embora a taxa de resposta à maioria desses fármacos seja baixa e os pacientes frequentemente desenvolvem resistência ao tratamento, o PTX tem demonstrado elevada eficácia, com uma taxa de resposta em pacientes com câncer de mama metastático de aproximadamente 56% (FRAGUAS-SÁNCHEZ et al., 2019; LANG et al., 2013; LU et al., 2013a; SURAPANENI; DAS; DAS, 2012).

2.2 Diagnóstico por imagem cintilográfica do câncer

O diagnóstico clínico inicial do câncer é baseado na anamnese e no exame físico do paciente, os quais direcionam a escolha dos exames complementares a serem realizados. Os exames complementares tais como os laboratoriais, endoscópicos e de diagnóstico por imagem auxiliam na avaliação da extensão do tumor, detecção de recidivas, monitoramento da terapia bem como na confirmação do diagnóstico (NIH, 2019).

As técnicas de diagnóstico por imagem incluem métodos que se baseiam em alterações anatômicas, como a tomografia computadorizada (TC), a ressonância magnética (RM) e a ultrassonografia, bem como métodos em medicina nuclear, como a tomografia por emissão de pósitrons (PET, do inglês *Positron Emission Tomography*) e tomografia computadorizada por emissão de fóton único (SPECT- do inglês *Single Photon Emission Computed Tomography*) (BLANCO et al., 2009; GRALLERT et al., 2012; RYVOLOVA et al., 2012). Nesse último

caso, o diagnóstico é baseado em alterações fisiológicas e/ou bioquímicas do órgão, permitindo uma detecção precoce e não invasiva da doença (DE BARROS et al., 2012a; HONG et al., 2009; OERLEMANS et al., 2010; STACY; MAXFIELD; SINUSAS, 2012).

O uso de técnicas cintilográficas é amplamente favorecido por uma variedade de sondas de imagem disponíveis, entre emissores de radiação gama (Tecnécio-99m -^{99m}Tc, o Índio-111 - ^{111}In, o Iodo-131 -^{131}I, Gálio-67 - ^{67}Ga) e emissores de pósitron (Fluor-18 - ^{18}F e Cobre-64 - ^{64}Cu) (DE BARROS et al., 2012a). Além disso, não possuem limite de penetração nos tecidos e permitem a quantificação do radiotraçador captado na região de interesse (DE BARROS et al., 2012a; HONG et al., 2009; STACY; MAXFIELD; SINUSAS, 2012). Dentre os emissores de radiação gama, o tecnécio-99m (^{99m}Tc) vem sendo muito utilizado por apresentar propriedades favoráveis para a utilização como radiofármaco. Elemento químico de número atômico 43, possui um total de 21 isótopos, sendo o Tecnécio-99 metaestável (^{99m}Tc) o isótopo que apresenta as melhores propriedades físicas e químicas para a aplicação em imagens cintilográficas (JONES, 1997; SCHWOCHAU, 2000; THRALL, J. H.; ZIESSMAN, 2003; ZHU et al., 2014). Tais propriedades incluem meia-vida física de 6,02 horas, emissão gama de baixa energia com fóton único de 140 keV, facilidade de obtenção por meio de geradores de Molibdênio-99/Tecnécio-99m (^{99}Mo/^{99m}Tc), além de apresentar um custo relativamente baixo (DE BARROS et al., 2013a; VARSHNEY et al., 2012; ZHU et al., 2014). O tempo de meia-vida apresentado pelo ^{99m}Tc é longo o suficiente para permitir uma preparação farmacêutica e obter imagens *in vivo*, mas não demasiadamente longo, uma vez que a meia-vida é determinante no tempo de exposição dos pacientes à radiação (THRALL, J. H.; ZIESSMAN, 2003; VARSHNEY et al., 2012).

A complexação do ^{99m}Tc com ligantes polidentados tais como o ácido dietilenotriaminopentaacético (DTPA), o ácido etilenodiaminotetraacético (EDTA) e o ácido tetraazaciclododecanotetracético (DOTA) tem proporcionado um aumento no contraste da imagem e na estabilidade do radionuclídeo *in vivo* uma vez que previne a transquelação durante o tempo de circulação desse na corrente sanguínea (VARSHNEY et al., 2012). Em particular, a complexação do DTPA (**Figura 1**) com ^{99m}Tc tem mostrado bons resultados como um agente de imagem nuclear (HAZARI et al., 2010) sendo, portanto, uma excelente alternativa para associar o radioisótopo a um nanocarreador.

Figura 1. Representação química do ^{99m}Tc complexado ao DTPA.

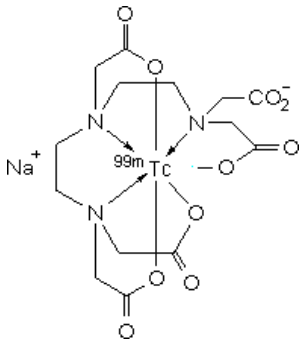

Reproduzido de (WHO, 2018).

2.3 Paclitaxel

O PTX é um agente antineoplásico de origem natural, pseudo-alcalóide, derivado originalmente da árvore *Taxus brevifolia* ou Teixo do Pacífico, que atualmente é obtido semi-sinteticamente pela acilação da 10-desacetilbacatina III, que é um precursor presente nas agulhas da *T. brevifolia* e *T. baccata* (BERNABEU et al., 2017; HENNENFENT; GOVINDAN, 2006; ZHANG; MEI; FENG, 2013).

Esse fármaco possui fórmula molecular $C_{47}H_{51}NO_{14}$, peso molecular de aproximadamente 854 Da e consiste em uma estrutura diterpenóide centrada em um anel taxano volumoso, de conformação rígida, composto por vários substituintes hidrofóbicos, o que contribui para uma baixa hidrofilicidade (log P igual a 3,96) e solubilidade em água inferior a 1 µg/mL (**Figura 2**). Sua atividade anticâncer é, principalmente, devido à presença do grupo benzoíla no carbono C2 e do anel oxetano localizados no anel taxano. Além disso, os grupamentos presentes nos carbonos C3' e C13 são responsáveis por manter a atividade antineoplásica e a hidroxila no C2' potencializa essa atividade (ZHANG; MEI; FENG, 2013). O mecanismo de ação desse fármaco ocorre na fase mitótica de divisão celular e envolve a ligação irreversível à subunidade-beta da tubulina, o que resulta na estabilização dos microtúbulos impedindo sua reorganização. A perda da funcionalidade dessas estruturas e a inibição da mitose na fase G2 leva as células neoplásicas à morte celular por apoptose (BINDER, 2013; SURAPANENI; DAS; DAS, 2012; ZHANG et al., 2014). Alguns pesquisadores têm relacionado ainda a eficácia antitumoral à atividade antiangiogênica

promovida pelo PTX. Esses estudos relataram a inibição da quimiotaxia e da capacidade de invasão de células endoteliais, em decorrência do efeito de supressão da expressão do fator de crescimento do endotélio vascular (VEGF) no tumor. No entanto, não há um consenso sobre o efeito antiangiogênico promovido pelo fármaco *in vivo*, devido à variação nas respostas obtidas em diferentes modelos experimentais (BELOTTI et al., 1996; BOCCI; DI PAOLO; DANESI, 2013; SURAPANENI; DAS; DAS, 2012).

Figura 2. Estrutura química do Paclitaxel.

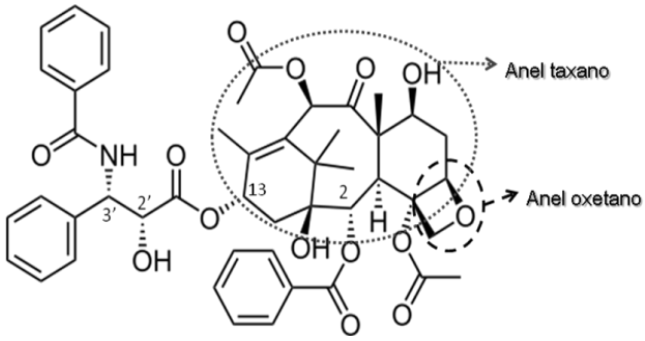

Adaptado de (SURAPANENI; DAS; DAS, 2012; ZHANG; ZHANG, 2013).

O PTX na forma da formulação comercial Taxol® (Bristol-Myers Squibb), na qual é preparado com uma mistura de co-solventes contendo óleo de rícino polioxietilado (Cremophor® EL, CrEL) e etanol desidratado na proporção de 1:1 (v/v) é aprovado pela Food and Drug Administration (FDA) para ser usado isoladamente, ou em combinação com outros tratamentos antineoplásicos, no tratamento de sarcoma de Kaposi, câncer de mama, incluindo metastático, câncer de pulmão de células não pequenas (NSCLC) e câncer de ovário. Mas apresenta atividade frente outros tipos de câncer, incluindo câncer de cabeça e pescoço, esôfago, bexiga, endométrio e colo do útero (BARBUTI; CHEN, 2015; BOCCI; DI PAOLO; DANESI, 2013). Entretanto, apesar da sua elevada potência anticâncer, o PTX apresenta características que limitam a sua aplicação clínica, entre elas a baixa solubilidade em água e a alta taxa de ligação a proteínas plasmáticas, o que resulta em uma baixa biodisponibilidade do fármaco por via oral e dificulta a obtenção de preparações farmacêuticas para via parenteral (SURAPANENI; DAS; DAS, 2012; ZHANG et al., 2014).

O uso do solvente Cremophor® EL possibilita a veiculação do PTX para administração por via endovenosa, porém, além dos efeitos adversos já conhecidos dos citotóxicos, como a mielossupressão e toxicidade gastrointestinal, estudos demonstraram que o Taxol® apresentou,

também, nefrotoxicidade, neurotoxicidade periférica, broncoespasmos, hipotensão e reações de hipersensibilidade. Esses efeitos podem ser atribuídos à elevada concentração do CrEL utilizada na preparação, limitando de forma significativa a terapia com esse fármaco (HENNENFENT; GOVINDAN, 2006; STIRLAND et al., 2013; VAN ZUYLEN; VERWEIJ; SPARREBOOM, 2001).

Dentre os efeitos adversos observados em pacientes usuários do PTX destaca-se o surgimento de neuropatias sensoriais periféricas (BERNABEU et al., 2017; OOSTENDORP; BUCKLE; LAMBERT, 2011). As neuropatias periféricas induzidas por quimioterápicos estão entre as toxicidades que mais limitam a dose e a continuidade dos tratamento e o PTX é um dos quimioterápicos com maior incidência desse tipo de toxicidade. Além disso, diferente dos outros antineoplásicos que causam esse sintoma normalmente após um tempo ou somente após repetidas doses, o PTX pode causa-lo imediatamente após ou mesmo durante a infusão do fármaco. Entre os sintomas mais comuns da neurotoxicidade periférica pode-se citar dormência, formigamento, sensação de toque alterada, parestesias e disestesias induzidas por toque e temperatura, além disso, sensações dolorosas, incluindo queimação, dor semelhante a choque elétrico e hiperalgesia. Em casos graves, esses sintomas podem progredir para a perda da percepção sensorial. Ainda, alguns sintomas motores são relatados entre eles fraqueza distal, distúrbios da marcha e do equilíbrio e movimentos prejudicados. E em casos mais graves, pode levar à imobilização completa do paciente (ZAJACZKOWSKA et al.,2019).

Diante disso, observa-se a real necessidade de desenvolver novas estratégias para veicular o PTX, de forma a reduzir a toxicidade e aumentar sua atividade antitumoral. Nesse sentido, o emprego da nanotecnologia tem se mostrado uma abordagem promissora (HENNENFENT; GOVINDAN, 2006; STIRLAND et al., 2013; WAN et al., 2013; WANG; PETRENKO; TORCHILIN, 2010; ZHANG; ZHANG, 2013).

Estudos pré-clínicos e clínicos com nanoestruturas carreadoras como lipossomas (KAN et al., 2010; XU et al., 2013; ZHANG et al., 2015a; ZHOU et al., 2013), micelas poliméricas (EMAMI et al., 2015; KATRAGADDA et al., 2013; WANG; PETRENKO; TORCHILIN, 2010; WU; ZHU; TORCHILIN, 2013), nanopartículas lipídicas sólidas (BAEK; CHO, 2015; CHIRIO et al., 2014; KIM et al., 2015), entre outras, têm demonstrado vantagens no tratamento de diversos tipos de câncer. No entanto, apenas três preparações veiculando o PTX foram aprovadas para o uso clínico: Abraxane® (nanopartículas de albumina), Lipusu® (lipossomas) e Genexol-PM® (micelas poliméricas).

Dentre essas formulações o Abraxane® (Abraxis-Celgene), aprovado pela FDA para tratamento de câncer de mama, tem ganhado grande parte do mercado do Taxol®, uma vez que

apresenta uma maior dose máxima tolerada (DMT), menor toxicidade, elimina a necessidade de pré medicações e infusões demoradas (BERNABEU et al., 2017). Entretanto, não foi comprovada superioridade quanto a atividade em relação a formulação convencional, além disso neurotoxicidade periférica ainda é uma preocupação com relação a esse medicamento, sendo que alguns levantamentos mostram que a incidência dessa toxicidade é ainda maior em pacientes em tratamento com Abraxane® (BERNABEU et al., 2017; GUO et al., 2019).

Quanto ao Genexol-PM® (Samyang Corporation), atualmente tem o uso clínico aprovado para o tratamento de câncer de mama na Coréia do Sul, Índia, Vietnã, Filipinas e Indonésia, também apresentou ganhos quanto a DMT e apresentou melhor atividade em comparação ao Taxol, quando ambos usados na sua DMT. No entanto, a incidência de neutropenia e neuropatias periféricas ainda é alto nos pacientes tratados com o Genexol-PM (BERNABEU et al., 2017).

Pode-se perceber, portanto, que a viabilidade da nanomedicina para entrega do PTX foi comprovada, entretanto, a questão de segurança, ainda é uma preocupação e a busca por novas preparações que apresentem vantagens quanto à segurança e eficácia sobre aquelas já relatadas é de extrema relevância.

2.4 Sistemas nanoestruturados carreadores de fármacos na oncologia

Sistemas nanoestruturados carreadores de fármacos são estruturas de tamanho nanométrico, que apresentam grande potencial para encapsular substâncias fracamente hidrossolúveis (HUH et al., 2008), proteger moléculas (GREGORY; TITBALL; WILLIAMSON, 2013), modificar o perfil farmacocinético e farmacodinâmico de substâncias (LEITE et al., 2012; YOU et al., 2014) e direcioná-los para um sítio alvo (LU et al., 2013b), como objetivo de tratar sistemas biológicos, bem como diagnosticar e monitorar processos físicos e patológicos (BERTRAND et al., 2014; PEER et al., 2007; SHARMA; JAIN; SAREEN, 2013).

O fator que favorece o uso de nanocarreadores na oncologia é a característica peculiar da maioria dos tumores sólidos, que, devido à grande necessidade de suprimento de oxigênio e de nutrientes para o seu crescimento, apresenta regiões com alta taxa de angiogênese. No entanto, os vasos são malformados e altamente permeáveis com fenestrações maiores que 100 nm. Essa neovascularização não é uniforme, assim como a distribuição dos vasos linfáticos, provocando uma drenagem linfática na massa tumoral heterogênea e ineficiente (BERTRAND et al., 2014; FANG; NAKAMURA; MAEDA, 2011; SVENSON, 2012). Essas características

inerentes aos tumores favorecem o acúmulo das nanopartículas nessa região, efeito que foi descoberto por Hiroshi Maeda e colaboradores (1986) e foi denominado efeito de "aumento da permeabilidade e retenção" ou efeito EPR (do inglês *Enhanced Permeability and Retention*) (**Figura 3**) (FANG; NAKAMURA; MAEDA, 2011; MAEDA, 2010). A maior parte dos sistemas nanoestruturados aprovados para uso e em fases de estudos clínicos são constituídos por polímeros e lípides naturais e sintéticos (PEER et al., 2007; RAMOS-CABRER; CAMPOS, 2013; SAWANT; TORCHILIN, 2010; TORCHILIN, 2007a) e incluem os lipossomas, as nanopartículas poliméricas e as micelas poliméricas (SVENSON, 2014).

Figura 3. Acúmulo de nanopartículas em tecidos tumorais em decorrência do efeito EPR.

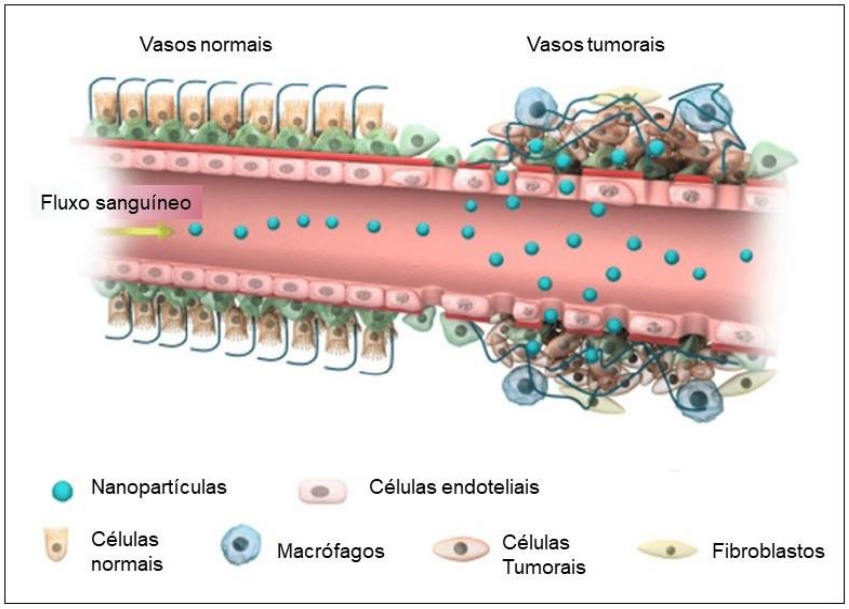

Adaptado de (ABDALLA et al., 2018).

2.5 Micelas poliméricas

Micelas poliméricas são estruturas supramoleculares, de tamanho na faixa de 5 a 100 nm, formadas por copolímeros de bloco ou de enxerto, com uma composição bifásica, consistindo em um núcleo hidrofóbico interior e uma "casca" hidrofílica exterior, ou estrutura "*core-shell"* (KAZUNORI et al., 1993; TORCHILIN, 2006; YOKOYAMA, 2014).

Figura 4. Representação da formação de micelas a partir da concentração micelar crítica.

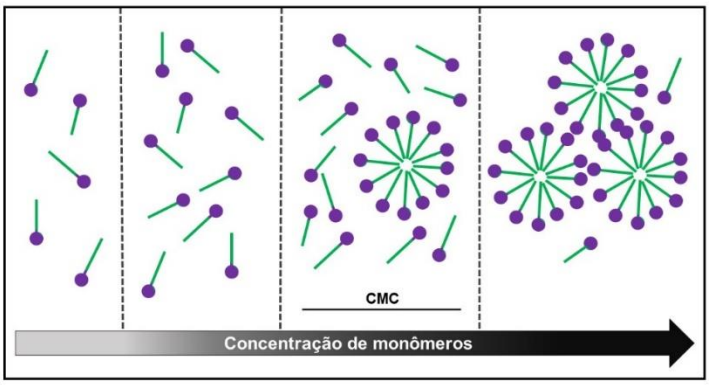

Os copolímeros anfifílicos em soluções aquosas muito diluídas se encontram na forma de monômeros, no entanto, com o aumento da concentração no meio alcançam a concentração micelar crítica (CMC), na qual as micelas começam a ser formadas, como representado na **Figura 4.** (OERLEMANS et al., 2010; TORCHILIN, 2007b; TRIVEDI; KOMPELLA, 2010).

A composição da micela é determinante para as suas características físico-químicas, tais como o tamanho, a forma e principalmente a CMC, determinando, portanto, a estabilidade física do sistema (CROY; KWON, 2006). Sabe-se que quanto menor o peso molecular da componente estrutural da micela, maior é a sua CMC e maior à sensibilidade à diluição. Nesse sentido, as micelas poliméricas usualmente apresentam uma CMC menor (10^{-6} a 10^{-7} mol/L) quando comparado a outros surfactantes (10^{-3}a 10^{-4} mol/L) (OERLEMANS et al., 2010; SAWANT; TORCHILIN, 2010). A obtenção de uma baixa CMC é particularmente interessante, do ponto de vista farmacológico, para sistemas administrados por via intravenosa. Ao atingir a corrente sanguínea, micelas com valores de CMC alto podem se dissociar em monômeros e seu conteúdo pode ser liberado, visto que o volume do meio em que as micelas estão presentes aumenta muito e uma concentração abaixo da CMC pode ser alcançada. Em função disso, micelas baseadas em polímeros, possuem um tempo de circulação sanguínea aumentado quando comparadas às micelas de surfactantes de baixo peso molecular (GRALLERT et al., 2012; OERLEMANS et al., 2010).

As propriedades inerentes à composição micelar são responsáveis por controlar importantes características biológicas do nanocarreador, como perfil farmacocinético, perfil de biodistribuição, adsorção de macromoléculas na sua superfície e adesão a biossuperfícies (DESHMUKH et al., 2017; TORCHILIN, 2007b). A "casca" hidrofílica da micela é responsável por uma efetiva proteção estérica e é determinante em algumas características como hidrofilia, carga, tamanho, densidade de superfície e permite a modificação da superfície por

meio de grupos reativos. O núcleo hidrofóbico determinará a capacidade de armazenamento, perfil de liberação do fármaco e compatibilidade com fármaco encapsulado (DESHMUKH et al., 2017; OERLEMANS et al., 2010). Portanto, geralmente as micelas permitem a encapsulação de inúmeros fármacos hidrofóbicos incluindo agentes antineoplásicos como o PTX.

O grande interesse por sistemas micelares no tratamento do câncer se deve, principalmente, às suas características estruturais, uma vez que essas resultam em importantes vantagens biológicas, relacionadas à farmacodinâmica e farmacocinética, levando a um tempo de circulação sanguínea aumentado e direcionamento passivo na região tumoral, além de um caráter de liberação sustentada de fármacos (GRALLERT et al., 2012; NISHIYAMA; MATSUMURA; KATAOKA, 2016; YOKOYAMA, 2014). A liberação sustentada ocorre, porque, à medida que as micelas poliméricas são depuradas da circulação elas são, gradualmente, diluídas no meio fisiológico, se desfazem e liberam o seu conteúdo de forma gradativa e sustentada (CROY; KWON, 2006; TRIVEDI; KOMPELLA, 2010).

O tempo de circulação sanguínea aumentado e direcionamento passivo na região tumoral se devem, principalmente, ao seu tamanho reduzido. Esse compreende uma faixa ideal para escapar dos mecanismos fisiológicos de eliminação do organismo, pois partículas com tamanho inferior a 5 – 10 nm são rapidamente eliminadas via renal e partículas maiores são rapidamente reconhecidas pelo sistema fagocitário mononuclear (SFM) e eliminadas por essa via. Além disso, estruturas com tamanho inferior a 100 nm são preferencialmente acumuladas no interstício da região tumoral via efeito EPR. Portanto, as micelas apresentam todas as características favoráveis para levar a um direcionamento passivo do fármaco à região tumoral (CABRAL et al., 2011; CROY; KWON, 2006; JONES; LEROUX, 1999; MOHAMED et al., 2014; YOKOYAMA, 2014).

Com relação à composição, o polietilenoglicol (PEG), com peso molecular de 1 a 15 kDa, é o componente hidrofílico mais utilizado (CROY; KWON, 2006; LUKYANOV; TORCHILIN, 2004; MOHAMED et al., 2014; SAWANT; TORCHILIN, 2010). O PEG é um polímero altamente hidratável, atóxico, não antigênico e biocompatível, aprovado por agências regulatórias, para o uso interno em humanos (CHENG et al., 2011; KWON; KATAOKA, 1995). Uma importante propriedade do PEG é a sua eficiente capacidade de estabilizar estericamente superfícies em meio aquoso. Isso ocorre porque as cadeias de PEG formam uma densa “cabeleira” ou “escova” altamente hidratada o que resulta em uma grande camada de solvatação em torno do núcleo hidrofóbico da estrutura micelar (JOKERST et al., 2012; KWON; KATAOKA, 1995). Essa característica é particularmente interessante porque previne

a adsorção de proteínas, como imunoglobulinas, as quais identificam as nanoestruturas como um material estranho e previnem a adesão de células fagocitárias, mecanismos que levariam à eliminação da partícula do organismo (CROY; KWON, 2006; KOLATE et al., 2014; KWON; KATAOKA, 1995).

O material constituinte do núcleo da micela depende da natureza do fármaco a ser encapsulado e geralmente consiste de polímeros biodegradáveis como o poli ácido D,L-lático (PDLLA), poli ácido L-aspártico e poli ε-caprolactona (PCL) e, em alguns casos, resíduos fosfolipídicos são utilizados (KOLATE et al., 2014; SAWANT; TORCHILIN, 2010).

O uso de uma porção lipídica como bloco hidrofóbico da composição de micelas, como a fosfatidiletanolamina (PE), fornece vantagens adicionais para a estabilidade da nanoestrutura, quando comparado às micelas poliméricas convencionais, pois a presença de duas cadeias de ácidos graxos pode contribuir para as interações hidrofóbicas no núcleo entre as unidades constituintes da micela polimérica (SAWANT; TORCHILIN, 2010). Vários estudos têm demonstrado sucesso ao utilizar micelas compostas por diestearoilfosfatidiletanolamina associado ao PEG (DSPE-PEG) (**Figura 5A**) para solubilizar fármacos fracamente solúveis (GILL; KADDOUMI; NAZZAL, 2012; SARISOZEN et al., 2012; WU; ZHU; TORCHILIN, 2013). O diâmetro desse tipo de micela varia de 7 a 35 nm, dependendo do comprimento da cadeia de PEG, e os valores de CMC são baixos, na ordem de 10^{-5} a 10^{-6} mol/L (LUKYANOV; TORCHILIN, 2004) .

2.6 Micelas como uma plataforma teranóstica

A modificação da superfície das micelas poliméricas com agentes de imagem é particularmente vantajosa, pois permite a combinação da entrega de um agente terapêutico juntamente com um agente de diagnóstico (MI et al., 2017; TORCHILIN, 2007a).

Considerando que uma grande preocupação quanto ao uso de nanopartículas é a sua utilização em quantidades excessivamente elevadas o que pode levar à toxicidade inerente ao metabolismo e eliminação insuficiente do carreador, o uso de um mesmo sistema com multifunções é de grande interesse (**Figura 5B**) (ALLEN, 2004).

A essa combinação de terapia e diagnóstico, dá se o nome de teranóstico (ARRANJA et al., 2017; MUTHU et al., 2014). O uso de micelas com função teranóstica permite a visualização da distribuição das micelas no interior do corpo e no tumor em tempo real possibilitando a otimização do protocolo de tratamento de acordo com as características particulares dos tumores de cada paciente. Portanto, o uso de sistemas teranósticos é promissor

do ponto de vista do desenvolvimento de uma medicina personalizada, que busca tratar o paciente na sua individualidade para obter um resultado final mais satisfatório (KAIDA et al., 2010; KUMAR et al., 2012; MI et al., 2017).

Figura 5. Esquema representativo de um sistema micelar de DSPE-PEG multifuncionalizado carreador de PTX.

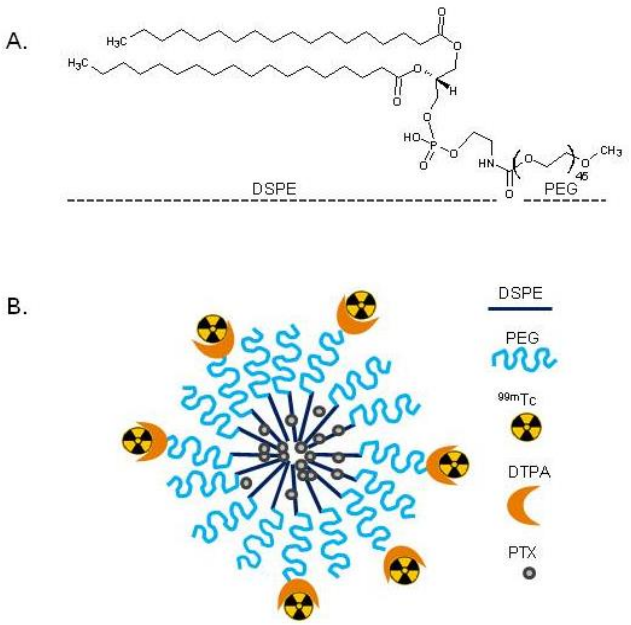

A. Estrutura química do DSPE-PEG; B. Esquema representativo de micelas poliméricas radiomarcadas com ^{99m}Tc, carreadoras de PTX.

Com base no exposto, um análogo do DSPE-PEG funcionalizado com o agente quelante DTPA foi sintetizado por nosso grupo (ODA et al., 2017) e utilizado no desenvolvimento de uma formulação de micelas poliméricas compostas por DSPE-PEG$_{2000}$ (10 mmol/L) contendo o fármaco antitumoral PTX (0,5 mg/mL). Baixos valores de CMC (1,8 x 10^{-5} mol/L), diâmetro médio de aproximadamente 10 nm e potencial zeta de -3,0 mV foram obtidos. Entretanto, quando concentrações superiores a 0,5 mg/mL foram associadas ao sistema, observou-se uma rápida liberação do fármaco a partir das micelas. A avaliação biológica quanto ao perfil de biodistribuição e tempo de depuração, demonstrou características promissoras, uma vez que foi possível observar a capacidade do sistema de acumular na região tumoral em modelo animal experimental de câncer de mama 4T1 e um tempo de circulação prolongado (ODA, 2015). Esses dados nos motivaram a investigar de forma mais detalhada as interações entre o fármaco e o

núcleo hidrofóbico no intuito de elucidar parâmetros essenciais para o processo de otimização dessa formulação, permitindo prosseguir a avaliação biológica.

2.7 Avaliação estrutural de micelas poliméricas

No desenvolvimento de um novo nanossistema, na maioria das vezes, acaba por se demonstrar somente os ganhos em relação a aplicações práticas, se tornando um sistema apenas "fenomenalístico", sem muito detalhamento sobre a estrutura e a arquitetura dessas micelas contendo o fármaco. Entretanto, sabe-se que o conhecimento sobre a organização estrutural e a liberação do fármaco, fornece importantes informações que contribuem para o aperfeiçoamento necessário e para uma melhor aplicação e funcionamento *in vivo* desse sistema (SANADA et al., 2013; SHIRAISHI et al., 2015). Algumas técnicas utilizadas para se obter as mais diferentes informações estruturais de micelas poliméricas estão apresentadas na **Tabela 1.**

Tabela 1. Técnicas de caracterização de micelas poliméricas.

Informações estruturais	Técnicas	Referências
Diâmetro; número de agregação; forma; padrão e periodicidade de organização; interação fármaco-estrutura; localização do fármaco	SAXS/WAXS	(GILROY et al., 2011; PEDERSEN et al., 2003; SANADA et al., 2013; SHIRAISHI et al., 2015)
Diâmetro; número de agregação; índice de polidispersividade	DLS; SLS/ AF4	(GIACOMELLI et al., 2011; MILLER et al., 2012; SANADA et al., 2013; WANG; PETRENKO; TORCHILIN, 2010)
CMC	Fluorescência	(AHN et al., 2014; DABHOLKAR et al., 2006; LV et al., 2013)
Diâmetro; morfologia	Microscopias: MET/ AFM	(CHEN et al., 2015; GILROY et al., 2011; LV et al., 2013; WANG et al., 2014)
Teor de fármaco encapsulado e perfil de liberação	Técnicas cromatográficas e espectrométricas	(CHEN et al., 2015; GUO et al., 2014; ZHANG et al., 2015b)
Potencial Zeta	DLS associado a mobilidade eletroforética (ou ELS)	(GIACOMELLI et al., 2011; WANG et al., 2014)

*SAXS/WAXS: Espalhamento de Raios-x a Baixo Ângulo e a Ângulo Amplo; DLS/SLS: Espalhamento de Luz Dinâmico e Estático; AF4: Fracionamento por campo de fluxo assimétrico; MET: Microscopia Eletrônica de Transmissão; AFM: Microscopia de força atômica; ELS: Espalhamento de luz eletroforética.

Embora cada uma apresente particularidades e aplicações distintas, nesse tópico, abordaremos com mais detalhes as técnicas de espalhamento de raios-x a baixo ângulo (SAXS/WAXS) e de fracionamento em campo de fluxo assimétrico (AF4, do inglês *asymmetric flow-field-flow fractionation*), que são técnicas complexas e menos utilizadas rotineiramente, mas fornecem uma ampla quantidade de informações estruturais sobre um sistema nanocarreador.

2.7.1 *Espalhamento de raios-X a baixo ângulo*

Dentre as técnicas mencionadas, o espalhamento de raios-x a baixo ângulo (SAXS) são técnicas bem estabelecidas para explorar a estrutura em escala nanométrica e as interações de materiais coloidais, portanto, têm sido fundamentais no esclarecimento das estruturas de micelas poliméricas (SANADA et al., 2013; SATO et al., 2007).

Essas técnicas oferecem resolução temporal e espacial nanométrica em um intervalo de milissegundos, permitindo elucidar a nanoestrutura de objetos muito pequenos ou deduzir informações altamente localizadas mediante varredura de uma amostra fina com resolução de espaço real micrométrica (NARAYANAN, 2009). As medidas são conceitualmente muito simples e seus princípios básicos são semelhantes aos da dispersão de luz aplicadas nas técnicas de microscopia. No caso dos raios-X, a dispersão ocorre a partir de elétrons originados de uma fonte síncrotron. Um raio altamente colimado e monocromático atinge uma amostra e a intensidade espalhada é coletada por um detector bidimensional (**Figura 6**) (DI COLA; GRILLO; RISTORI, 2016).

Figura 6. Esquema representativo de um equipamento de SAXS

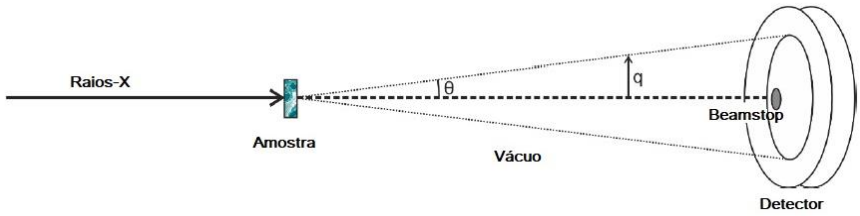

Adaptado de DI COLA et al., 2015.

Para que se tenha qualidade no padrão de espalhamento, o feixe primário, que possui alta intensidade, não é espalhado pela amostra e pode danificar o detector, precisa ser totalmente absorvido por um "*beamstop"*, o qual é colocado na frente do detector. Outro aspecto importante é que o percurso de voo, antes e depois da amostra, exige vácuo para evitar a

absorção e a dispersão dos raios-x pelo ar. No detector, o padrão de espalhamento bidimensional é radialmente integrado para proporcionar a função de dispersão unidimensional "I (q)", em que q é o comprimento do vetor de espalhamento, e é definido por $q=\frac{4\pi}{\lambda} sin\frac{\theta}{2}$, sendo λ o comprimento de onda incidente e θ o ângulo de espalhamento (CRAIEVICH, 2002; DI COLA; GRILLO; RISTORI, 2016; NARAYANAN, 2009). O espalhamento de raios-X pode fornecer informações sobre uma ampla faixa de ângulos de espalhamento, desde ângulos ultra baixos (USAXS), ângulos baixos (SAXS) e ângulos amplos (WAXS), compreendendo a faixa de "q" de 0,001 nm^{-1} a 50 nm^{-1}, o que corresponde em dimensões do espaço real, do micrometro até abaixo do nanômetro (DI COLA; GRILLO; RISTORI, 2016; SANADA et al., 2013). A intensidade do espalhamento I (q) produzida pela amostra dependerá do ângulo de espalhamento. Nesse sentido, a incidência na região de SAXS fornece informações principalmente quanto à morfologia das nanopartículas, incluindo raio, número de agregação e formato (GIACOMELLI et al., 2011; GILROY et al., 2011; SATO et al., 2007). Por outro lado, na região característica para WAXS, é possível obter informações sobre parâmetros da organização do material estudado, como periodicidade, espaçamento de rede, quantidade em volume do material estudado e padrões de organização, como exemplo estruturas com padrões caracteristicamente lamelares e não lamelares (GILROY et al., 2011).

2.7.2 *Fracionamento em campo de fluxo assimétrico*

Outra técnica que nos permite obter maiores informações a respeito de nanossistemas é o fracionamento em campo de fluxo assimétrico. A técnica de fracionamento em campo de fluxo (FFF) foi desenvolvida em 1966 por J. C. Giddings e se baseia na aplicação de um campo de fluxo aplicado sob um canal plano e perpendicular à direção do fluxo da amostra, promovendo a separação (ESKELIN et al., 2016; WAGNER et al., 2014). O AF4 é uma técnica derivada da FFF, na qual a separação da amostra ocorre em um canal de plano trapezoidal sob a influência de dois fluxos: o fluxo do canal que tem um perfil parabólico e o fluxo cruzado que direciona os componentes da amostra para uma placa de acumulação. A força do fluxo cruzado é neutralizada pela difusão dos componentes da amostra, distanciando-as da placa de acumulação. Dessa forma, cada componente da amostra, dependendo do seu coeficiente de difusão e do seu tamanho, equilibra-se a uma distância diferente da placa de acumulação de maneira que, os componentes menores da amostra eluem antes dos maiores, conforme descrito na **Figura 7**. (ESKELIN et al., 2016; NILSSON, 2013). A versatílidade dessa técnica é que ela

pode ser acoplada a um ou mais diferentes detectores associados como infravermelho, ultravioleta, espalhamento de luz laser multiângulo (MALLS, do inglês *multiangle laser light scattering*) e espalhamento dinâmico da luz (DLS, do inglês *dynamic light scattering*), sendo estes dois últimos os mais comumente utilizados. Dessa maneira, inúmeros parâmetros podem ser obtidos como, por exemplo, massa molar, tamanho, densidade, difusividade, número de agregação, conformação ou forma (GALYEAN et al., 2016; WAGNER et al., 2014).

Figura 7. Representação esquemática do princípio da técnica AF4.

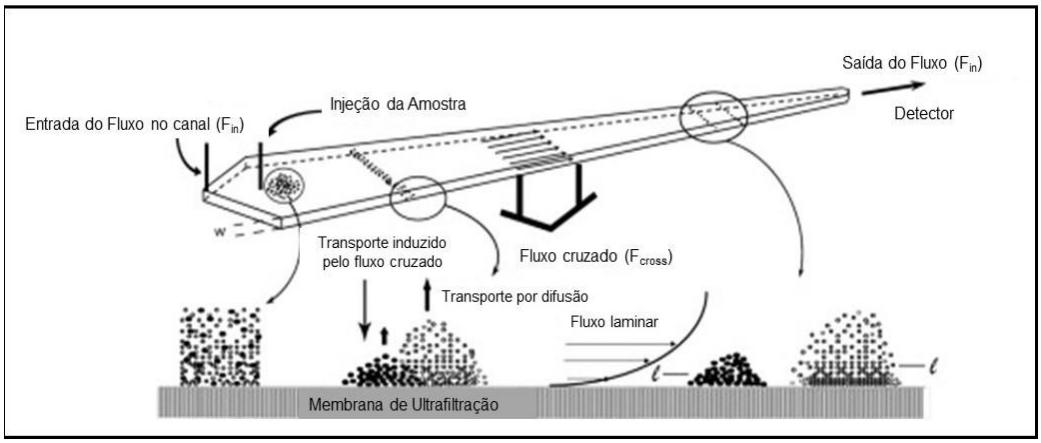

Adaptado de Nilsson, 2013.

2.8 Avaliação biológica de micelas poliméricas

Durante o desenvolvimento de um novo medicamento, seja ele um nanomedicamento ou não, logo após a etapa de desenvolvimento farmacotécnico e caracterização do sistema de entrega, a etapa seguinte é a sua avaliação biológica utilizando para isso ensaios *in vitro e in vivo*. Esses ensaios têm por finalidade avaliar algum comportamento desses sistemas em meio biológico, de maneira que seja possível correlaciona-los (EMAMI, 2006; EMAMI et al., 2015). Para isso, diversas abordagens podem ser utilizadas, seja utilizando de fato cobaias vivas para isso, seja pelo uso de cultura de células, ou até mesmo pelo uso de órgãos isolados ou de apenas um fluido biológico. O fato é que inúmeras perguntas podem ser respondidas por meio de desses estudos, seja simples ou complexo, e eles são extremamente essenciais para que se possa chegar à uma administração em humanos com algum nível de segurança.

Há uma grande discussão quanto ao uso de técnicas *in vitro e in vivo*, essas questões envolvem principalmente questões éticas. Uma vez que muitas respostas obtidas em experimentos *in vivo*, aparentemente, podem ser respondidas por ensaios *in vitro*, dessa forma

surge a dúvida de porquê continuar a utilizar animais. O fato é que o principal aspecto a ser considerado nessa questão é a complexidade de um ser. E como o objetivo desses estudos é encontrar respostas próximas ao que seria encontrado em seres humanos, para evitar possíveis desastres, é extremamente importante que seja feita uma avaliação com uma complexidade mais próxima ao do organismo humano. Entretanto, vale destacar a ética e respeito a vida, dessa maneira, entra a grande importância dos ensaios *in vitro*, uma vez que por meio deles é possível reduzir drasticamente a quantidade de animais utilizados numa experimentação *in vivo* (RASSI FERNANDES; RIBEIRO PEDROSO, 2017). Dessa maneira, foi sumarizado na **Tabela 2** alguns ensaios biológicos comumente utilizados e exemplos da sua aplicação em relatos da literatura, sendo alguns deles realizados neste trabalho.

Tabela 2 - Principais ensaios biológicos *in vitro* e *in vivo* utilizados na avaliação pré-clinica de formulações farmacêuticas e exemplos da sua aplicação em relatos da literatura.

Ensaio	Material utilizado	Aplicação	Referências
Estudos biológicos *in vitro*			
Estudos de permeabilidade	Tecido obtido por cultura 3D de células, tecido extraído de animais, membrana sintética	Avaliação a permeação de determinada substância através de tecidos como tumorais, intestinal, cutâneo, etc.	(FAN et al., 2015; JAHANSHAHI et al., 2020; VOLPE; VOLPE, 2020)
Estudos de captação e internalização celular	Células de cultivo	Avalia e quantifica a captação de substâncias no interior das células de interesse	(FAN et al., 2015; MONTEIRO et al., 2019; ZHANG et al., 2015a)
Estudos de viabilidade celular	Células de cultivo	Avaliação de potência do fármaco, toxicidade in vitro, atividade citotóxica, etc.	(WANG et al., 2019; ZHANG et al., 2015a)
Estudos de hemocompatibilidade	Sangue humano ou animal.	Avaliar o potencial da substância de provocar hemólise.	(DOBROVOLSKAIA; MCNEIL, 2013; MONTEIRO et al., 2019)
Estudos biológicos *in vivo*			
Estudos de atividade antitumoral	Tumores experimentais ou espontâneos em modelos animais.	Avaliar o potencial da substância como um antitumoral, por meio da avaliação da evolução/regressão do tumor.	(KIM et al., 2015; ZHANG et al., 2015a)
Estudos de toxicidade	Modelos animais e seus diferentes órgãos, tecidos e fuidos.	Avaliar os efeitos tóxicos de diferentes naturezas no organismo vivo: teciduais (avaliação histopatológica) hematológicos, bioquímicos, comportamentais, etc.	(LEITE et al., 2011; RABAH, 2010; YOU et al., 2014)
Estudos de biodistribuição	Órgãos e tecidos *ex vivo* ou *in vivo* (imagens)	Verifica como a substância se distribui nos órgãos e tecidos.	(KIM et al., 2015; OLIVEIRA et al., 2018; SILVA et al., 2019)
Estudos de depuração	Sangue, urina	Avalia qual a velocidade de excreção de uma substância	(MONTEIRO et al., 2017; YOU et al., 2014)

2.9 Considerações finais

Com base no exposto e na potencialidade observada previamente nas micelas funcionalizadas com DTPA contendo PTX, considerou-se de grande importância a avaliação estrutural das MP/PTX utilizando essas técnicas (SAXS e AF4) que são mais robustas e sensíveis. A elucidação da organização entre os componentes do sistema permite direcionar a otimização dessa formulação, que apresentou previamente problemas relacionados à estabilidade (ODA, 2015). Uma vez conhecidas as características físicas e químicas, o entendimento sobre o seu comportamento biológico desses sistemas é imprescindível para se verificar a sua potencialidade no tratamento do câncer e, portanto, estudos pré-clínicos de atividade antitumoral e toxicidade são etapas de extrema relevância. Foi a partir dessas premissas que o presente trabalho foi conduzido.

3 OBJETIVOS

3.1 Objetivo geral

Avaliar a potencialidade de micelas poliméricas de DSPE-PEG contendo PTX como estratégia para tratamento e diagnóstico do tumor de mama murino da linhagem 4T1.

3.2 Objetivos específicos

- Avaliar o efeito da encapsulação do PTX na estrutura e na organização supramolecular das micelas por técnicas de espalhamento de raios X a baixo ângulo (SAXS e WAXS).
- Caracterizar as formulações micelares quanto ao diâmetro médio, potencial zeta e teor de encapsulação do PTX.
- Desenvolver um kit liofilizado multifuncional contendo MP-DTPA/PTX para obtenção de um radiofármaco.Avaliar a estabilidade do kit quanto às características físico e radio químicas em relação ao teor de PTX e potencial de radiomarcação.
- Avaliar *in vivo* a aplicabilidade do kit como um radiotraçador após o tempo de armazenamento.
- Verificar o potencial hemolítico das micelas desenvolvidas.
- Realizar um estudo de captação da formulação desenvolvida em células 4T1 utilizando técnicas de radiomarcação isotópica com ^{99m}Tc e cromatografia líquida de alta eficiência.
- Comparar a atividade biológica e a toxicidade das MP/PTX com uma formulação contendo Cremophor/Etanol e PTX

4 DESENVOLVIMENTO

Esta sessão do documento foi dividida em três capítulos que representam os manuscritos dos artigos científicos desenvolvidos a partir do projeto de doutorado. Esses capítulos, embora abordem fases diferentes do estudo, eles são complementares e se complementam para se alcançar o objetivo do trabalho. São eles:

1. Capítulo 1: Efeitos físicos e biológicos da encapsulação do paclitaxel em micelas poliméricas de diestearoil fosfatidiletanolaina-polietilenoglicol.

O primeiro capítulo aborda principalmente a elucidação estrutural do sistema desenvolvido. Essa etapa foi primordial para a melhor compreensão de como o sistema se comporta *in vivo* e para entender como o sistema funciona. Dessa forma, foi possível entender quais as melhores condições para se obter uma formulação pronta para a aplicação *in vivo.*

2. Capítulo 2: Micelas poliméricas contendo paclitaxel funcionalizadas com ácido dietilenotriaminopentacético: kit para aplicação teranóstica no câncer.

A partir do profundo conhecimento sobre como o sistema se comporta e das melhores condições para se obter as MP/PTX, a etapa seguinte foi desenvolver um kit estável e robusto para aplicação simples e segura *in vivo.* Dessa maneira, esse segundo capítulo descreve o desenvolvimento desse kit e sua avaliação físico-química e biológica.

3. Capítulo 3: Encapsulação de paclitaxel em nanomicelas poliméricas aumenta a atividade antitumoral e previne neuropatia periférica.

Uma vez que foi obtido um sistema adequado para aplicação *in vivo* de forma simples e segura, partiu-se para a avaliação pré-clínica dessa formulação desenvolvida. Sendo assim, o capítulo três aborda a avaliação da efetividade antitumoral desse sistema, assim como a avaliação quanto a toxicidade das MP/PTX.

CAPÍTULO 1 – Efeitos físicos e biológicos da encapsulação do paclitaxel em micelas poliméricas de diestearoil fosfatidiletanolaina-polietilenoglicol.

Artigo publicado: Oda, C.M.R. et al. Physical and biological effects of paclitaxelencapsulation on disteraroylphosphatidylethanolamine-polyethyleneglycol polymeric micelles. **Colloids and Surfaces B: Biointerfaces.** v. 188 (2020)

CAPÍTULO 1

Physical and biological effects of paclitaxel encapsulation on disteraroylphosphatidylethanolamine-polyethyleneglycol polymeric micelles.

Caroline Mari Ramos Oda, Antônio Augusto Malfatti-Gasperini, Angelo Malachias, Gwenaelle Pound-Lana, Vanessa Carla Furtado Mosqueira, Renata Salgado Fernandes, Mônica Cristina de Oliveira, André Luis Branco de Barros, Elaine Amaral Leite

Figure 1.1 Graphical Table of Contents.

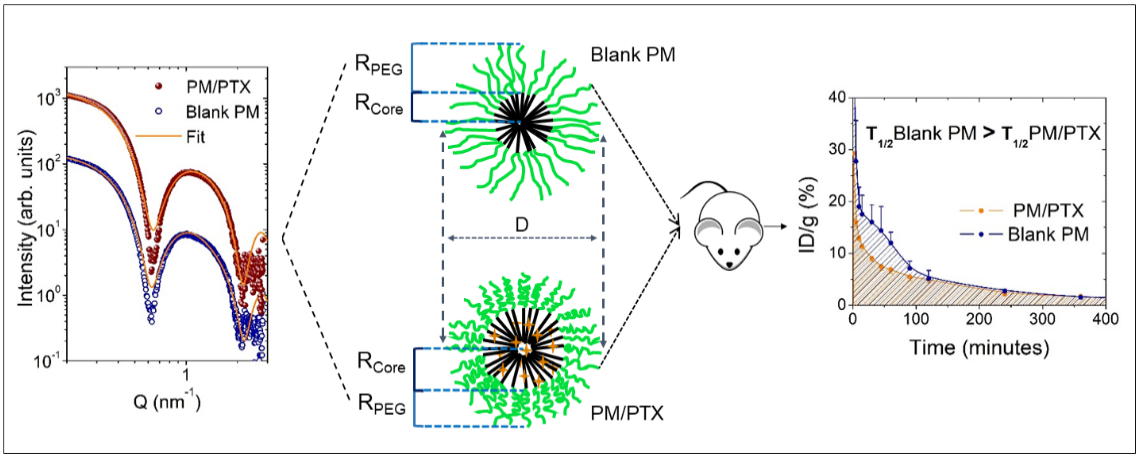

CAPÍTULO 1

Abstract

Simple size observations of 1,2-distearoyl-sn-glycero-3-phosphoethanolamine-N-[methoxy(polyethyleneglycol)-2000] (DSPE-mPEG2000) polymeric micelles (PM) with different compositions including or not paclitaxel (PTX) are unable to evidence changes on the nanocarrier structure. In such system a detailed characterization using highly sensitive techniques such as X-ray scattering and asymmetric flow field flow fractionation coupled to multi-angle laser light scattering and dynamic light scattering (AF4-MALS-DLS) is mandatory to observe effects that take place by the addition of PTX and/or more lipid-polymer at PM, leading to complex changes on the structure of micelles, as well as in their supramolecular organization. SAXS and AF4-MALS-DLS suggested that PM can be found in the medium separately and highly organized, forming clusters of PM in the latter case. SAXS fitted parameters showed that adding the drug does not change the average PM size since the increase in core radius is compensated by the decrease in shell radius. SAXS observations indicate that PEG conformation takes place, changing from brush to mushroom depending on the PM composition. These findings directly reflect in *in vivo* studies of blood clearance that showed a longer circulation time of blank PM when compared to PM containing PTX.

Keywords: polymeric micelles; paclitaxel; DSPE-PEG; SAXS analysis; cancer.

1 Introduction

Polymeric micelles (PM) are promising nanometric structures for poorly water-soluble drug delivery (MOHAMED et al., 2014). They have shown excellent stability and good effectiveness to anticancer drugs delivery at tumor site-specific (CHO et al., 2015). These nanostructures are formed by the self-assembly of amphiphilic block copolymers in an aqueous medium. Hydrophilic blocks form an outer shell interfacing water while hydrophobic blocks are segregated to the inner core, forming a densely packed region. Such arrangement allows the solubilization of hydrophobic molecules (CAGEL et al., 2017; YOKOYAMA, 2010).

The combination of poly(ethylene glycol) (PEG) and phospholipid, such as 1,2-distearoyl-sn-glycero-3-phosphoethanolamine (DSPE) is a prominent strategy for the development of PM with low toxicity, biodegradability, and biocompatibility (KOLATE et al., 2014; SAWANT; TORCHILIN, 2010). The presence of the phospholipid containing two fatty acid chains can increase the number of hydrophobic interactions in the core, promoting higher stability of this system (TORCHILIN, 2006).

Our research group recently developed PM composed by 1,2-distearoyl-sn-glycero-3-phosphoethanolamine-N-[methoxy(polyethyleneglycol)-2000] (DSPE-PEG_{2000}) carrier to paclitaxel (PTX) (ODA et al., 2018). This system was developed as simple and stable kit formulation that presented promising features as a platform to tumor delivery of PTX and/or imaging agent via enhanced permeability and retention (EPR) effect (ODA et al., 2018). Worth mentioning that this formulation represent an alternative to the most used and highly toxic PTX formulation Cremophor EL-based one. Investigating alternatives formulations of PTX is relevant since it is an effective antineoplastic agent and covers a broad spectrum of solid tumors, including ovarian and breast cancer (BERNABEU et al., 2017). PTX triggers the apoptotic cell death by stabilizing the microtubules and impairing the normal function of the mitotic spindle (JORDAN; WILSON, 2004; WANG et al., 2015). It is well established that the length of polymer blocks, the hydrophobicity of hydrophobic blocks as well as the interactions between the hydrophilic blocks in swollen corona can affect the shape and size of micelles (AKIBA et al., 2012). Thus, proper knowledge of micelles internal structure is pivotal information to guarantee a suitable preparation of a potential new drug delivery system.

Small-angle X-ray scattering (SAXS) is a well-adapted technique to evaluate the structure and the interactions of colloidal materials. With a proper data modeling and fitting, SAXS gives information about size, shape, and core size of PM (SANADA et al., 2013; SATO et al., 2007), which permits to elucidate the mechanisms of interaction/complexation of nanocarriers-drugs

systems and correlate them with the preparation process. Besides, the packing of the micellar nanostructure can be inferred by this technique [16].

Previous studies have shown that the PEG domains of PM close to the core/shell interface have enough hydrophobicity to tolerate the presence of hydrophobic compounds (SANADA et al., 2013). In addition, the PEG surface density of PM characterized using SAXS and field flow fractionation with multi-angle light scattering has been found to influence the *in vivo* behavior of the micelles (SHIRAISHI et al., 2015). In the present study, we have used complementary scattering techniques (SAXS and AF4-MALS-DLS) to evaluate the structural characteristics of the PM containing PTX (PM-PTX) and their correlation with *in vivo* behavior.

2 Experimental

2.1 Material

1,2-distearoyl-sn-glycero-3-phosphoethanolamine-N-[methoxy(polyethyleneglycol)-2000] (DSPE-mPEG2000) was acquired from Lipod GmbH (Ludwigshafen, Germany). Diethylenetriaminepentaacetic acid-functionalized 1,2-distearoyl-sn-glycero-3-phosphoethanolamine-N-[methoxy(polyethyleneglycol)-2000] (DSPE-PEG_{2000}-DTPA) was synthesized in our laboratory. PTX was supplied by Quiral Química do Brasil S/A (Juiz de Fora, Brazil) with a purity greater than 97%. The water was purified using Milli-Q® equipment (Millipore, USA). Technetium–99m was obtained from an alumina-based $^{99}Mo/^{99m}Tc$ generator from the Institute of Energy and Nuclear Research (IPEN, São Paulo, Brazil). All other reagents were acquired from Sigma-Aldrich Co (Missouri, USA). The female BALB/c mice (6-8-week-old, 20 ± 2g) were obtained from CEBIO-UFMG (Belo Horizonte, Brazil). Animal study was approved by the local Ethics Committee for Animal Experiments (CEUA/UFMG) under the protocol number 205/2013.

2.2 Preparation of PM/PTX

PM/PTX were prepared using the method described previously (ODA et al., 2017a). Briefly, chloroformic solutions in equivalent quantities of 5, 10 or 15 mmol/L of DSPE-$mPEG_{2000}$ and PTX (0.6 mg/mL) were transferred to a round bottom flask and the solvent was completely removed by evaporation under reduced pressure until a thin lipid film was obtained. The resulting film was hydrated with saline 0.9% (w/v), in a water bath at 40 °C for 5 min,

followed by vortexing at 1000 rpm for 3 min. Lastly, the preparation was filtered on a 0.22 μm pore size polycarbonate membranes in order to remove non-encapsulated PTX.

2.3 Syncrotron Small-Angle X-ray Scattering (SAXS)

Structural information such as the shape and size of micelles was obtained via SAXS analysis. The experiments were performed at the SAXS-1 beamline at the Brazilian Synchrotron (LNLS, Campinas, Brazil) in two different configurations. For freeze-dried samples, the X-ray energy used was 8.3 keV (λ = 0.1488 nm) and a Pilatus 300k detector was positioned 1.0 m from the sample, providing a reciprocal space vector range (Q) spamming from 0.15 nm^{-1} to 2.5 nm^{-1}. These samples were encapsulated by two polyimide films (Kapton®) and analyzed at 25 °C in transmission mode. For the liquid samples, the X-ray energy used was 8 keV (λ = 0.155 nm) with the Pilatus 300k detector positioned 1.5 m from sample, providing a Q range from 0.05 to 3 nm^{-1}. The liquid samples were placed in a temperature-controlled cell constituted by two mica windows separated by 1 mm, and the experiment performed in vacuum.

For all SAXS data, the 2D images obtained were normalized by incoming beam intensity and sample's absorption. For liquid samples, the background scattering contributions from sample chamber (mica) and solvent (saline) were subtracted and converted to intensity profiles I(Q) as a function of the scattering vector Q using the Fit2D software.

Evaluation of the core surface PEG clouding

The surface packing of the PEG chains at the interface between the core and the shell region of micelles can be evaluated by the parameter σ consering the core radius (R_{core}), shell radius (R_{PEG}), and aggregation number (N_{agg}) according to the equation 1:

Equation 1: $$\sigma = \frac{N_{agg}\,\pi\,{R_{PEG}}^2}{4\,\pi\,(R_{Core}+R_{PEG})^2}$$

This means that the higher σ-values, higher packing on core surfaces.

The conformation of PEG chains was also determined from the reduced tethering density ($\tilde{\sigma}$-value), by using the equation 2 (CHEN et al., 2004; SHIRAISHI et al., 2015)

Equation 2 $$\tilde{\sigma} = \sigma\pi R_{PEG}^2$$

By this $\tilde{\sigma}$-value is possible to estimate the interacting regime of the tethered PEG chains as non and weak, cross-over or strongly stretched. This classification follows a score directly related to the increase in $\tilde{\sigma}$-value.

2.4 AF4-MALS-DLS

PM fractionation was carried out on a Postnova analytics (Landberg, Germany) AF2000 MT AF4 system comprising two PN1130 HPLC pumps (tip and focus pumps) and an AF2000 module (crossflow pump), PN5300 auto sampler thermostated at 25°C, PN4020 channel oven set at 25°C, a separation channel fitted with a Postnova AF2000 MT Series Nova RC AQU 5 kDa cut-off regenerated cellulose membrane and a 350 µm spacer. The channel eluent was characterized by a set of three detectors in series, a PN3211 UV detector set for detection of absorbance at 254 nm, a PN3621 multi-angle laser light scattering (MALS) detector (12°-164°, 20 operating angles) with a 532 nm laser at 35°C and a Malvern PN3702 Zetasizer NanoZS (Malvern Instruments, UK) DLS detector with a 633 nm laser, a Hellma Analytics Suprasil® 3 mm light path quartz flow cell, for 173° back scattered light detection recorded at 5 s time intervals, at 25°C. The carrier liquid was 10 mmol/L NaCl in ultrapure water filtered through a 0.1 µm pore size PTFE membrane filter (Millipore). The detector flow rate was constant at 0.5 mL/min. Undiluted formulations (20 µL) were injected with an injection flow of 0.2 mL/min and an initial crossflow of 2.0 mL/min and injection and transition times of 1 min each. The crossflow rate was maintained at 2.0 mL/min for another 3 min and it was set to decrease exponentially from 2.0 to 0.05 mL/min over a period of 15 min, kept at 0.05 mL/min for 15 min followed by 12 min at 0 mL/min to guarantee complete sample elution. Particle diameter of gyration (D_g) were determined in flow mode using the angular variation of the scattered light intensity at angles 12°-164° recorded on the MALS detector normalized with a 60 nm (D_h) monodisperse polystyrene latex, using the Postnova AF2000 software calculation for spherical shape model. The hydrodynamic diameters (D_h) in flow mode were determined using the Malvern Zetasizer 7.11 data analysis software, as described above.

2.5 PTX content

PTX encapsulated in the formulation was evaluated by high performance liquid chromatography (HPLC) using a previously validated analytical method (BARBOSA et al., 2015). The chromatographic conditions were: eluent system consisting of acetonitrile: water, in the ratio of 55:45 (v / v); Lichrospher®, C18, 5 µm, 4 mm x 25 cm reverse phase column

(Merck Millipore, Darmstadt, Germany); flow rate of 1.2 mL/min; temperature of 25 °C; volume of injection equal to 10 μL. The equipment used was an Agilent HPLC, model Agilent 1260 Infinity Quaternary LC (Germany).

2.6 Blood clearance

PM, containing PTX (0.6mg/mL) or not, prepared from a mixture of DSPE-mPEG$_{2000}$ and DSPE-PEG$_{2000}$-DTPA 99:1 (w/w), respectively (10 mmol/L final concentration) were radiolabeled with ^{99m}Tc (^{99m}Tc-DTPA-PM) (ODA et al., 2017a). An aliquot of 3.7MBq of ^{99m}Tc-DTPA-PM (100 μL per 20 g of animal) was injected through the tail vein of healthy mice (n = 5) and blood samples were collected at 1, 5, 10, 15, 30, 45, 60, 120, 240, 360, 480 and 1440 min after administration. A small incision was made in the distal tail to facilitate rapid and reliable blood collection. Each sample was weighed, and the associated radioactivity was determined in an automatic scintillation apparatus. A standard dosage containing the same injected amount was counted simultaneously in a separate tube, which was defined as 100% radioactivity. A blood decay curve was plotted using the percentage of injected dose per gram (%ID/g) of blood as a function of time. Data were expressed as mean ± standard deviation (SD). Normality and homogeneity of variance was evaluated by the D'Agostino and Pearson, and Bartlett's tests, respectively. Data were tested using unpaired t test (GraphPadPrism version 6.00). The 95% confidence interval was adopted and differences were considered significant when the p value was lower or equal to 0.05 ($p \leq 0.05$).

3 Results and discussion

3.1 Syncrotron Small-Angle X-ray Scattering

Small-angle X-ray scattering is an extremely sensitive tool to study the structural organization of nanocarriers and to elucidate the different interactions among the constituents (SANADA et al., 2013; SATO et al., 2007). In this study, PM were analyzed in two ranges of X-ray scattering angles, including the q range between 0.05 nm^{-1} and 2.0 nm^{-1} as well as 0.15 nm^{-1} and 4.0 nm^{-1}. These analyses allow us to correlate information about micelle organization itself and its behavior in an aqueous medium.

First of all, the influence of the concentration (5, 10 and 15 mmol/L) of the structural component (DSPE-PEG$_{2000}$), either in the absence or in the presence of PTX (at 0.6 mg/mL) was evaluated. The scattering patterns are shown in Figure 1.2A.

Figure 1.2 **Evaluation of supramolecular organization of polymeric micelles containing PTX.**

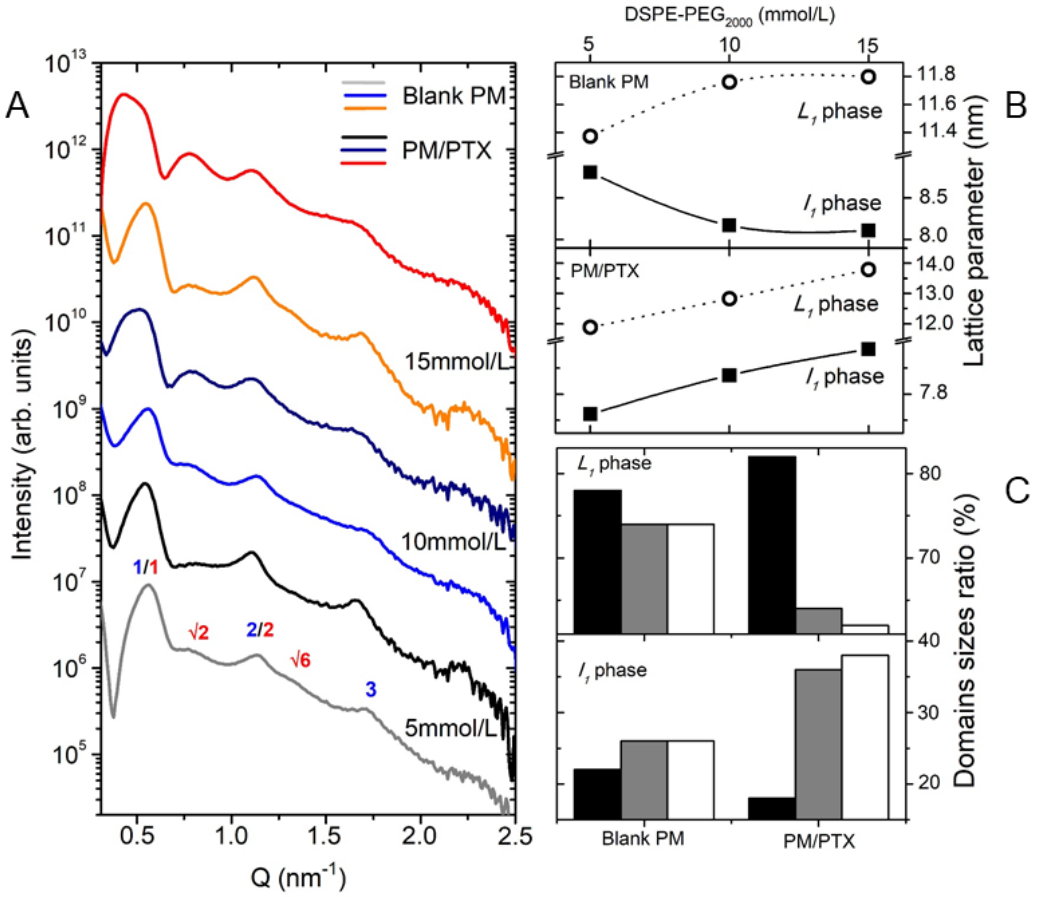

(A) SAXS patterns of blank freeze-dried PM at 5 (grey), 10 (light blue) and 15 (yellow) mmol/L of DSPE-PEG_{2000}, and respective formulations containing PTX, represented by black, dark blue and red colors, respectively. (B) Observed lattice parameter for the L_1 (○) and I_1 (■) phases of blank PM (upper panel) and PM containing PTX (lower panel). (C) Domains sizes fraction between L_1 phase (upper panel) and I_1 phase (lower panel) with and without the presence of PTX at 5 mmol/L (black), 10 mmol/L (dark grey) and 15 mmol/L (white) of DSPE-PEG_{2000}.

The coexistence of two domains with lamellar and non-lamellar supramolecular organization was clearly observed in all samples. The first order type was identified at Q ≈ 0.55, 1.10 and 1.65 nm^{-1} with Bragg indexes of 1, 2, 3, indicating the existence of a lamellar phase (L_1) (ALEXANDRIDIS; OLSSON; LINDMAN, 1998; MONTEIRO et al., 2016). The second sequence of peaks verified at Q ≈ 0.55, 0.78, 1.10 and 1.35 nm^{-1}, corresponding to Bragg reflection position ratios close to 1, √2, √4, √6, characteristic of micellar cubic phase (I_1). The low intensity of the reflection at Q = 1.35 nm^{-1} and the inability to discern higher order reflections from this space group are also characteristics of structures with cubic organization, more specifically, from the centrosymmetric *Im3m* space group (ALEXANDRIDIS; OLSSON;

LINDMAN, 1998). The coexistence of the two domains could be attributed to the ratio among water and components of the system. In general, an excess of water is able to favor a lamellar organization (L_1). On the other hand, when the ratio between water and PM decreases, the cubic phase (I_1) formation is more pronounced than in other phases (ALEXANDRIDIS; OLSSON; LINDMAN, 1998; PERSSON; EDLUND; LINDBLOM, 2003).

The peaks were fit independently, and the average domain size and the lattice parameter were extracted from the peaks at Q = 0.55 and 1.10 nm^{-1} for L_1 domain and Q equal 0.78 nm^{-1} for the I_1 domain; their values are shown in Figure 1.2B. All domain sizes were evaluated using the width (ΔQ) of the first Bragg peak and the relation $L = 2\pi/(\Delta Q)$. The L_1 domains were larger than I_1 for all evaluated samples. For blank PM, the ratio between the domain sizes was around 3:1 (L_1:I_1), however, the presence of PTX leads an increase of I_1 domain size at 10 and 15 mmol/L, resulting in a ratio approximately of 1.7:1 (Figure 1.2C). Concerning the lattice spacing, the SAXS data clearly showed that the lamellar lattice spacing is directly proportional to the DSPE-PEG_{2000} concentration and the presence of PTX. In contrast, the lattice parameter of I_1 phase is considerably reduced for the DSPE-PEG_{2000}, at 15 mmol/L, in the absence of PTX. It is worth to underscore that the PM containing PTX formulations always present lattice parameter of lamellar phase greater than blank PM, while the inverse occurs in the cubic phase. These results suggest that the increase of DSPE-PEG_{2000} concentration and the presence of PTX significantly contribute to a greater aggregation of the system.

Figure 1.3 Structural analysis of polymeric micelles containing PTX.

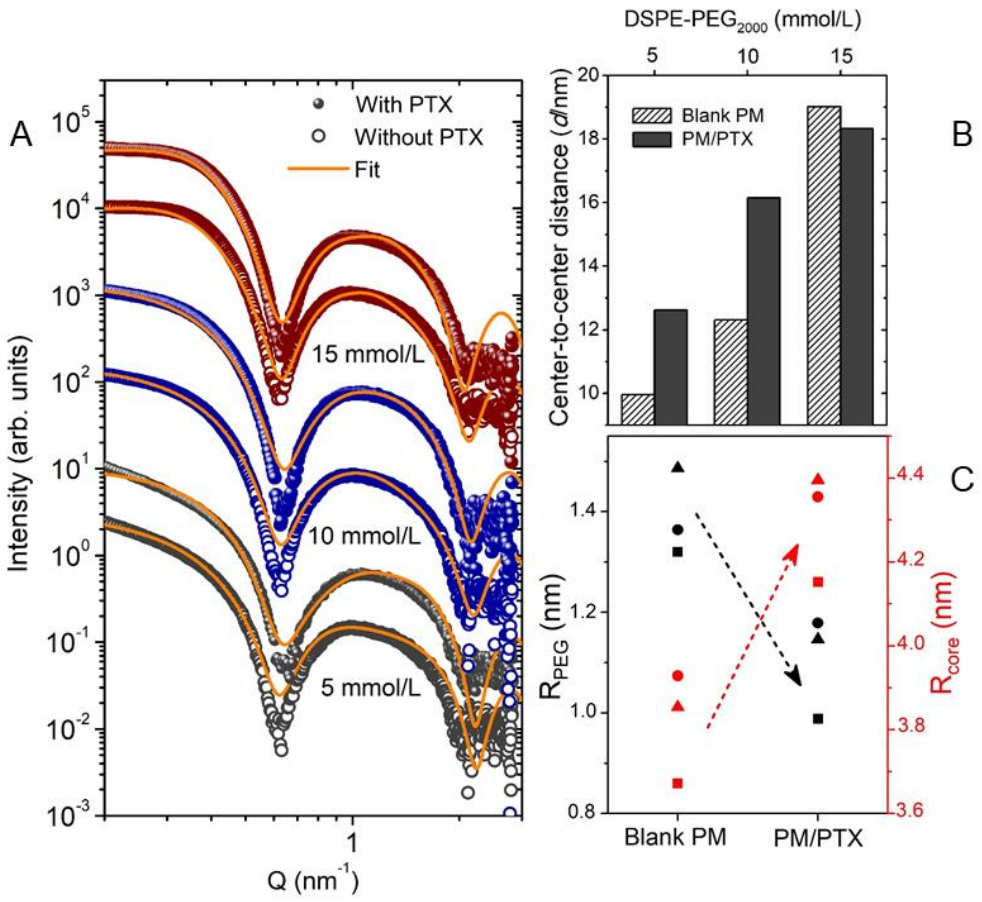

(A) SAXS patterns of PM dispersed in saline solution containing PTX (●) and blank (○) at 5 (grey), 10 (blue) and 15 (red) mmol/L of DSPE-PEG$_{2000}$ with respective curve fitting (orange lines). (B) Effect of DSPE-PEG$_{2000}$ concentration in solution on the mean center-to-center distance between micelles in system containing PTX or not. (C) Effect of PTX presence in shell radius (R_{PEG}, black) and core radius (R_{core}, red) of PM at 5 (■), 10 (●) and 15 (▲) mmol/L of DSPE-PEG$_{2000}$.

The SAXS patterns shown in Figure 2-A, which correspond to a saline solution of PM, describe nanoparticles with spheroidal shape and core-shell structure, containing a hydrophobic core and hydrophilic polymer chains, compatible with the scattering profile of the structure of the polymeric micelles. While the position of the local minima along the q axis is deterministic to retrieve the correct particle shape (spherical micelles), the relative intensity of successive maxima (y-axis) depends on the distribution of electron density within the studied objects and points out in this case for a core-shell structure (DISCH et al., 2012). It is important to note that these profiles converge to a plateau at very low Q-values (lower as 0.2 nm^{-1}), suggesting that DSPE-PEG$_{2000}$ formulations, with drug or not, actually form isolated micelles (AKIBA et al., 2010). A minimum in the scattering profile, located between Q = 0.6 and 0.7 nm^{-1} can also be observed for all curves, which can be correlated with well-defined nanostructure with a

narrow distribution range (AKIBA et al., 2010; SANADA et al., 2013). The scattering vector Q which corresponds to the position of the first minimum in the intensity I (Q) provides a quick estimation of the micelle diameter (*D*) using $D=2\pi/Q$ (SATO et al., 2007). *D* values estimated for our samples were all close to 10 nm, and are considered here as a rough guide to the aggregation number used in our model (Table 1.1).

SAXS patterns were fitted to the theoretical curves (Figure 1.3A, solid orange lines) in the range of $q < 2.5\ nm^{-1}$ using equation 2S of supplementary material, where the model used to fit is described briefly.

The distance center-to-center (*d)* was calculated by "$d=2\ R_{total}\ c$", where R_{total} was given by *D/2*. The parameter *c* comes from the model of Sanada et al., (2013) and Akiba et al., 2010, and accounts for the average clustering of neighbor micelles. Physical contact of micelles is achieved at c = 1, while we obtained values for our fits of approximately c ~ 1.5, meaning that the center-to-center distance of micelles is of the order of $3R_{total}$. As can be observed in Figure 2-B, *d* value increases with increasing of the DSPE-PEG_{2000} concentration and in the presence of PTX. Noteworthy is that at 5 and 10 mmol/L of DSPE-PEG_{2000}, *d* for PM/PTX is approximately 3 and 4 nm greater than those found for the respective blank micelle, while at high DSPE-PEG_{2000} concentration the *d* values in the formulations PM/PTX and blank PM are almost the same. These data are in agreement with the lattice spacing observed by analyses on freeze-dried samples.

N_{agg} parameter analysis showed that the addition of DSPE-PEG_{2000} in the system led to an increase in N_{agg} (Table 1.1), which was more expressive at 15 mmol/L for both systems. Furthermore, the presence of PTX also influenced the DSPE-PEG_{2000} monomers aggregation inducing an increase of N_{agg} equal to 15% compared to 7% for blank when the concentration was 15 mmol/L. However, this relation did not affect the *D* of nanostructures. This can be explained by the conformation of the PEG on the micelles shell, where α value closer to 1 represents stretched PEG chains (Table 1.1). In both systems, blank and PTX micelles, α value decreases with increasing of DSPE-PEG_{2000} concentration and in the presence of PTX.

It is known that PEG chains can acquire two main conformations depending on grafting density: mushroom or brush. In the first case, due to a low density of PEG, the chains are not fully extended, resulting in a thin PEG layer. The brush conformation is dictated by increased grafting densities and the chains are more stretched/extended (JOKERST et al., 2012). According to Akiba and coworkers (2010), the formation of PM from asymmetric block

copolymers can be understood by packing parameter theory considering the volumetric balance between the hydrophilic and hydrophobic chains. This equilibrium involves the elastic deformation of the micellar core, the osmotic energy of the shell chains, and the interfacial tension between the core and the solvent in which the micelles are dispersed (AKIBA et al., 2010). Thus, if the free osmotic energy of the PEG chains is high, they will tend a brush conformation. It is well-established that N_{agg} has an inverse relationship with the amount of free energy, which will be lower when the number of chemical units in the core is higher than in the shell (AKIBA et al., 2010; ISRAELACHVILI; MITCHELL, JOHN; NINHAM, 1976). In our case, one of the most important effect which should be taken into account is the hydrophobic core hydration caused by the curvature of the micelle surface, close to the lipid head position. The hydration level depends on the N_{agg} (since it determines the micelle diameter) and on the presence or not of PTX molecules. By analyzing data from Table 1.1, we can infer that the increase of N_{agg} and the reduction of α-values decrease the free osmotic energy and the PEG chains interactions, which favor the mushroom conformation. In addition, the presence of PTX represents an increase of chemical units in the micelles core, leading to a lower PEG chains interaction, and consequently, the brush conformation is unfavorable.

Recent studies have reported that knowing about the transition between the two conformations can give additional information about the surface packing of the PEG chains at the interface between the core and the shell region (SHIRAISHI et al., 2015). Thus, in order to clarify the tethered PEG chains on micelles core surface, the obtained structural characteristics were applied to an index, known as σ-value or core surface PEG clouding. This σ-value is understood as a crowding of tethered chain on a flat surface. The blank PM showed higher σ-values compared with PM/PTX, suggesting that there is a higher density on core surfaces and the PEG chains are closer to each other in the blank micelles compared to PM/PTX. On the other hand, the $\tilde{\sigma}$-value (Table 1.1) allows estimating the tethered chains behavior as non and weak interacting regime ($\tilde{\sigma}$ < 3.7-3.8), cross-over regime (3.7-3.8 < $\tilde{\sigma}$ < 6-12) or strongly stretched regime ($\tilde{\sigma}$ > 6-12). The data revealed $\tilde{\sigma}$-values higher than 12 for blank PM indicating a strongly stretched regime. Meanwhile, PM/PTX showed $\tilde{\sigma}$-values significantly lower, equal to 3.8, 6.6 and 6.7 for DSPE-PEG_{2000} at 5, 10 and 15 mmol/L, respectively, suggesting that PTX presence in PM core, leads to “shrinkage” of the PEG chains. To demonstrate the events observed by this technique a scheme was proposed (Figure 1S).

Figure 1S. Scheme representing micellar structure changing core and shell radiuses, without changing size after encapsulating PTX (1), and detailed PEG conformation changing from the brush (α = 1) to mushroom (α < 1) when PTX is present in the core.

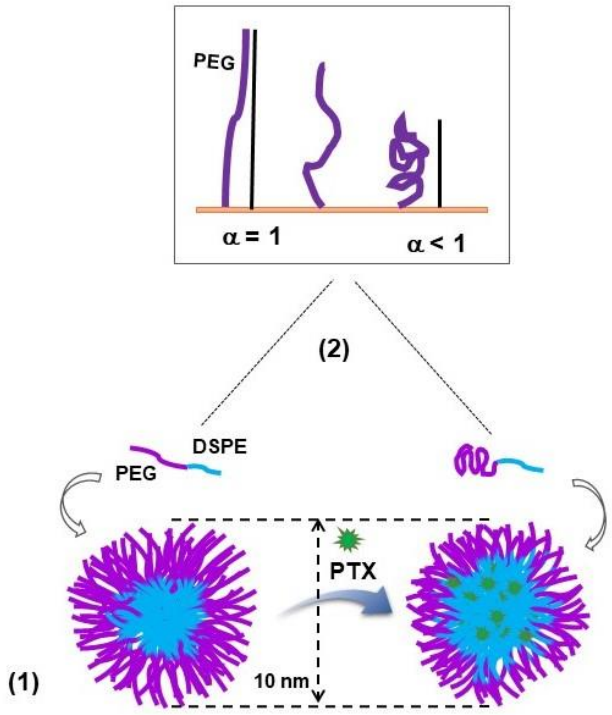

Table 1.1 Properties of PM and PM/PTX obtained by SAXS analysis.

DSPE-PEG$_{2000}$ (mmol/L)	PTX (mg/mL)	N_{agg}	α	σ	$\tilde{\sigma}$
5	-	132	0.99	2.3	12.6
	0.6	131	0.60	1.2	3.7
10	-	134	0.85	2.2	13.0
	0.6	133	0.56	1.5	6.6
15	-	141	0.83	2.7	19.0
	0.6	151	0.51	1.6	6.7

We also evaluated the influence of the DSPE-PEG$_{2000}$ concentration on the shell (R_{PEG}) and core (R_{core}) radius. As can be observed in Figure 1.3C, the addition of drug leads to an increase in the micelles core and, as previously suggested, a reduction in R_{PEG}, reflecting in an unchanged micelles size.

Since the presence of PTX strongly influenced the structural organization of PM, we decided to keep the DSPE-PEG$_{2000}$ concentration at 10 mmol/L but change the PTX concentration (0.2, 0.6 and 1.0 mg/mL). SAXS data were again fitted, and the same parameters were evaluated. A proportional variation (reduction or increase depending on the parameter) was observed with increasing the drug concentration until 0.6 mg/mL (Figure 1.4). At 0.2 mg/mL, α and $\tilde{\sigma}$ reduced from 0.85 to 0.78 and from 13.0 to 10.0, respectively. Increasing to 0.6 mg/mL, these parameters reduced to 0.56 (α) and 6.6 ($\tilde{\sigma}$). These data are in agreement with previous data when compared with blank PM, which showed shrinkage of the PEG chains, reflected by α and σ values reduction when PTX was added (Figure 3-A). However, a data inversion was observed at the highest drug concentration. The analysis of the core behavior showed a R_{core} diminished after increasing of PTX to 1.0 mg/mL (Figure 3-B). This data suggests a micelle system destabilization and releasing of the drug, which allowed us to suppose that PM is able to carry a maximum of 0.6 mg/mL of PTX. The similar profile was observed when the DSPE-PEG$_{2000}$ concentrations were 5 and 15 mmol/L (data not shown).

Figure 1.4 **Influence of PTX concentration in (A) α-value *(*green) and $\tilde{\sigma}$-values (red) and (B) in R_{PEG} (yellow) and R_{core} (blue) of PM.**

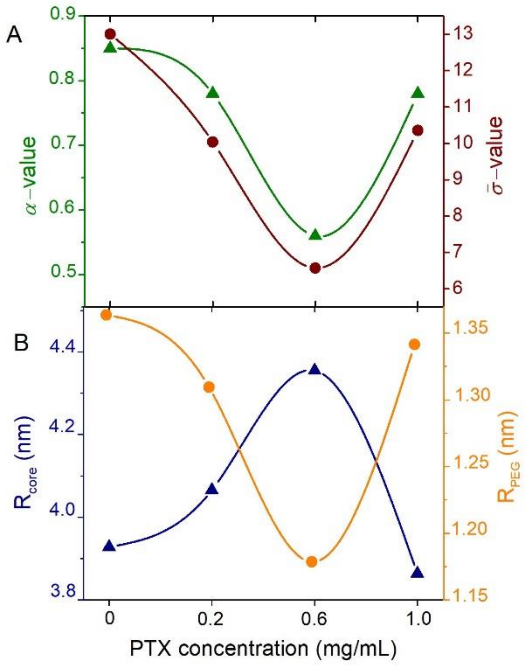

3.2 Fractionation and size characterization by AF4-MALS-DLS

AF4 separates nanoparticles according to their diffusion coefficient such that the retention time is proportional to the hydrodynamic diameter of the particles (MONTEIRO et al., 2018a). Our system is equipped with DLS and MALS to determine D_g and D_h of the fractions as they elute (Figure 1.5C). AF4 analysis was able to separate two populations of submicron-sized particles in all samples evaluated (Figure 1.5 and Table 1.2). One major peak eluted at short retention times, corresponding to small nanoparticles (5 to 10 min, peak 1, average D_h = 16.7 ± 2.0 nm, highly monodisperse) and a second peak at longer retention times (10 to 25 min, peak 2, average D_h = 132.0 ± 36.7 nm covering a range of D_h from approx. 160 nm to 260 nm) were detected, indicating the coexistence in the sample of distinct nanostructures (Figure 1.5). The low contribution of peak 2 to the UV signal (Figure 1.5A), although significant in the light scattering signal (Figure 1.5B) indicates the presence of few particles with greater size. This experiment emphasizes the strength of AF4 coupled to DLS rather than performing batch measurements, where the larger particles are overestimated. More specifically, peak 1 represents a contribution of 87% to 97% of the total UV signal, depending on the DSPE-PEG_{2000} concentration (Table 1.2). It is important to mention that the UV signal (254 nm) is used to determine the relative concentration of each fraction with respect to the total sample mass or volume. At 254 nm the UV signal is mostly a measure of the turbidity of the eluent (some of the incident light does not reach the detector because of scattering), although a small contribution of specific absorption may occur depending on the composition of the sample. Hence, an increase in the UV signal intensity with increasing DSPE-PEG_{2000} concentration and in the presence of PTX was clearly observed. We suspect that the gyration diameters determined by MALS for peak 1 (close to 40 nm) were not accurate. This may be due to angle normalization error (normalization of the MALS detector to correlate the angular variation of the scattered intensity with D_g was done with a sample of intermediate D_g of 46 nm, which may have introduced an error for particles of significantly different sizes) or to the lower size limit for this technique generally accepted as $1/20^{th}$ of the laser wavelength (here 532/20 = 27 nm), whereas other techniques suggest that the size of the main population in this sample should be less than 20 nm.

While the diameters determined for peak 1 are consistent with well-defined DSPE-PEG_{2000} micelles, this is not the case for peak 2. By SAXS, the core radius was approximately 4 nm. As the chain theoretical length of fully stretched PEG_{2000} is 12.7 nm (corresponding to 45 units of ethylene glycol of 0.28 nm each), the maximum diameter of the blank micelles

would be about 33.4 nm. On the other hand, the PEG_{2000} chain size in an aqueous medium, according to Flory radius, is 2.8 nm (MA et al., 2014), thus, our MP could have a hydrodynamic diameter as low as 13.6 nm, close to the D_h values determined for the main population (peak 1). Therefore, the large particle population identified by AF4-MALS-DLS can be attributed to clusters of micelles. This finding corroborates our SAXS data, which suggested that the increase in DSPE-PEG_{2000} concentration and the presence of PTX contributed to a greater aggregation of the system.

Table 1.2 Micelle sizes by dynamic light scattering coupled to AF4.

DSPE-PE G_{2000} (mmol/L)	PTX (mg/mL)	Average D_h (nm)		Contribution of AF4 peak 1 to the total UV signal (%)
		Peak 1	Peak 2	
5	-	19.4 ± 1.0	128 ± 1.0	89
	0.6	15.2 ± 0.3	96 ± 13	87
10	-	15.1 ± 0.5	84 ± 6	93
	0.6	14.5 ± 0.3	144 ± 21	>97
15	-	17.7 ± 1.3	164 ± 8	89
	0.6	18.3 ± 1.7	176 ± 18	97

Figure 1.5 Asymmetric flow field-flow fractionation results.

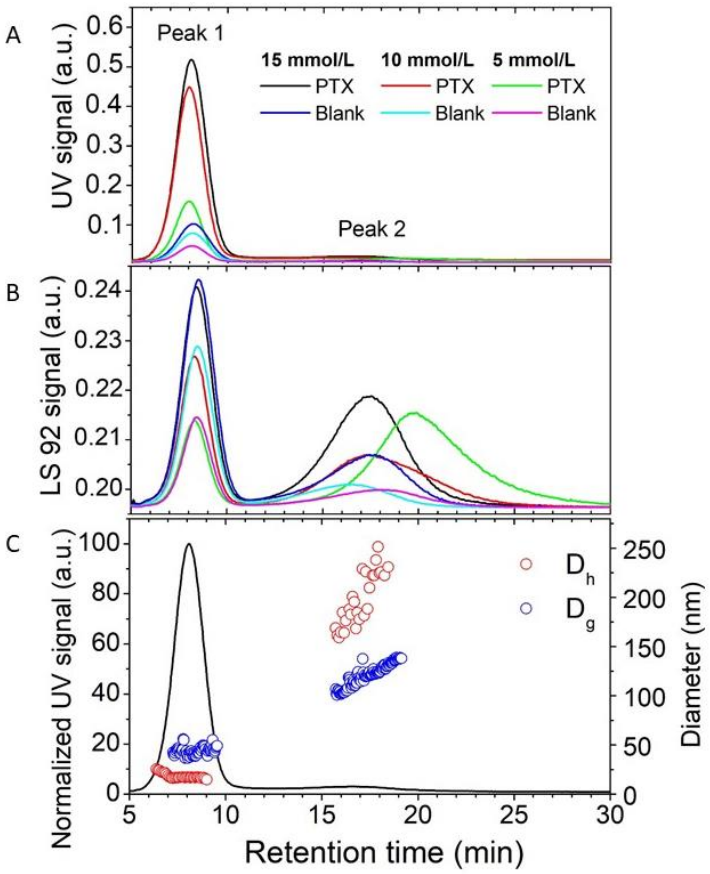

Comparison of the fractograms consisting of the UV signal (A) and 92º angle light scattering signal (B) of all blank and PTX loaded PM at concentrations of 5, 10 and 15 mmol/L of DSPE-PEG_{2000}, as indicated in the figure legend inserts. (C) Fractogram of PTX loaded PM at 15 mM of DSPE-PEG_{2000} illustrating the hydrodynamic radius (R_h) and gyration radius (R_g) determination within each sample peak.

3.3 Blood clearance

PEG is frequently used to prolong the blood circulation time of drug nanocarriers (KIM et al., 2008; MONTEIRO et al., 2018b). Since the presence of PTX changed the PEG conformation on the surface of the PM, as indicated by our SAXS data, we evaluated the influence of this change on the blood clearance of the PM after intravenous injection in BALB/c mice. First, PM were radiolabeled with ^{99m}Tc and the radiocomplexing exhibited high stability for at least 8 h, allowing its use for *in vivo* application as previously demonstrated [8]. Also, the amount of PTX encapsulated in PM was determined by HPLC, indicating a drug content of 0.68 ± 0.06 mg/mL, which represents a 98.3 ± 5.1% of encapsulation efficiency. The data of %ID/g as a function of time obtained for PM prepared with DSPE-PEG_{2000} (10 mmol/L) with PTX or blank are shown in Figure 5.

Blood clearance of both PM showed biphasic decay with α half-life ($T_{1/2}$) of 34 ± 2 and 40 ± 1 min, and a β $T_{1/2}$ of 421 ± 20 and 223 ± 2 min for blank and PTX loaded PM, respectively. Significant difference was observed between both formulations which P-values for α and β $T_{1/2}$ were 0.032 and 0.0001, respectively. This finding suggests that a small fraction of the micelles may undergo an initial burst-effect upon entering the bloodstream due to osmotic forces, however, the majority of them remained in the circulation (PEARSON; JUETTNER; HONG, 2014). In addition, a higher AUC was detected for blank PM (3139 ± 235 %ID/g min^{-1}) compared to PM/PTX (2317± 81 %ID/g min^{-1}) after 24 hours of administration (P = 0.0108). Since the composition is the same for both formulations, this difference may be due to the PEG conformation. Previous studies do have shown that the conformation of the PEG chains influences the plasma half-life of nanocarriers. The brush conformation has a higher grafting density than the mushroom conformation, promoting the formation of a hydrophilic barrier that sterically prevents the serum protein adsorption and reduces the uptake by the mononuclear phagocytic system, which consequently increases the time circulation (JOKERST et al., 2012; SHIRAISHI et al., 2015). As described before, stretched PEG chains were observed for blank PM, while mushroom conformation was found to PM containing PTX. Thus, these results are compatible with higher circulation time obtained to blank PM compared to PTX loaded PM. Despite the reduction in blood circulation time observed for the drug-loaded micelles, the β $T_{1/2}$ was close to an optimal half-life (2–6 h) to allow adequate accumulation at the targeted site, as previously demonstrated by Oda et al [8].

Figure 1.6 Blood clearance profile of blank PM (blue line and symbol) and PM/PTX (yellow line and symbol) obtained by the injected dose (%) of respective 99mTc-labeled micelles over 24 hours. Data represent thes mean ± standard deviation (n=5).

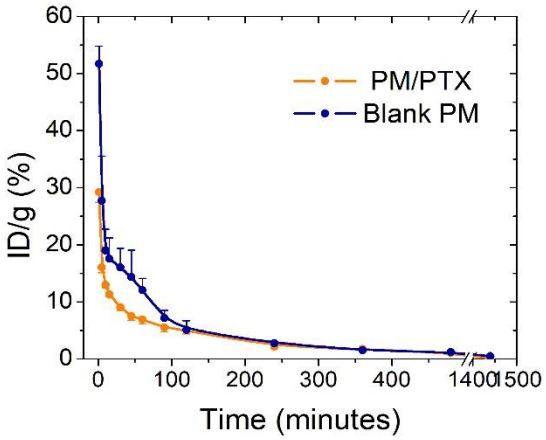

4 Conclusions

PM differing in their composition concerning their DSPE-PEG_{2000} and PTX concentrations showed structural differences that suggest some particularities of this nanocarrier. The presence of PM clusters without or with PTX was observed by SAXS and AF4-MALS-DLS. In addition, SAXS analysis on solution samples indicated an increase in the core radius and shrinkage in PEG chains upon PTX loading, which influenced the *in vivo* behavior. Blood clearance study found longer circulation time for the blank PM compared to PTX loaded PM, however, the last one still presented a half-life recommended for tumor accumulation. Importantly, our data raise the point in which micellar preparations can be affected by the encapsulation of drugs without increasing their external size. Pure size distribution measurements, such as dynamic light scattering would not differentiate this scenario. In our case, PTX might disturb the supramolecular organization of micelles resulting in packing/micelle core differences that affect *in vivo* behavior.

ACKNOWLEDGEMENTS

The authors thank Brazilian Synchrotron Light Laboratory (LNLS), Conselho Nacional de Desenvolvimento Científico e Tecnológico (CNPq,- Brazil), Fundação de Amparo à Pesquisa do Estado de Minas Gerais (FAPEMIG, -Brazil), and Coordenação de Aperfeiçoamento de Pessoal de Nível Superior (CAPES) for their financial support and fellowships.

SUPPORTING INFORMATION

1. SAXS modeling for DSPE-PEG micelles

The SAXS intensity for the different DSPE-PEG micelle systems were simulated and fitted using a model based on the scattering intensity of spherical diblock copolymers micelles proposed in reference Pedersen and Gerstenberg, 1996 (PEDERSEN; GERSTENBERG, 1996). On that model, the block copolymers micelles self-organize to form a sphere-with-brushes conformation, where the sphere is formed by the hydrophobic part of the copolymer and the brushes represent the hydrophilic part. The model used to fit our data was changed since the sphere, in our case, is now a core-shell structure, where the core is composed by the hydrophobic phospholipid (DSPE) plus the PTX molecules (when present) and the shell is

composed by polyethylene glycol. The equation (6) of reference Pedersen and Gerstenberg, 1996, which corresponds to the scattering intensity of the sphere-with-brushes conformation is now rewritten to correspond to the scattering of a core-shell sphere-with-brushes:

$$I_{micelle}(Q) = {N_{agg}}^2 FF_{csh}(Q) + N_{agg} FF_{br}(Q) + N_{agg}(N_{agg} - 1) S_{br-br}(Q) + 2{N_{agg}}^2 S_{csh-br}(Q), \quad \text{Eq. 1}$$

where N_{agg} is the aggregation number of (in our case) DSPE-PEGs molecules forming a micelle, $FF_{csh}(Q)$ $(FF_{br}(Q))$ is the form factor of the core-shell (brush) structures and $S_{br\text{-}br}(Q)$ $(S_{csh\text{-}br}(Q))$ is the brush-brush (core-shell – brush) cross term. The micellar agglomeration is taken into account adding a hard-sphere structure factor $S_{mm}(Q)$ multiplying the scattered intensity of a micelle. Then the total scattered intensity is given by:

$$I_{tot}(Q) = N\, I_{micelle}(Q) S_{mm}(Q), \quad \text{Eq. 2}$$

where N is a normalization factor. The details of the model can be found in references (Pedersen & Gerstenberg, 1996) and SASfit manual (Kohlbrecher & Breßler 2015).

In order to improve model reliability, the total number of variables used to fit the data was decreased using some approximations concerning DSPE and PEG_{2000} sizes and electronic densities.

References

(Pedersen & Gerstenberg, 1996) Pedersen JS; Gerstenberg MC. Scattering Form Factor of Block Copolymer Micelles, *Macromolecules* (1996) **29**:1363-1365.

(Kohlbrecher & Breßler 2015) Kohlbrecher J; Breßler I. SASfit Manual (2015) http://kur.web.psi.ch/sans1/SANSSoft/sasfit.pdf

CAPÍTULO 2

.

CAPÍTULO 2 – Micelas poliméricas contendo paclitaxel funcionalizadas com ácido dietilaminopentacético: kit para aplicação teranóstica no câncer.

Artigo publicado: ODA, C. M. R. et al. Freeze-dried diethylenetriaminepentaacetic acid-functionalized polymeric micelles containing paclitaxel: A kit formulation for theranostic application in cancer. **Journal of Drug Delivery Science and Technology**, v. 46, 2018.

CAPÍTULO 2

Freeze-dried diethylenetriaminepentaacetic acid-functionalized polymeric micelles containing paclitaxel: a kit formulation for theranostic application in cancer.

Caroline Mari Ramos Oda; André Luis Branco de Barros; Renata Salgado Fernandes; Sued Eustáquio Mendes Miranda; Marina Xavier Teixeira; Valbert Nascimento Cardoso; Mônica Cristina Oliveira; Elaine Amaral Leite.

Figura 2.1. Graphical abstract.

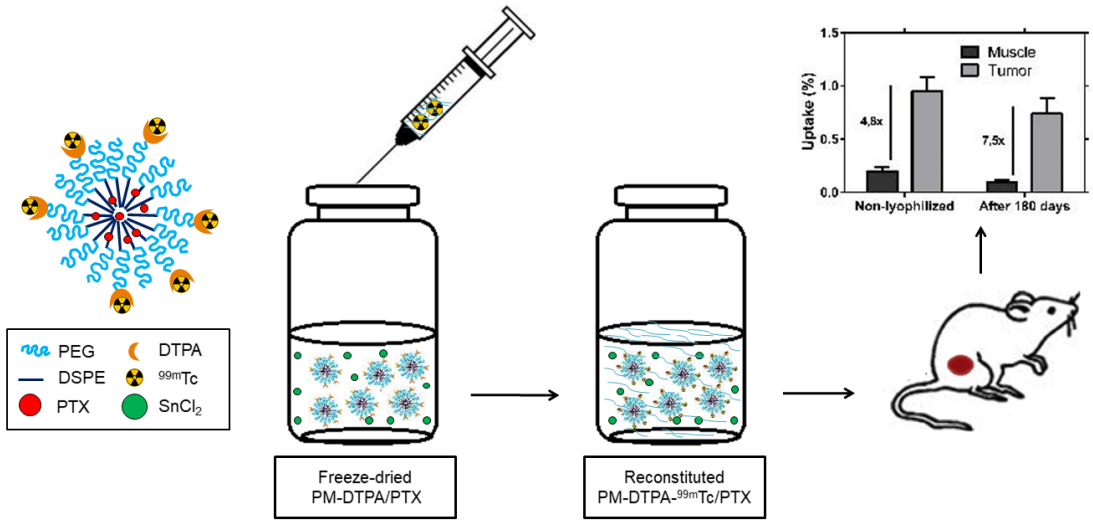

CAPÍTULO 2

Abstract

Polymeric micelles (PM) are versatile nanoparticles with suitable properties to tumor delivery of hydrophobic drugs such as paclitaxel (PTX) and imaging probes such as technetium-99m. However, instability of drug content in aqueous medium and obstacles related to lengthy radiolabeling procedures, high radiation exposure and risk of human error limit its clinical application. Freeze-dried kit formulation might be a strategy to overcome these issues. Thus, we developed a freeze-dried kit formulation containing diethylenetriaminepentaacetic acid (DTPA)-functionalized 1,2-distearoyl-sn-glycero-3-phosphoethanolamine-N-[methoxy(polyethyleneglycol)-2000] polymeric micelles carrying PTX (PM-DTPA/PTX) for application in the diagnosis and/or treatment of solid tumors. PM-DTPA/PTX were prepared and the physical and radiochemical characteristics (size, zeta potential, PTX content, and radiolabeling yields) evaluated before lyophilization process and after storage up to 180 days. In vivo biodistribution studies were performed in 4T1 breast tumor-bearing BALB/c mice. Freeze-dried kit containing PM-DTPA/PTX showed high storage stability in all parameters evaluate up to 180 days since no significant alteration was observed at all evaluated timeframes. Freeze-drying process did not change the physicochemical and biological properties of the PM, including the property of tumor targeting. Therefore, a stable freeze-dried kit containing PM-DTPA/PTX was developed as an easy and fast preparation and showed high potential for theranostic application in cancer treatment.

Keywords: Kit-formulation; polymeric micelle; paclitaxel; technetium; theranostic; cancer.

CAPÍTULO 2

1 Introduction

Polymeric micelles (PM) are nanostructures ranging in size from 5 to 100 nm, formed by block or graft copolymers with a biphasic composition, consisting of an inner hydrophobic core and an outer hydrophilic shell (KAZUNORI et al., 1993). Micellar systems have represented a promising tool for the application of cancer therapy (GAO; LI; LEE, 2013; KE et al., 2014; SHI et al., 2017). This is mainly due to their structural characteristics, since they result in important pharmacodynamics and pharmacokinetics advantages, leading to an increased blood circulation time, a passive targeting in the tumor region, and a sustained release of the drug (CROY; KWON, 2006; YOKOYAMA, 2014). These properties are mainly related to their reduced size, which comprises an ideal range in order to escape from physiological mechanisms of elimination from the organism. Particles which are smaller than 7 nm and larger than 80 nm are rapidly eliminated by renal excretion and captured by the mononuclear phagocytic system (MPS), respectively (MOHAMED et al., 2014). In addition, structures which are smaller than 100 nm are preferably accumulated in the interstitium of highly permeable tumors, and particles smaller than 30 nm penetrate in inclusive poorly permeable tumors (CABRAL et al., 2011). Therefore, micelles have all the favorable characteristics to lead to a passive targeting of substances to the tumor region (CROY; KWON, 2006; YOKOYAMA, 2014).

Furthermore, the micelles lipophilic core allows carrying hydrophobic drugs such as the antineoplastic drug paclitaxel (PTX). PTX has proven activity against various types of cancer, including metastatic breast cancer, lung, head and neck cancer, colon, advanced ovarian carcinoma and Kaposi's sarcoma (BOCCI; DI PAOLO; DANESI, 2013; ZHANG et al., 2014; ZHANG; MEI; FENG, 2013). However, the very low water solubility (< 1.0 μg/mL) and the high plasma protein binding rate have resulted in a low bioavailability of the drug limiting its clinical application. Thus, its association with a nanostructured carrier represents a potential alternative to allow the intravenous administration (SURAPANENI; DAS; DAS, 2012; ZHANG et al., 2014).

Micelles, with suitable stability i.e. low critical micelle concentration (CMC), carrying imaging probes along with therapeutic agents, as known as theranostic, permit the visualization of micelles biodistribution in real time, allowing the optimization of the treatment protocol according to the particular characteristics of the tumors of each patient (KAIDA et al., 2010; KUMAR et al., 2012). Additionally, imaging tests are extremely important in the detection of tumors, evaluation of tumor extension, detection of relapses, as well as monitoring of anticancer

therapy. Among the imaging techniques, nuclear medicine methods, such as positron emission tomography (PET) and single-photon emission computed tomography (SPECT) are widely used since they have no limits of tissue penetration and allow the quantification of the radiotracer captured in the region of interest (BLANCO et al., 2009; RYVOLOVA et al., 2012). Technetium-99m (^{99m}Tc) is often used to obtain scintigraphic images due its adequate physical and chemical properties such as physical half-life of 6.02 h, low emission energy with a single photon of 140 keV, relatively low cost by using Molybdenum-99/Technetium-99m generators (^{99}Mo/^{99m}Tc), and easy complexation with a variety of chelating agents as diethylenetriaminepentaacetic acid (DTPA)(DEWANJEE, 1990; ZHU et al., 2014).

Based on the foregoing, a DTPA-functionalized 1,2-distearoyl-sn-glycero-3-phosphoethanolamine-N-[methoxy(polyethyleneglycol)-2000] (DSPE-PEG$_{2000}$-DTPA) analog was synthesized by our research group and used on the development of a PM formulation showing favorable characteristics for application in solid tumors identification (ODA et al., 2017a). However, it is well-known that a radiolabeling procedure may present some obstacles, such as lengthy labeling procedures, high radiation exposure, and risk of human error. In this sense, the optimization of the labeling process is important for the clinical use of radiopharmaceuticals. Freeze-dried kit formulations represent an alternative to simplify the radiolabeling procedure, reduce the risk of human errors in the preparation and minimize radiation exposure during preparation (AHLGREN; ANDERSSON; TOLMACHEV, 2010; DE BARROS et al., 2012b; ZHAO; LI, 2012). Furthermore, the lyophilization process can prevent instability of micellar carriers in the aqueous medium, favoring drug retention in their hydrophobic core (DOKTOROVOVA et al., 2014; FONTE et al., 2014; MIYAJIMA, 1997).

Taking into account that developed PM have suitable physicochemical characteristics for carrying PTX, the aim of this study was to develop a kit formulation containing the PTX-loaded DSPE-PEG$_{2000}$/DSPE-PEG$_{2000}$-DTPA micelles (PM-DTPA/PTX) in order to achieve a straightforward preparation to the possible theranostic application in tumors.

2 Materials and Methods

2.1 Materials

1,2-distearoyl-sn-glycero-3-phosphoethanolamine-N-[methoxy (polyethyleneglycol)-2000] (DSPE-mPEG$_{2000}$) was acquired from LipoidGmbH (Ludwigshafen, Germany). 1,2-

distearoyl-sn-glycero-3-phosphoethanolamine-N-[amine(polyethylenegliycol)-2000] (DSPE-PEG_{2000}-NH_2) was obtained from Avanti Polar Lipids, Inc (Alabama, USA). Diethylenetriaminepentaacetic (DTPA) dianhydride and stannous chloride ($SnCl_2.2H_2O$) were purchased from Sigma-Aldrich Co. (Missouri, USA). PTX was supplied by QuiralQuímica do Brasil S/A (Juiz de Fora, Brazil) with purity greater than 97%. The water used was purified using Milli-Q® distillation and deionization equipment (Millipore, USA). Technetium–99m was obtained from an alumina-based $^{99}Mo/^{99m}Tc$ generator from Institute of Energy and Nuclear Research (IPEN, São Paulo, Brazil). All other reagents were acquired from Sigma-Aldrich Co (Missouri, USA).

Murine mammary carcinoma cell line (4T1) was purchased from the American Type Culture Collection (ATCC, Rockville, USA). Female BALB/c mice were purchased from Bioterism Center of Federal University of Minas Gerais (CEBIO-UFMG), aging 6–8 weeks and weighing 20 ± 2 g. The mice were housed in cages in a controlled environment to a temperature range of 25 ± 2 °C and a humidity range of 30–70% with a 12 h light-dark cycle and free access to food and water. All animals experiments were approved by Ethics Committee on Animal Use (CEUA) from UFMG, protocol number 205/2013 and follow the guide for the care and use laboratory animals recommended by European Community.

2.2 Preparation of PM-DTPA/PTX

PM-DTPA/PTX were prepared using a solvent evaporation method (SAWANT; TORCHILIN, 2010; WANG; PETRENKO; TORCHILIN, 2010). Firstly, DSPE-PEG_{2000}-DTPA was synthesized according to the method described previously (ODA et al., 2017a). Then, chloroformic solutions of DSPE-mPEG_{2000} and DSPE-PEG_{2000}-DTPA, 99:1 (w/w) respectively (10 mmol/L final concentration), and PTX (0.6 mg/mL) were transferred to a round bottom flask. The solvent was completely removed under reduced pressure. The thin film formed was hydrated with saline 0.9% (w/v), in a water bath at 40 °C for 5 min, followed by vortexing at 1000 rpm for 3 min. Lastly, the preparation was filtered in 0.22 μm polycarbonate membranes in order to remove non-encapsulated PTX.

2.3 Physical and chemical characterization

Size average was determined by dynamic light scattering (DLS) at 25ºC at a 90º angle using a Zetasizer NanoZS90 instrument (Malvern Instruments, England). Zeta potential was

evaluated by DLS associated with electrophoretic mobility, at 25ºC, at an angle of 90º, also using a Zetasizer NanoZS90 instrument. To carry out these analyzes, the samples were diluted 15-fold in saline 0.9% (w/v) solution previously filtered on a 0.45 μm pore membrane.

The content of PTX encapsulated in the formulation was evaluated by high-performance liquid chromatography (HPLC) using a previously validated analytical method (BARBOSA et al., 2015). The chromatographic conditions were: eluent system consisting of acetonitrile: water, in the ratio of 55:45 (v / v); Lichrospher®, C18, 5 μm, 4 mm x 25 cm reverse phase column (Merck Millipore, Darmstadt, Germany); flow rate of 1.2 mL / min; temperature of 25 °C; volume of injection equal to 10 μL. The equipment used was an Agilent HPLC, model Agilent 1260 Infinity Quaternary LC (Germany).

2.4 Preparation of kits

Aliquots (0.2 mL) of the PM-DTPA/PTX formulation were transferred to amber and cryo-resistant vials containing glucose as a cryoprotectant in a sugar:polymer ratio of 2:1 (w/w). In the flasks were also added different amounts (0.2 or 0.3 mg) of stannous chloride (reducing agent) in HCl 0.25 mol/L solution and NaOH 0.1 mol/L solution in a volume sufficient to neutralize the pH of the medium. Vials were vortexed then, frozen in liquid nitrogen for 5 minutes and lyophilized in a 24-hour cycle using a Modulyolyophilizer (Thermo Electron Corporation, USA). After the lyophilization cycle, the vials were sealed under vacuum, stored sheltered from the light and kept at -20 °C. In order to evaluate the best amount of stannous chloride to be used, on the following day, the kits obtained were reconstituted and evaluated for their radiolabeling yield. To reconstitute the kits, 0.2 ml of $Na^{99m}Tc$ solution (3.7 MBq) was added to each vial with a syringe, gently stirred for 15 minutes. Afterward, the vials were opened and the radiolabeled complex was evaluated.

2.5 Radiolabeling yield evaluation

The radiolabeling yield was determined by thin layer chromatography (TLC-SG, Merck, Darmstadt, Germany) using acetone to determine $^{99m}TcO_4^-$. PM-DTPA-^{99m}Tc/PTX were purified from $^{99m}TcO_2$ by a filtration through 0.22 μm polycarbonate membranes. Radioactivity was measured using a gamma counter (Perkin Elmer Inc., USA).

2.6 Kit Storage Stability

At days 1, 30, 90 and 180 after the preparation, the kits (n = 5) were reconstituted with 0.2 mL $Na^{99m}TcO_4$ solution (3.7 MBq) and kept under gentle shaking for 15 minutes. After this, the flasks were opened and the content was filtered by 0.22 μm for removing released PTX and radiochemical impurity $^{99m}TcO_2$. Size, zeta potential, PTX content and radiolabeling yields were evaluated at all timeframes.

2.7 In vitro radiocomplexing stability

After 180 days of storage, radiolabeling stability was evaluated. TLC was used to estimate the stability of PM-DTPA-^{99m}Tc/PTX in saline 0.9% (w/v), at room temperature (25 °C), and in the presence of mouse plasma, at 37 °C. For saline, at specific time points, the amount of free technetium presents in the radiolabeled MP was determined as mentioned previously. For plasma stability, 90 μL of labeled PM-DTPA solution was incubated, under agitation with 1.0 mL of mice fresh plasma. Radiochemical stability was determined from samples collected at 0, 1, 2, 6, 8 and 24 h after radiolabeling. The same procedure was used for freshly prepared micelles.

2.8 In vivo evaluation

2.8.1 Cell culture

4T1 cells were cultured in RPMI 1640 medium (Gibco, Waltham, MA, USA) containing 10% (v/v) fetal bovine serum, 100 IU/mL penicillin and 100 μg/mL streptomycin. Cells were grown in a humidified incubator with 5% CO_2 atmosphere at 37 °C until reaching confluence. After this, cells were harvested with 0.25% trypsin, subjected to centrifugation at 500g for 5 min, and the pellet of cells obtained was re-suspended in RPMI medium for inoculation into Balb/c mice.

2.8.2 4T1 breast tumor model

A 4T1 breast tumor was implanted in adult female BALB/c mice. For tumor implantation, 2.5×10^6 4T1 cells were injected subcutaneously into the right flank of the mice.

Tumors were allowed to grow and the biodistribution studies were performed when the tumors reach a volume of 100 mm^3.

2.8.3 Biodistribution studies of PM-DTPA-^{99m}Tc/PTX

In order to study biodistribution, every 4T1 tumor-bearing mice (n=4) received 3.7 MBq of PM-DTPA-^{99m}Tc/PTX intravenously through the tail vein. After 24 h, animals were anesthetized with ketamine (80 mg/kg) and xylazine (10 mg/kg) solution and then submitted to euthanasia by cervical displacement. The following organs and tissues were removed: heart, blood, kidneys, stomach, spleen, liver, thyroid, lung, muscle and tumor.Whole organs were washed with distilled water, dried on filter paper, placed in pre-weighed plastic test tubes, weighed and taken to an automatic scintillation apparatus to determine the radioactivity. Results were expressed as %ID/g of tissue.

2.9 Statistical analysis

All data are expressed as the mean ± standard deviation (SD). Normality and homogeneity of variance were evaluated by the D'Agostino and Pearson, and Bartlett's tests, respectively. Variables without a normal distribution were transformed when appropriate, by the equation: y = log (variable + 1). Storage stability data were tested using one-way analysis of variance (ANOVA) followed by Tukey's test and biodistribution data were tested by Student's t-test. The 95% confidence interval was adopted and differences were considered significant when the p-value was lower or equal to 0.05 ($p \leq 0.05$). All data were analyzed by GraphPadPrism version 6.00.

3 Results

3.1 Kit formulation

Considering that oxidation of tin (II) into tin (IV) is the main cause of instability of ^{99m}Tc radiolabeling kits (DE BARROS et al., 2012b; LEE et al., 2007), different amounts of stannous chloride were evaluated: 0.2 mg, amount efficient in radiolabeling non-lyophilized micelles (ODA et al., 2017a); and 0.3 mg, to guarantee the radiolabeling efficiency after

lyophilization. Radiochemical impurities were quantified after freeze-dried kits reconstitution. Kits containing 0.2 mg of stannous chloride presented 1.1 ± 0.9% of TcO_4^- and 10.3 ± 4.7% of TcO_2. Meanwhile, kits containing 0.3 mg of $SnCl_2$, showed 0.2 ± 0.2% and 8.2 ± 1.7% of TcO_4^- and TcO_2, respectively. Although no significant difference was found ($p>0.05$) between the two concentrations tested in this study, the amount of 0.3 mg was considered to assure high radiolabeling yields after long-term storage.

3.2 Non-lyophilized PM-DTPA/PTX characterization

Mean size, zeta potential, PTX content and radiolabeling yield of DTPA-functionalized polymeric micelles freshly prepared were evaluated and the results are presented in Table 2.1. The efficiency of loading of PTX in PM was 96.9 ± 5.6%.

Table 2.1 Physicochemical characteristics of PM-DTPA-^{99m}Tc/PTX before lyophilization process. Data shown as mean ± SD (n=3).

Radiolabeling yield		PTX (mg/mL)	Size (nm)	Zeta potencial (mV)
TcO_4^- (%)	TcO_2 (%)			
1.4 ± 0.8	4.3 ± 0.7	0.7 ± 0.1	12.8 ± 1.0	-1.2 ± 1.5

3.3 Storage Stability

The stability of the kits was verified over the course of 180 days, regarding the maintenance of physicochemical and radiolabelling characteristics. These characteristics were evaluated after purification of kits reconstituted with $Na^{99m}TcO_4$. Mean size and zeta potential of PM-DTPA-^{99m}Tc/PTX remained around 14 nm and -3.0 mV over the time evaluated (Fig. 2.2A). Approximately 85% of PTX remained trapped within the micelles, which represents around 0.65 mg/mL of PTX retained throughout the evaluated period (Fig.2.2B). Regarding the radiolabelling efficiency, no significant amount of radiochemical impurity $^{99m}TcO_4^-$ was observed after the kit reconstitution in all timeframes (Fig. 2.2B). Data analysis did not show significant variation ($p>0.05$) in any of the investigated parameters, indicating high physicochemical properties stability of the freeze-dried kit.

Figure 2.2 Storage stability evaluation of freeze-dried kit formulation.

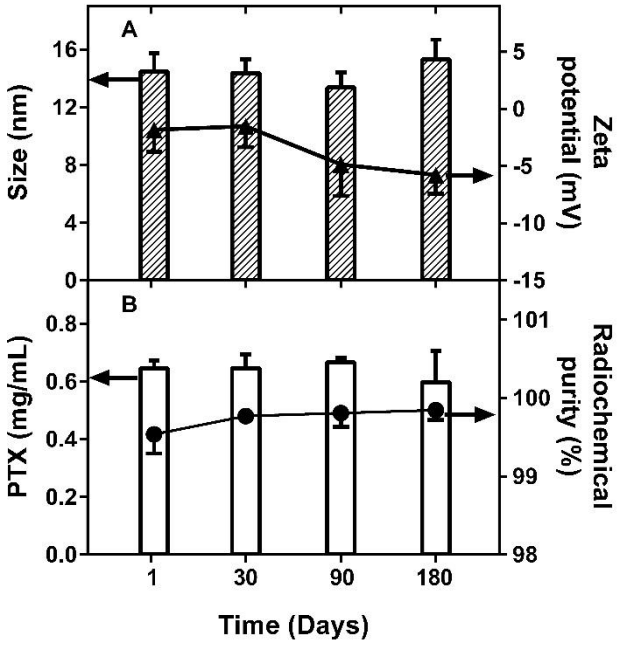

In (A), size (nm) is shown in bars and zeta potential (mV) as symbol and line. In (B), PTX retained (mg/mL) is shown in bars and radiochemical yields (%) as symbol and line. Data shown as mean ± SD (n=5).

3.4 Radiocomplexing stability

180 days-storage kits were tested for their ability to chelate with technetium-99m in high efficiency and their radiocomplexing stability over time. PM-DTPA-^{99m}Tc/PTX exhibited a high *in vitro* radiocomplexing stability (Fig. 2.3B) within 24 h of incubation (n = 4) in saline. However, in the presence of mouse plasma, a reduction of approximately 18% in the radiolabeling yield was verified 24 h post-incubation, although a high stability was observed up to 8 h. The kit showed a comparable radiocomplexing stability to freshly prepared micelles (Fig. 2.3A).

Figure 2.3. Radiolabeling stability evaluation of freshly prepared (A) and freeze-dried (B) PM-DTPA-99mTc/PTX in presence of normal saline (●) and murine plasma(▲).

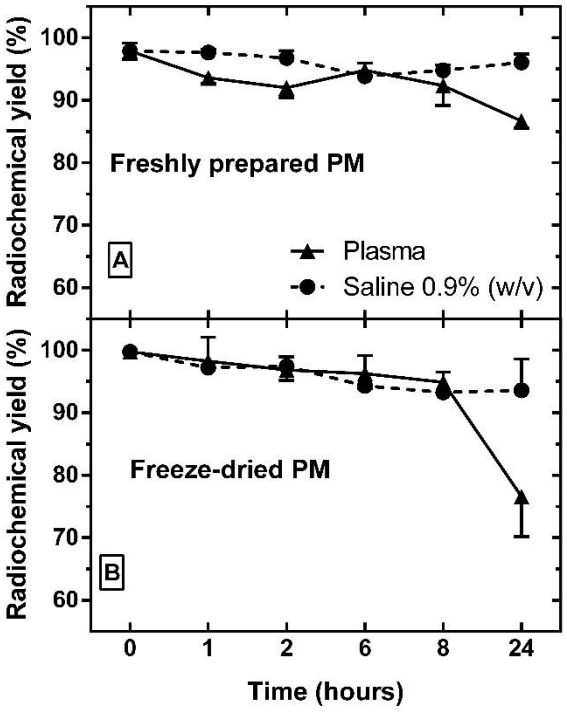

3.5 Biodistribution studies of PM-DTPA-^{99m}Tc/PTX kit

After 180 days of storage, the biodistribution profile of freeze-dried PM-DTPA-^{99m}Tc/PTX was evaluated in tumor-bearing mice model. The results obtained were compared with the non-lyophilized and freshly prepared micelles. The biodistribution profile (Fig.2.4) was obtained for both radiolabeled micelles at 24 h post-injection.

Despite significantly ($p<0.05$) lower uptakes in liver, thyroid, stomach, muscle, and tumor were observed for mice that received freeze-dried micelles when compared to those animals that received the freshly prepared micelles, both groups had similar biodistribution profiles. In both cases, a high uptake in kidney, liver, and spleen was observed, thus, suggesting that micelles are possibly eliminated by these routes. A very low uptake in thyroid and stomach was also observed indicating high radiochemical stability of PM-DTPA-^{99m}Tc/PTX. Noteworthy that tumor uptake was consistently higher than muscle uptake, indicated by the high tumor-to-muscle ratio (Fig. 2.4 – inset). However, no significant change ($p>0.05$) in the tumor-to-muscle ratio (7.9 ± 2.9) was observed in freeze-dried PM-DTPA-^{99m}Tc/PTX compared to non-lyophilized micelles (4.7 ± 1.2).

Figure 2.4. Biodistribution profiles of non-lyophilized micelles (dark grey) and freeze-dried kit after 180 days of storage (light grey).

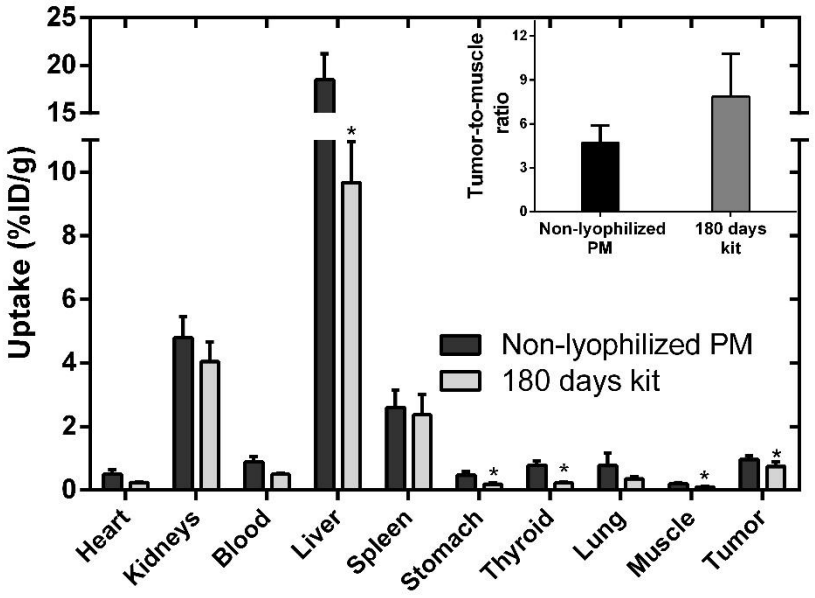

Inset: Tumor-to-muscle ratio obtained by biodistribution study. Each animal received 3.7 MBq of PM-DTPA-99mTc/PTX by intravenous tail-vein administration. A solution of xylazine (10 mg/kg) and ketamine (80 mg/kg) was used to anesthetize animals. Data expressed as the mean ± standard deviation. *Represents significant difference compared to non-lyophilized PM. P-values less than 0.05 were set as the level of significance (Student's t-test).

4 Discussion

PM-DTPA/PTX was developed to passively target solid tumors, however, instability of micellar carriers in an aqueous medium is often reported problems. Thus lyophilization is a potential alternative to prevent instability in these cases (FONTE et al., 2014; KAMIYA; NAKASHIMA, 2017; MIYAJIMA, 1997). Given that freeze-dried kits for radiodiagnosis are reported as an easy, fast, safe and reproducible way to obtain radiopharmaceuticals, it has been seen as a safe and effective alternative to prepare the PM-DTPA/PTX formulation(KUMAR et al., 2015; VIDAL et al., 2015; ZHAO; LI, 2012). However, considering that a lyophilization process involves conditions of stress, such as freezing and removal of water (ABDELWAHED et al., 2006; YANG et al., 2008), and freeze-dried kits should be stable for long period of storage, a detailed study of the lyophilized kit is indispensable.

Our kit was formulated with PTX-loaded micelles, glucose (as a cryoprotectant to prevent micelles aggregation/fusion), and stannous chloride (as reducing agent). The main concern was related to the amount of reducing agent, once it may undergo oxidation during kit preparation and/or storage, resulting in an inefficient reduction of $^{99m}TcO_4^-$. Pertechnetate is a non-reactive form of ^{99m}Tc and its presence in high amounts results in low quality *in vivo* data (DEWANJEE, 1990). Although putting a higher concentration of the reducing agent appeared to be the most obvious alternative, it is known that the use of large quantities of $SnCl_2$ might lead to a decrease in radiolabelling yield by the formation of radiocolloids (AHLGREN; ANDERSSON; TOLMACHEV, 2010). In this way, two different amounts of stannous chloride were evaluated showing low levels of radiochemical impurities. As a result, the kit preparation with the higher amount of reducing agent was selected for further studies in order to guarantee the best radiolabeling efficiency after long periods of storage.

Micelles from the kit preparation were characterized after storage for 1, 30, 90, and 180 days, indicating no significant differences in size and zeta potential. These findings suggest that glucose, used as a cryoprotectant, was efficient in avoiding micelles aggregation. It is well established that the use of cryoprotectants in freeze-drying processes and in a certain proportion have the ability to protect nanoparticles from stresses and subsequent aggregation, maintaining characteristics of shape and size. This is possible since, at low temperatures, the cryoprotectant forms a glassy matrix which can protect nanoparticles from the mechanical stress of ice (KAMIYA; NAKASHIMA, 2017; LEE, MIN KYUNG; KIM, MIN YOUNG; KIM, SUJUNG; LEE, 2009). It is noteworthy that the high retention (about 90%) of PTX into micelles even after 180 days of storage, indicating that the kit can be safely used after preparation and storage.

High radiolabeling yields were attained for all kits from 1 to 180 days of storage. However, in addition to an efficient radiolabeling process, it is important for radiodiagnostic agents that the radioisotope binding remains stable over a long period. In the development of a radiopharmaceutical, this time should be adequate to obtain a reliable and reproducible biodistribution profile in order to predict the real destination of the radiolabeled material (VARSHNEY et al., 2012). On the other hand, for clinical application, this time should allow radiopharmaceutical administration and acquisition of scintigraphic images (DE BARROS et al., 2013a; ZHU et al., 2014). In this sense, the evaluation of labeling stability is extremely important, since unstable radiopharmaceuticals result in undesirable biodistribution imparting data interpretation (SAHA, 2010; ZHU et al., 2014). Polymeric micelles from the kits storage for 180 days exhibited high radiolabeling stability for at least 8 h, which allow their use for *in vivo* application. It is important to underscore that, although a reduction in the stability in

presence of plasma at 24 h has been observed, the biodistribution study did not show significant uptake in thyroid or stomach even at 24 h post-injection. This finding indicates that the slight reduction in stability does not compromise in vivo studies. It is worthy mentioning that micelles freshly prepare exhibited the same radiocomplexing stability after 24 h of incubation in mice plasma, indicating that freeze-drying process did not alter the characteristics of PM-DTPA-^{99m}Tc/PTX.

PM-DTPA-^{99m}Tc/PTX, after 180 days of storage, showed biodistribution profile, in tumor-bearing mice, similar to non-lyophilized micelles suggesting that freeze-drying process did not alter in vivo micelles properties. As it was expected, biodistribution and imaging studies showed high uptake in liver and spleen, which might be attributed to the activation of the MPS (KIESSLING et al., 2014; KOLATE et al., 2014). The reduction in thyroid uptake ($p = 0.007$) and stomach ($p = 0.028$) observed may be due to the lower level of $^{99m}TcO_4^-$ in freeze-dried PM-DTPA-^{99m}Tc/PTX, which can be explained by the greater amount of stannous chloride used in the kit when compared to the system freshly prepared. Despite a lower uptake in tumor observed for micelles from the kit, no significant change ($p>0.05$) in tumor-to-muscle ratio was observed when compared to non-lyophilized micelles. Importantly, micelles lyophilized or not showed signal-to-noise ratios over than 4.0. It has been established that radiotracers showing tumor-to-muscle ratio higher than 1.5 (50% more uptake in the targeting tissue) can be considered as promising imaging probes for tumor identification(DE BARROS et al., 2010; PHILLIPS, 1999). These results indicate that the freeze-dried system, after 180 days of storage, maintains similar properties than those found in the freshly prepared micelles, indicating that kit is feasible for application in tumor targeting.

5 Conclusion

A freeze-dried kit containing PM-DTPA/PTX was successfully developed to be considered as a theranostic tool in cancer. Results showed that the prepared kit was able to keep the physicochemical and radiochemical properties as well as biological profiles of PM freshly prepared, including tumor targeting. Thus, our kit proved to be an easy, fast and safe preparation with potential for application in the treatment and diagnosis of cancer.

ACKNOWLEDGEMENTS

The authors thank Conselho Nacional de Desenvolvimento Científico e Tecnológico (CNPq-Brazil), Fundação de Amparo à Pesquisa do Estado de Minas Gerais (FAPEMIG-Brazil), and

Coordenação de Aperfeiçoamento de Pessoal de Nível Superior (CAPES) for their financial support and fellowships.

CONFLICTS OF INTEREST

There are no conflicts of interest.

CAPÍTULO 3 – Encapsulação de paclitaxel em nanomicelas poliméricas aumenta a atividade antitumoral e previne neuropatia periférica.

CAPÍTULO 3

Encapsulating paclitaxel in polymeric nanomicelles increases antitumor activity and prevents peripheral neuropathy

Caroline Mari Ramos Oda; Juliana de Oliveira Silva; Alysson Vinícius Braga; Renes de Resende Machado; Renata Salgado Fernandes; Geovanni Dantas Cassali; André Luís Branco de Barros; Elaine Amaral Leite.

Figura 3.1 Graphical abstract.

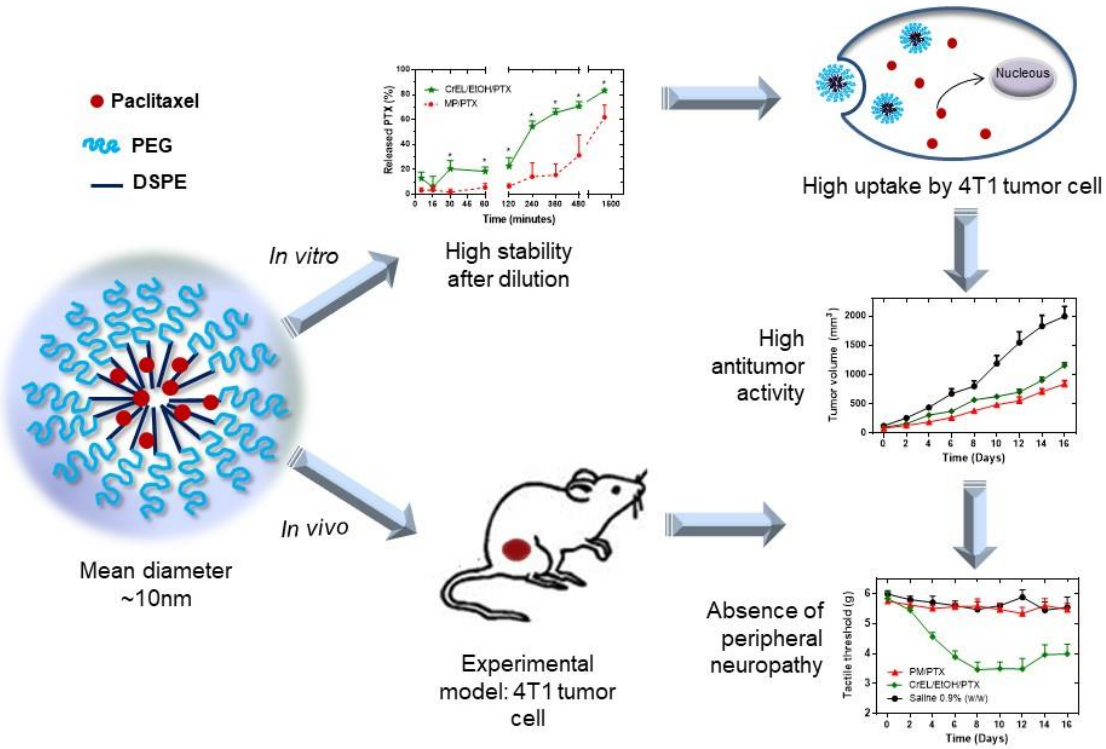

CAPÍTULO 3

Abstract

Paclitaxel (PTX) has a great clinical significance as an antitumor drug, although several side effects are strongly dose-limiting. In this way, we prepared a PTX-loaded 1,2-distearoyl-sn-glycero-3-phosphoethanolamine-N-[methoxy (polyethylene glycol)-2000] polymeric micelle (PM/PTX) in the attempt to improve safety and effectiveness of the conventional PTX formulation (CrEL/EtOH/PTX). In this study, we evaluated from both formulations: stability after dilution, hemocompatibility, 4T1 cell uptake, acute toxicity in healthy and tumor-bearing mice, and antitumor activity. PM/PTX higher stability after dilution than CrEL/EtOH/PTX . PM/PTX did not show hemolytic activity (values <1%), even at high concentrations. *In vitro* cell uptake study indicated that PM was able to deliver more PTX (5.8%) than CrEL/EtOH (2.7%) to 4T1 cells. Peripheral neuropathy was observed in healthy mice treated with a single dose of CrEL/EtOH/PTX (20 mg/kg), while the absence of this effect was observed in PM/PTX group. Similar results were observed in tumor-bearing mice after multiple-dose of treatment (7 doses of 10 mg/kg). Worth mentioning that the vehicle (CrEL/EtOH) was not capable of inducing neuropathic pain. Reduction in the tactile threshold only occurred in CrEL/EtOH/PTX group. In addition, PM/PTX presented a higher antitumor activity with an inhibition ratio approximately 1.5-fold higher than CrEL/EtOH/PTX group. These findings suggested that PM/PTX was safer than CrEL/EtOH/PTX, and in addition, PM/PTX was able to improve the antitumor effectiveness in a 4T1 breast cancer model.

Keywords: cancer; nanoparticles; paclitaxel; polymeric micelles; toxicity.

CAPÍTULO 3

1 Introduction

Paclitaxel (PTX) is a chemotherapeutic agent with proven effectiveness for the treatment of metastatic and non-metastatic breast cancer, ovarian cancer, non-small cell lung cancer, prostate cancer, melanoma, esophageal cancer, and other types of solid tumors (WEAVER; BEMENT, 2014). However, this drug has poor aqueous solubility, low bioavailability and is often associated with dose-limiting toxicities, such as nephrotoxicity and chemotherapy-induced peripheral neuropathy (CIPN) (BERNABEU et al., 2017; OOSTENDORP; BUCKLE; LAMBERT, 2011). The first commercial product named Taxol® was approved by the Food and Drug Administration (FDA) for clinical use in ovarian cancer in 1992. This product and its generic versions are micellar formulations prepared with ethanol and Cremophor EL (CrEL), a synthetic and nonionic surfactant (GELDERBLOM et al., 2001). Even though CrEL has been used as a vehicle to PTX, it is associated with severe and sometimes fatal anaphylactic reactions, and pre-treatments with steroids and/or antihistamine are commonly required (WANG et al., 2015; YANG; HORWITZ, 2017).

In recent years, pharmaceutical companies have heavily invested in alternatives to carrier PTX (BERNABEU et al., 2017). In search of new PTX formulations, nanoparticle albumin-bound PTX (nab-PTX), called Abraxane®, emerged with great advantages over Taxol®, such as higher maximum tolerated dose, and therefore it has been taking much of the PTX market (LUCA; PROFITA; CICERO, 2019; PENG et al., 2017). However, Abraxane® has still shown a high incidence of CIPN, which is dose-limiting, painful, and cumulative, often interfering with continuous PTX treatment (KAMEI et al., 2017).

Therefore, the development of new and advantageous PTX formulations is of great clinical and economic interest. At this time there are at least 18 companies focused on the pre-clinical and/or clinical development of nanoformulations of this drug. These PTX-nanocarriers may favor a higher antitumor efficacy with fewer side effects due to a remarkable enhanced permeability and retention (EPR) effect (FANG; NAKAMURA; MAEDA, 2011). Among the studied nanosystems, polymeric micelles (PM) have shown as a promising tool for cancer therapy. These nanostructures with size ranging from 5 to 100 nm are formed by block or graft copolymers with a biphasic composition, consisting of an inner hydrophobic core and an outer hydrophilic shell (KAZUNORI et al., 1993). Structural characteristics of PM can provide important pharmacodynamic and pharmacokinetic advantages, which lead to an increased blood circulation time, a passive targeting in the tumor region, and/or a sustained release of the drug, properties that bypass free PTX drawbacks (OERLEMANS et al., 2010). PM made up of

1,2-distearoyl-sn-glycero-3-phosphoethanolamine-N-methoxy(polyethyleneglycol)-2000] (DSPE-PEG_{2000}) are one of the most studied micelles worldwide due to their biocompatibility, biodegradability, and other advantageous properties (CHEN et al., 2013; CROY; KWON, 2006; DABHOLKAR et al., 2006). Our research group developed recently a kit formulation of PM composed of DSPE-PEG_{2000} containing PTX. This formulation showed tumor targeting and enabled the theranostic use in a solid tumor by ^{99m}Tc-radiolabeling (ODA et al., 2018). In the meantime, the *in vivo* effectiveness and the ability of this system to reduce PTX side effects remain to be investigated. Thus, in this work, we aimed to investigate the ability of PTX-loaded PM to treat a murine breast tumor model. In addition, we evaluated the toxicity using laboratory tests, histological evaluation, and peripheral neuropathy of the proposed micelle in comparison with the conventional formulation.

2 Material and methods

2.1 *Material*

1,2-distearoyl-sn-glycero-3-phosphoethanolamine-N-[methoxy (polyethylene glycol)-2000] (DSPE-$mPEG_{2000}$) was acquired from Lipoid GmbH (Ludwigshafen, Germany). PTX was supplied by Quiral Química do Brasil S/A (Juiz de Fora, Brazil) with purity greater than 97%. Cremophor® EL was acquired from Sigma-Aldrich Co (Missouri, USA). Ultra-pure water was obtained using Milli-Q® distillation and deionization equipment (Millipore, USA). Technetium–99m was obtained from an alumina-based ^{99}Mo/^{99m}Tc generator from the Institute of Energy and Nuclear Research (IPEN, São Paulo, Brazil). All other reagents were acquired from Sigma-Aldrich Co (Missouri, USA).

Murine mammary carcinoma cell line (4T1) was purchased from the American Type Culture Collection (ATCC, Rockville, USA). Female BALB/c mice were purchased from Bioterism Center of Federal University of Minas Gerais (CEBIO-UFMG). Female Swiss mice were acquired from the Faculty of Pharmacy of the UFMG. All mice were aging 6–8 weeks and weighing 20 ± 2 g. The mice were housed in cages in a controlled environment to a temperature range of 25 ± 2 °C and a humidity range of 30–70% with a 12 h light-dark cycle and free access to food and water.

2.2 *Paclitaxel dispersion preparation*

A micellar dispersion of PTX (CrEL/EtOH/PTX) was prepared by dissolving 30.0 mg of the drug in 5.0 mL of a mixture of Cremophor EL™:dehydrated ethanol (1:1 v/v) under vigorous stirring. Before intravenous injection, this dispersion was diluted in NaCl 0.9% (w/v) solution at a concentration of 0.6 mg/mL.

2.3 *Preparation of PM*

PM formulations were prepared using a solvent evaporation method (SAWANT; TORCHILIN, 2010; WANG; PETRENKO; TORCHILIN, 2010). For DTPA-functionalized PM, DSPE-PEG_{2000}-DTPA was synthesized according to the method described previously (ODA et al., 2017a). Chloroformic solutions of DSPE-$mPEG_{2000}$ and DSPE-PEG_{2000}-DTPA 99:1 (w/w), respectively (10 mmol/L final concentration), and PTX (0.6 mg/mL) were transferred to a round bottom flask. The solvent was completely removed under reduced pressure. The thin film formed was hydrated with NaCl 0.9% (w/v), in a water bath at 40 °C for 5 min, followed by vortexing at 1500 g for 3 min. Then, the formulations were transferred to amber and cryo-resistant vials containing glucose as a cryoprotectant in a sugar:polymer ratio of 2:1 (w/w). Vials were frozen in liquid nitrogen and lyophilized in a 24-hour cycle using a Modulyo lyophilizer (Thermo Electron Corporation, USA). After lyophilization cycle, vials were sealed under vacuum, stored sheltered from the light and kept at -20 °C.

At the time of use, the freeze-dried PM was reconstituted by adding ultra-pure water, and after 15 minutes, the preparation was filtered in 0.22 μm polycarbonate membranes to remove non-encapsulated PTX.

2.4 *Physicochemical characterization*

Mean diameter was determined by dynamic light scattering (DLS) and zeta potential was evaluated by DLS associated with electrophoretic mobility. Both were investigated at 25ºC and an angle of 90º, using a Zetasizer NanoZS90 instrument (Malvern Instruments, England). For these analyzes, all the samples were diluted 15-fold in NaCl 0.9% (w/v) solution previously filtered on a 0.45 μm pore membrane.

The content of PTX encapsulated in the formulation was evaluated by high-performance liquid chromatography (HPLC) using a previously validated analytical method (BARBOSA et al., 2015).

2.5 *Formulations stability after dilution*

This study was conducted according to the dilution method proposed by De Barros et al. (DE BARROS et al., 2013b). An aliquot of 92 μL of the MP/PTX or Cremophor/Ethanol/PTX were incubated in 1.0 mL of pH 7.4 saline-phosphate buffer (PBS) at 37 °C under stirring at 500 bpm (Dubnoff Metabolic Bath MA-95/CF Marconi, Brazil). After 5, 15, 30, 60, 120, 240, 360, 480, and 1440 minutes, vials (n = 4) were centrifuged at 24000 g for 15 minutes to remove released PTX. Amount of remaining encapsulated PTX present in the supernatant at different time (Q_T), as well as the initial amount of drug encapsulated (Q_0), were determined. PTX in Q_T and Q_0 was extracted from PM/PTX using isopropyl alcohol and quantified in HPLC. The release profile was calculated indirectly by the percentage of PTX retained within micelles over time and calculated by equation 1.

$$\text{Released PTX}(\%) = 100 - \left(\frac{Q_T}{Q_0} x 100\right) \qquad \text{Eq.1}$$

2.6 *Cellular uptake*

Cellular uptake evaluation was investigated according to the protocols previously described in the literature (MIAO et al., 2013; NIE et al., 2011) Briefly, PM-DTPA/PTX and CrEL/EtOH/PTX were radiolabeled with ^{99m}Tc as reported by our group (MONTEIRO et al., 2017; ODA et al., 2017a). 4T1 cells ($1.5x10^6$ cells), in culture medium, were incubated with 0.021 μmol of each ^{99m}Tc-labeled formulation at 37°C under stirring (Metabolic Bath Dubnoff MA-95/CF Marconi, Brazil). At different times (15, 30, 60, and 120 min) after incubation, the samples were centrifuged at 500 g for 5 min at room temperature. The supernatant was conditioned in a vial and pellet was washed with 1.0 mL of PBS to remove the non-uptaken micelles. Then, the radioactivity presented in the pellet and the supernatant (n=5) was quantified in a gamma counter and the percentage of uptake was calculated according to equation 2:

$$\text{Uptake}(\%) = \frac{\text{radioactivity}_{\text{pellet}}}{\text{radioactivity}_{\text{pellet}} + \text{radioactivity}_{\text{supernatant}}} \text{x}100 \qquad \text{Eq. 2}$$

The amount of PTX associated with 4T1 cells was quantified by HPLC. After quantifying the radioactivity, 1.0 mL of acetonitrile was added to the pellet and the preparation was taken to the ultrasonic bath for 5.0 minutes to lyse the cells and precipitate the protein. The samples were centrifuged at 3100 g for 15 min at room temperature and an aliquot of the supernatant was used for quantifying PTX (PTX sample). The percentage of PTX uptake was calculated by using the following equation 3:

$$\text{Uptake of PTX } (\%) = \frac{[\text{PTX}]_{\text{sample}}}{[\text{PTX}]_{\text{total}}} \text{ x}100 \qquad \text{Eq. 3}$$

2.7 *Hemocompatibility evaluation*

The hemolytic potential of PM was assessed according to reported in the literature and compared to CrEL/EtOH formulation (JAIN et al., 2012; MONTEIRO et al., 2019; ZHANG et al., 2015b). Fresh blood was obtained from female Swiss mice, 8 weeks, 20.0 ± 2.0 g (Ethics Committee on Animal Use - CEUA from UFMG, protocol number 148/2017). Blood samples were collected in tubes containing 10% w/v EDTA solution. The red blood cells (RBC) were separated by centrifugation at 1100 g for 10 min at room temperature (Heraeus Multifage X1R Centrifuge, Germany). RBC collected from the bottom were washed with NaCl 0.9% (w/v) until a colorless supernatant was obtained. The final pellet was diluted with NaCl 0.9% (w/v) solution to obtain a 2% (w/v) RBC concentration. The formulations evaluated were MP/PTX and CrEL/EtOH/PTX at concentrations of 0.05 and 0.1 mg/mL and their respective controls. The samples were added to 500 μL of 2% RBC suspension (n=5), the volume was completed to 1 mL with NaCl 0.9% (w/v), and then, the samples were incubated for 1 h at 37 °C under agitation at 500 bpm (Metabolic Bath Dubnoff MA-95/CF Marconi, Brazil). After the incubation time, the cell suspensions were centrifuged at 500 g for 5 min and the amount of hemoglobin released to the supernatant absorbance was measured in a spectrophotometer (Evolution 201 UV-Visible Spectrophotometer Thermo Scientific, USA) at 540 nm. NaCl 0.9% (w/v) was used as a negative control (NC), while ultra-pure water and was used as a positive (PC) control. The percent hemolysis was calculated using the following equation 4:

$$\text{Hemolysis (\%)} = \frac{\text{Sample}_{\text{Absorbance}} - \text{NC}_{\text{Absorbance}}}{\text{PC}_{\text{Absorbance}} - \text{NC}_{\text{Absorbance}}} \text{ x100} \qquad \text{Eq. 4}$$

2.8 *Acute toxicity*

A single dose of PM/PTX or CrEL/EtOH/PTX (20 mg/kg) was intravenously administrated into healthy mice (n=6). After treatments, the animals were observed for 14 days and behavioral/clinical modifications, body weight, morbidity, and mortality were evaluated (OECD Guideline for Testing of Chemicals, 2001). After this time, the mice were anesthetized with a mixture of ketamine (80 mg/kg) and xylazine (15 mg/kg) and blood was collected by puncture of the brachial plexus in tubes containing anticoagulant EDTA (Ethics Committee on Animal Use - CEUA from UFMG, protocol number 310/2017). Hematological parameters such as hemoglobin (HGB), number of red blood cells (RBC), hematocrit (HTC), platelets (PLT) total white blood cells (WBC), granulocytes and non-granulocytes were evaluated for each group. For biochemical analysis, blood was centrifuged (1100 g, 15 min) and the plasma obtained was frozen at −70 °C. The tests were performed in the Bioplus BIO-2000 semiautomatic analyzer (São Paulo, Brazil) using commercial kits (Labtest, Lagoa Santa, Brazil). Renal function was evaluated by the measurement of urea and creatinine; liver function by determination alanine aminotransferase (ALT) and aspartate aminotransferase (AST) activity.

After collecting the blood, the mice were euthanized, then liver, spleen, and kidneys were removed for histopathologic evaluation. Organs were set in 10% (v/v) buffered formalin, then, they were embedded in paraffin blocks and a 4-μm thickness tissue was placed onto glass slides and stained with hematoxylin-eosin. Images of cross-sections were obtained for evaluation using a microcamera (Spot Insight Color, SPOT Imaging Solutions, Sterling Heights, Michigan, USA) attached to a microscope (Olympus BX-40, Olympus, Tokyo, Japan). SPOT software (version 3.4.5) was used for image analysis.

2.9 *Peripheral neuropathy evaluation*

PTX peripheral neurotoxicity from both formulations was evaluated by mechanical allodynia following a model of neuropathic pain induced by an antineoplastic (MORAIS et al., 2018). Mechanical allodynia was evaluated at the right hind paw of healthy female BALB/c mice using an electronic von Frey apparatus (Model EFF 301, Insight, Brazil). Initially, the mice were acclimatized at the experimental apparatus for 1 h per day during 2 days, and the

basal paw withdrawal threshold of each animal was determined (mean of three measurements). Afterward, PM/PTX or CrEL/EtOH/PTX (20 mg/kg) was administrated by the tail vein of mice (n=6) and mechanical allodynia was evaluated every 2 days during 14 days after administration.

2.10 *Antitumor activity*

Aliquots of 100 µL containing 5×10^6 4T1 cells in RPMI were injected subcutaneously into the right flank of female BALB/c mice (6-weeks old, 20.0 ± 2.0g). Tumor cells were allowed to grow for 7 days. When the tumor volume reached approximately 100 mm^3, animals were randomly divided into five experimental groups, six animals per group (saline 0.9% (w/w); CrEL/EtOH, CrEL/EtOH/PTX, blank PM and PM/PTX). Each treated animal received a cumulative dose of 70 mg/kg split into 7 administrations, or correspondent volume (control group), via the tail vein, each other day. The first day of treatment was considered day zero (D0) of the study. Antitumor activity was evaluated over 16 days and was based on the tumor volume and the tumor growth inhibition ratio determination, tumor-to-muscle ratio using the ^{99m}Tc-radiolabeled polymeric micelles. This study was approved by CEUA from UFMG with the protocol number 205/2013.

The tumor volume (V) was evaluated twice a week by the measurements of two orthogonal diameters (d1and d2) with a slide caliper (Mitutoyo, MIP/E-103), where d1 and d2 were the smallest and the largest perpendicular diameters, respectively, and it was calculated as follows: $v = d1^2 x\ d2 \times 0.5$ (MONTEIRO et al., 2019). Tumor growth was monitored before the treatment (D0) and prior to the administration of each dose. Mice body weight was also monitored at the same time. At the end of the experimental period (D16), the relative tumor volume (RTV) and the inhibition ratio (IR) for each experimental group was determined as follows in the equation 5 and 6, respectively.

$$RTV = \frac{\text{Tumor volume on D16}}{\text{Tumor volume on D0}} \qquad \text{Eq. 5}$$

$$IR(\%) = \frac{\text{mean RTV from each treatment}}{\text{mean RTV from control group}} x100 \qquad \text{Eq.6}$$

Ex vivo tumor-to-muscle ratio was also determined in order to evaluate viable tissue in the tumoral area. For this, at D16 mice received, intravenously, 37 MBq of ^{99m}Tc-DTPA-PM. At 4 h post-administration, mice were anesthetized with a mixture of ketamine (60mg/kg) and xylazine (8 mg/kg) and sacrificed. After euthanasia, muscle of contralateral flank and tumor of

the animal were collected, weighted and taken to an automatic scintillation apparatus to determine the radioactivity. Results were expressed as the percentage of injected dose per gram (%ID/g) of tissue.

2.11 *Treatment toxicity evaluation*

It was observed behavioral/clinical modifications, body weight, and peripherical neuropathy during treatment. At the end of treatment, a laboratory investigation was performed (hematological and biochemical) in animals blood.

2.12 *Statistical analysis*

Statistical analyses were performed using GraphPad Prism 5.0 software. The normality and homogeneity of the variance analysis were verified by D'Agostino-Pearson's and Bartlett's tests, respectively. The difference among experimental groups was tested using the one-way analysis of variance (ANOVA), followed by the Tukey's test. The hemolytic activity data were transformed as cubic root (variable). Differences were considered significant when p values were lower or equal to 0.05 (p <0.05).

3 Results

3.1 *Physicochemical characterization*

The results of the physicochemical characteristics of PM are presented in Table 3.1. No significant differences were observed among blank PM, PM/PTX, and PM-DTPA/PTX in mean diameter and zeta potential. Size distribution analysis of all formulations showed that over 99% of particles present less than 20nm, indicating uniformity in the particle size. About 100% of drug content (around 0.6 mg/mL) was encapsulated in both formulations containing PTX.

Table 3.1. Physicochemical characterization of PM formulations.

Sample	Mean diameter (nm)	Size distribution	Zeta potential (mV)	PTX content* (%)
Blank PM	10.4 ± 0.3	~99%, 7 to 18nm	-2.9 ± 1.3	-
PM/PTX	10.7 ± 0.8	~99% , 7 to 16nm	-3.0 ± 0.4	98 ± 5
PM-DTPA/PTX (99:1)	9.5 ± 0.8	~99%, 6 to 16nm	-2.4 ± 1.2	99 ± 8

*PTX content is the percentage encapsulated from an initial concentration of 0.6 mg/mL. Data represent the mean ± standard deviation (n=3).

3.2 *Stability of PTX in PM after dilution*

The amount of PTX released from PM over time was analyzed to evaluate the stability after dilution and compared with the CrEL/EtOH/PTX formulation (Fig. 3.2). The data indicate that PM is able to control drug release overtime. From 30 min, the release of PTX from PM was significantly lower ($p < 0.05$) than CrEL/EtOH/PTX. Besides, after 6h, CrEL/EtOH/PTX released around 66% of the drug against approximately 16% released from the PM. Thus, these data suggest that the micellar dispersion for CrEL/EtOH is less stable after dilution compared to the studied PM.

Figure 3.2. Evaluation of PTX released from PM/PTX and CrEL/EtOH/PTX formulations overtime after dilution in PBS pH7.4.

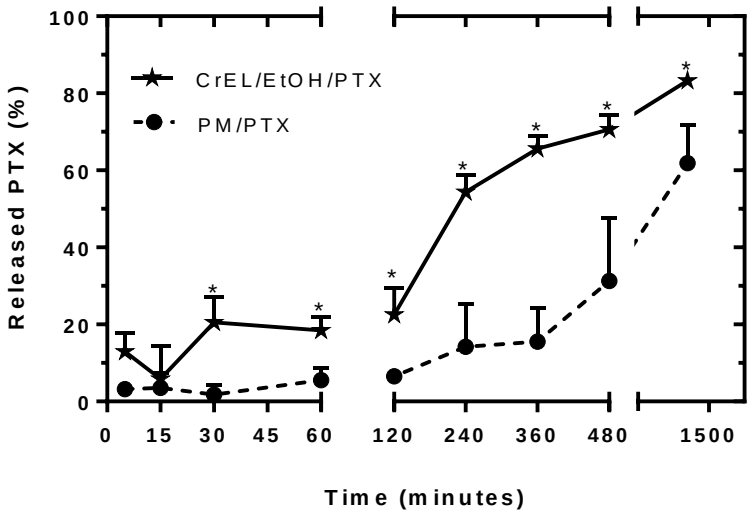

* Represents significant difference when compared to the PM/PTX at the respective time ($p \leq 0.05$).

3.3 *Cellular uptake of DTPA-PM/PTX and CrEL/EtOH/PTX*

The results of cellular uptake of ^{99m}Tc-radiolabeled nanosystems and the drug content are shown in Fig. 3.3. A higher uptake ($p \leq 0.05$) of ^{99m}Tc-CrEL/EtOH/PTX formulation at incubation times of 15 (2.4 ± 0.6%) and 30 (2.4 ± 0.2%) minutes when compared to ^{99m}Tc-DTPA-PM/PTX (1.0 ± 0.2% and 1.2 ± 0.1%, respectively) was observed (Fig. 2A), although no differences between them were found after 60 minutes. In contrast, a higher amount of PTX ($p \leq 0.05$) in the 4T1 cells was observed for PM/PTX throughout the study.

Figure 3.3. PTX and 99mTc-labeled formulation uptake in 4T1 tumor cells.

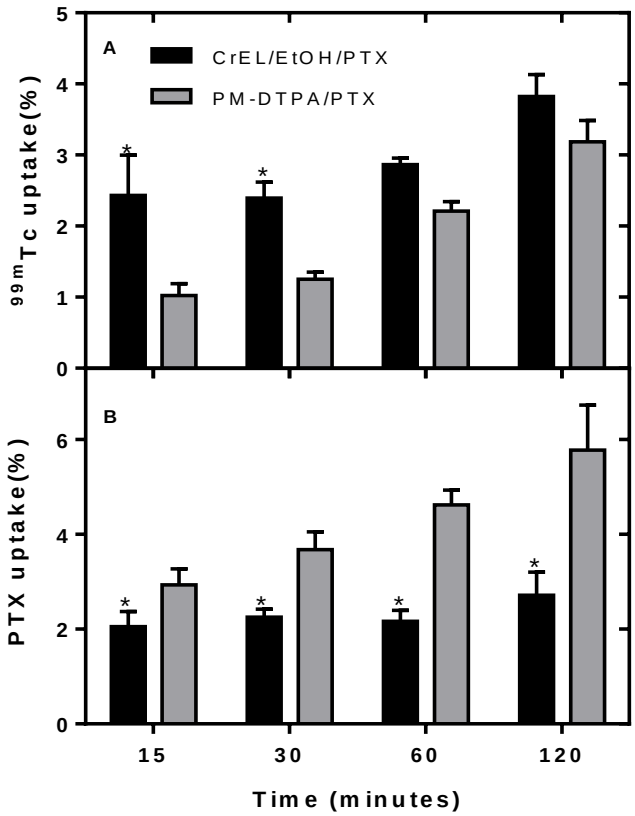

*Represents significant difference when compared with PM/PTX in the respective time ($p \leq 0.05$). Data were expressed as the mean ± standard deviation, n=5.

3.4 *Hemocompatibility evaluation*

Hemolytic studies were performed on the PM/PTX and CrEL/EtOH/PTX, as well as their respective vehicles, as can be seen in Fig. 3.4. The results were classified as non-hemolytic (up to 2% hemolysis), moderately hemolytic (above 2% and less than 5%) and hemolytic (more than 5%) as recommended by the International protocol E2524-08 of American Society for Testing and Materials (DOBROVOLSKAIA; MCNEIL, 2013).

The comparison of the hemolytic activity among all the groups in the same concentration showed that CrEL/EtOH was significantly ($p < 0.05$) more hemolytic than PM, except at the smallest concentration. CrEL/EtOH/PTX was classified as highly hemolytic (6% and 16% for 0.05 and 0.10 mg/mL, respectively) and the vehicle at the same dilution showed moderate hemolytic activity (4% of hemolysis) at the concentration of 0.10 mg/mL. On the other hand, incorporating PTX into PM, the hemolysis was remarkably reduced to values lower than 0.5% in both concentrations. The hemolytic activity observed for blank PM at the same dilution was also less than 0.5%. Thus, the values obtained for PM containing or not PTX are considered predictive of low toxicity.

Figure 3.4. Hemolytic toxicity of PM and CrEL/EtOH micelles containing or not PTX.

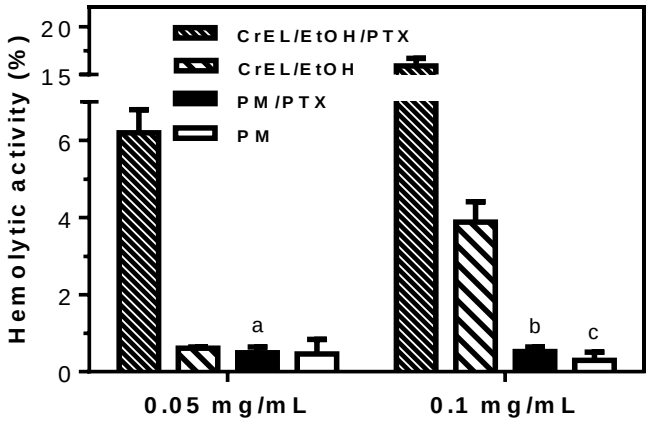

Data were expressed as the mean ± standard error mean, n=5. [a]Represents significant difference when compared to CrEL/EtOH/PTX 0.05mg/mL. [b] Represents significant difference when compared to CrEL/EtOH/PTX 0.1 mg/mL. [c] Represents significant difference when compared to CrEL/EtOH 0.1 mg/mL

3.5 *Acute toxicity*

Hematological investigation of a single dose of PM/PTX and CrEL/EtOH/PTX was compared to healthy mice blood and the data are shown in Table 3.2. RBC, hemoglobin, hematocrit, and platelets levels were similar in both groups and presented no significant difference ($p > 0.05$) when compared to the control group (healthy mice). In addition, there was no change in leucocytes series for all groups.

Biochemical parameters indicative of renal (urea and creatinine) and hepatic (ALT and AST) toxicity are also presented in Table 3.2. Hepatic parameters did not show significant changes among groups. CrEL/EtOH/PTX group presented a significant increase in the urea levels compared to PM/PTX and control group. The creatinine values in both treated groups were significantly different from the control group. By calculating the index urea/creatinine, the results suggest an initial renal toxicity for the treated groups since it was about 2.7 and 2.0-fold higher than the control group. However, the value obtained for the PM/PTX group was significantly lower than that of CrEL/EtOH/PTX group. Nevertheless, no histological alteration was observed in the renal tissue of the mice treated with different formulations containing PTX (data not shown).

Table 3.2. Hematological and biochemical parameters obtained at 14 days after treatment with a single dose of PTX formulations.

Parameters	Healthy mice	CrEL/EtOH/PTX	PM/PTX
RBC ($x10^6/\mu L$)	6.8 ± 0.2	6.4 ± 0.3	6.5 ± 0.3
HGB (g/dL)	13.4 ± 0.5	12.6 ± 0.9	12.4 ± 0.9
HCT (%)	33.4 ± 1.1	32.0 ± 1.9	32.9 ± 1.4
PLT ($x10^3/\mu L$)	396.5 ± 113.8	329.0 ± 63.1	316.8 ± 30.1
WBC ($x10^3/\mu L$)	6.17 ± 1.27	6.56 ± 0.88	5.30 ± 0.71
Granulocytes ($x10^3/\mu L$)	2.27 ± 0.21	2.82 ± 0.38	2.33 ± 0.44
Non-granulocytes ($x10^3/\mu L$)	3.90 ± 1.08	3.74 ± 0.63	2.97 ± 0.37[a]
Urea (mg/dL)	33.4 ± 3.7	51.8 ± 6.0 [a,b]	40.5 ± 4.7
Creatinine (mg/dL)	0.38 ± 0.07	0.22 ± 0.05[b]	0.23 ± 0.04[b]
Blood urea/creatinine	90.8 ± 23.1	247.6 ± 44.8[a,b]	178.3 ± 29.1 [b]
ALT (U/L)	42.8 ± 3.8	35.1 ± 3.7	35.8 ± 7.8
AST (U/L)	95.7 ± 23.5	83.8 ± 22.9	87.4 ± 15.5

Results were expressed as mean ± standard deviation. [a] Represents significant difference when compared to PM/PTX group ($p \leq 0.05$). [b] Represents significant difference when compared to healthy mice group ($p \leq 0.05$). Abrev.: HGB (hemoglobin), RBC (red blood cells), (HTC) hematocrit, PLT (platelets), WBC (total white blood cells), ALT (alanine aminotransferase), and AST (aspartate aminotransferase).

Concerning the body weight, no significant variation over time was observed in both studied groups ($p > 0.05$), as is shown in Fig. 3.5A. A slight weight loss only in CrEL/EtOH/PTX group at 2 days after drug administration was observed, but at the end of the study, all groups presented a weight gain. Absence of mortality or clinical toxicity signs such as prostration and intense piloerection were observed in all groups.

The appearance of toxicity in the form of neuropathic pain was also evaluated in BALB/c mice after a single dose (20 mg/kg) of PM/PTX and CrEL/EtOH/PTX using mechanical allodynia method (Fig. 3.5B). After 2 days from the dose administration, CrEL/EtOH/PTX group has already presented a reduction in the nociceptive threshold, indicating neuropathic pain, and within the first eight days of treatment, the nociceptive threshold was remarkably reduced. By contrast, no significant ($p > 0.05$) change over time was observed in PM/PTX group. This data suggests that PM had a protective effect against the PTX-induced peripheral neuropathy.

Figure 3.5. In vivo evaluation of (A) percentage of body weight variation and (B) mechanical allodynia in BALB/c mice after administration of a single dose (20 mg/kg) of two different formulations containing PTX.

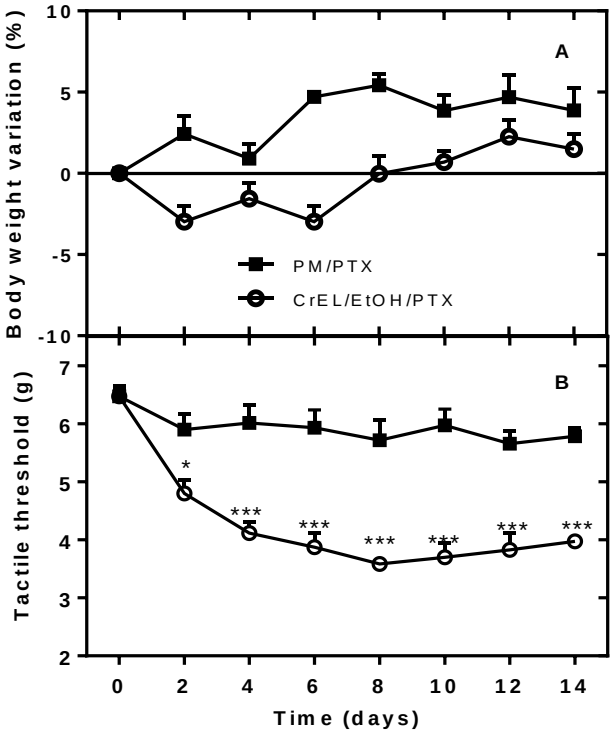

Data were expressed as mean ± standard error mean. *Represents significant difference when compared to PM/PTX group, $p < 0.05$, *** $p < 0.001$ (n=7).

3.5. Antitumor activity

The antitumor efficacy was evaluated in 4T1 tumor-bearing BALB/c mice after treatment with a total dose of 70 mg/kg of PTX. Tumor volume was measured each other day. Although we evaluated control groups for each treatment formulations (blank formulations), no significant difference among these control groups could be observed, thus, only the data from the saline group were presented as the control group in Fig. 5A. In order to detect the changes in the tumor growth after treatment with the different PTX formulations, regression analysis was also performed. The best-fit models and their respective determination coefficients are shown in Table 3.3. Although the same mathematical model fits (first-order) have been obtained for all groups, the analyses of intercept and inclination were significantly different in all groups, suggesting that the tumor growth was altered by treatment. These data are in accordance with the IR data, which showed that both treatments were able to reduce tumor growth when compared to control group, however, PM/PTX group presented a higher IR (approximately 1.5-fold) than CrEL/EtOH/PTX (Table 3.3).

In addition, the *ex-vivo* tumor-to-muscle ratio evaluation also demonstrated the high efficacy of PM/PTX compared to CrEL/EtOH/PTX. As can be seen in Table 3.3, a significant reduction on the uptake in the tumor area could be observed for the PM/PTX group in comparison to CrEL/EtOH/PTX and control groups (p <0.05).

Table 3.3. Parameters of the antitumor evaluation of PTX treatments in 4T1 tumor-bearing BALB/c mice.

Group	Regression model	R^2	RTV	IR (%)	Tumor-to-muscle ratio
Saline 0.9% (w/w)	Y = 124.8X - 882.4	0.8486	16.3 ± 1.4	-	1.97 ± 0.40
CrEL/EtOH/PTX	Y = 62.26X - 387.7	0.8822	11.7 ± 1.2	29	1.81 ± 0.50
PM/PTX	Y = 45.23X - 264.9	0.9284	9.5 ± 1.3	42	1.05 ± 0.22[a]

Data were expressed as mean ± standard deviation. [a] Represents significant difference when compared to other groups (p < 0.05). Abbreviations: RTV - Relative Tumor Volume; IR – Inhibition Ratio.

Figure 3.6 Evaluation of (A) tumor volume, (B) percentage of body weight variation and (C) mechanical allodynia evaluation, in 4T1 tumor-bearing BALB/c mice after treatment.

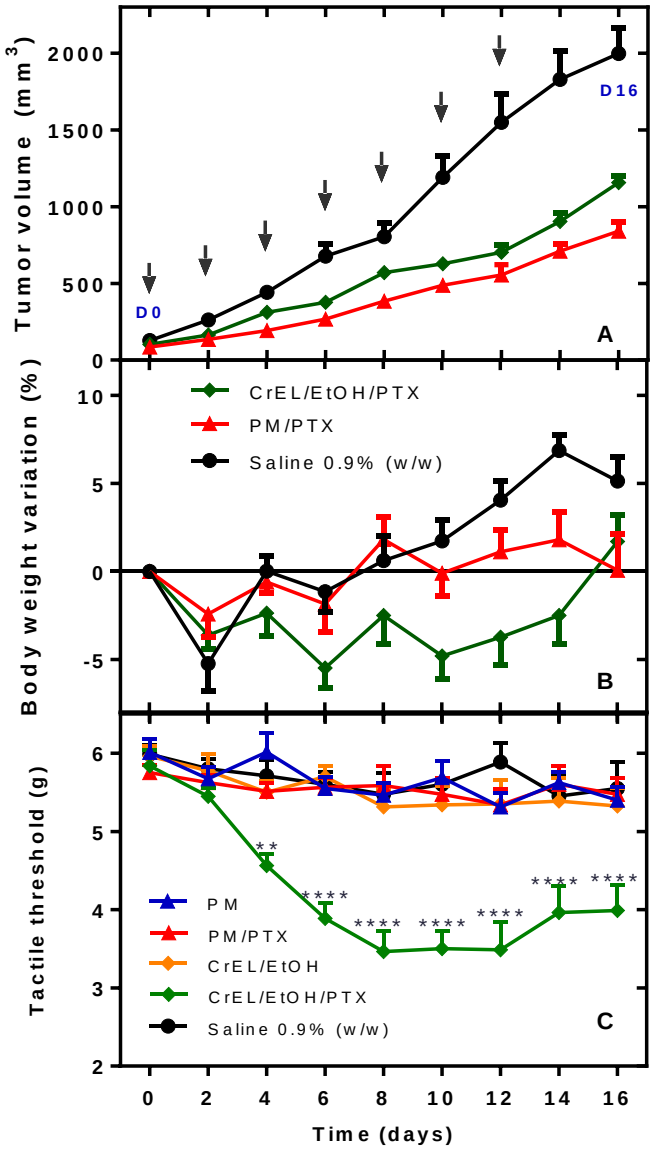

Arrows in (A) indicate the days of treatment. Data were expressed as mean ± standard error mean. *Represents significant difference when compared to other groups at the respective time **(p <0.01), ****(p <0.0001).

In these experimental groups, we also evaluated the effect of the treatment in the toxicity parameters. Behavioral observation of the animals showed that CrEL/EtOH/PTX group presented more stressed than other groups. The percentage of weight variation of the animals during treatment is presented in Fig. 3.6B. As can be observed, the CrEL/EtOH/PTX group presented a body weight loss until the 14th day of monitoring, while the other groups showed

an initial body weight reduction, nevertheless no significant difference at the end of the experiment was observed.

Hematological and biochemical parameters of PM/PTX, CrEL/EtOH/PTX, and saline groups are shown in Table 3.4. No significant difference was observed among groups in hematological parameters. However, the comparison of these data with those obtained from healthy mice without treatment (Table 3.2) demonstrated a substantial increase in WBC (around 6 x 10^3 cell/µL *versus* 100 x 10^3 cell/µL). By contrast, no difference was observed in hepatic and renal function parameters (p >0.05).

Tabela 3.4. Hematological and biochemical parameters of tumor-bearing BALB/c mice treated with cumulative doses of PTX formulations.

Parameter	Saline 0.9 (w/w)	CrEL/EtOH/PTX	PM/PTX
RBC ($x10^6/\mu L$)	6.5 ± 0.5	5.4 ± 1.0	5.8 ± 0.8
HGB (g/dL)	13.3 ± 1.5	11.3 ± 2.8	12.0 ± 2.2
HCT (%)	31.7 ± 2.8	28.1 ± 5.5	30.1 ± 4.5
PLT ($x10^3/\mu L$)	453.0 ± 112.3	363.2 ± 159.1	393.3 ± 158.6
WBC ($x10^3/\mu L$)	94.4 ± 26.3	113.5 ± 5.4	106.2 ± 6.2
Granulocytes ($x10^3/\mu L$)	85.8 ± 26.3	101.1 ± 15.4	100.5 ± 5.3
Non-granulocytes ($x10^3/\mu L$)	8.6 ± 1.9	6.2 ± 0.8	5.8 ± 1.0
Urea (mg/dL)	48.1 ± 8.2	53.5 ± 12.1	45.0 ± 3.0
Creatinine (mg/dL)	0.36 ±0.05	0.36 ± 0.06	0.32 ± 0.04
ALT (U/L)	36.3 ± 6.4	33.0 ± 7.2	32.5 ± 5.5
AST (U/L)	142.9 ± 11.2	147.3 ± 15.3	178.5 ± 26.7

Data are expressed as mean ± standart deviation.

Peripheral neuropathy of repeated doses of PM/PTX and CrEL/EtOH/PTX were also evaluated. As can be observed in Fig. 3.6C, only CrEL/EtOH/PTX sensitized tumor-bearing BALB/c mice, leading to a significant reduction in the nociceptive threshold in these animals. Formulations vehicles (blank PM and CrEL/EtOH) were also evaluated to verify if they contribute to the sensitization. However, none of them affected mice basal tactile threshold, suggesting that the neuropathic pain is indeed caused by PTX. Thus, these data reinforce the hypothesis that PM had a protective effect on the peripheral neuropathy induced by PTX.

CAPÍTULO 3

4. Discussion

PTX as a single agent or in combination with other chemotherapeutic drug is frequently used in the treatment of metastatic breast cancer and other types of solid tumors (WEAVER; BEMENT, 2014). Despite the effective activity achieved with CrEL-based PTX formulation, this solvent is often associated with severe toxicities. In addition, it cannot prevent the unspecific PTX side effects, such as neutropenia, anemia, and hair loss or other more limiting which include bone marrow suppression and neurotoxicity, the major dose-limiting PTX toxicity (BERNABEU et al., 2017). An ideal PTX formulation requires stability after dilution, no systemic toxicity or hypersensitivity reactions besides specific and high accumulation in the tumor region. Drug delivery nanosystems are promising tools to overcome these issues and have been widely studied leading to heavy investments of pharmaceutical and biotech companies (SOFIAS et al., 2017) [HAN S. ET AL., 2018;]. New PTX formulations nanotechnology-based were approved recently for clinical applications, such as Abraxane™ (PTX albumin-bound nanoparticle) and Genexol-PM™ (polymeric micelles containing PTX)(ZHANG; MEI; FENG, 2013). Enhanced cytotoxic activity against some cancer cells has been reported, however, myelosuppression and sensory neuropathy are adverse effects often related to the use of these nanoformulations (DESAI et al., 2006; GRADISHAR, 2006). Thus, we developed lipid-polymer PM composed of DSPE-PEG_{2000} to carrier the PTX and evaluated the advantages of this system to treat tumors as well as to reduce the toxicity compared to CrEL-based PTX formulation.

The PM/PTX proposed in this study for intravenous administration presented a narrow size distribution of approximately 10nm and neutral zeta potential. These characteristics are important since they can favor the increase of blood circulation time and lead to accumulation in the tumor tissue by EPR effect (JOKERST et al., 2012; MAEDA, 2010). PM/PTX presented better stability after dilution than CrEL/EtOH/PTX within 24 hours studied. This fact was evidenced at 2 hours after dilution since a rapid release of PTX from CrEL/EtOH, around 4-fold higher than PM, was observed. This finding suggests that the PM are suitable as a delivery system and they are not disrupted after dilution as occur in the bloodstream dilution. Additionally, 4T1 uptake studies indicated that PM/PTX deliver a high amount of drug to cells. On the other hand, although the nanoparticle uptake pathway cannot be predicted by this study, data suggest that the uptake of the two systems involves different pathways of cellular internalization once they present different uptake profiles over time. It is known that some nanoparticles properties, such as size, zeta potential, and composition are directly related to the

cellular uptake mechanism of these systems (CHEN et al., 2016; JIANG et al., 2015). However, PM presented similar size (10 nm) of CrEL-based micelles as previously described by Monteiro et al. (MONTEIRO et al., 2017). Therefore, probably the composition of the systems was the main parameter that affected the uptake mechanism of each formulation.

Since the intravenous route is the main choice for the administration of PTX due to its low oral absorption, we firstly evaluated the potential of the PM/PTX to reduce hemolytic toxicity (BARBUTI; CHEN, 2015). It is well-described that after administering pharmaceutical formulations by the intravenous pathway, they unavoidably interact with RBC, thus the hemolytic activity study can be a good indication for the toxicity of the developed formulation (DOBROVOLSKAIA; MCNEIL, 2013; SERRANO et al., 2013). This study evidenced that PM, containing or not PTX, did not cause lysis of RBC, whereas CrEL/EtOH/PTX was classified as hemolytic at the lower concentration evaluated, suggesting that PM is safer as a PTX carrier than CrEL/EtOH. *In vivo* toxicity studies were also performed in healthy mice, after injecting IV a high and single dose of PTX. An important observation verified immediately after CrEL/EtOH/PTX administration was the aggressiveness followed by weakness and inability to move off the mice. Similar behavior has already been reported by Rabah (RABAH, 2010). By contrast, these effects did not occur in mice treated with PM/PTX. We supposed that this behavior was due to the presence of the CrEL that can cause many side-effects, including tachycardia and hypotension (GELDERBLOM et al., 2001). Besides, the biochemical analysis indicated early nephrotoxicity in both treated groups verified by an increased in the urea/creatinine index compared to the control. This index is a good parameter to indicate early renal damage when there is no apparent reduction in the glomerular filtration rate, but there is some tubular damage, reflecting in an alteration only in the urea levels. As kidney injury is common toxicity of PTX, it is interesting to note that the nephrotoxicity was more pronounced in CrEL/EtOH/PTX group, evidenced by a significant increase in urea levels compared to control (BAEK; CHO, 2015; RABAH, 2010).

It is also well-known that PTX leads to axonal degeneration in peripheral sensory nerves causing neuropathy, which is dose-limiting. This effect has substantially worsened the quality of patients' life due to clinical manifestations as painful paresthesia or numbness, sensory ataxia, gait disturbance, and weakness (KAMEI et al., 2017; LI et al., 2018; TSUBAKI; TAKEDA; MATSUMOTO, 2018). In this sense, we also evaluated the induction of neuropathic pain by mechanic allodynia after administrating of PTX in different formulations. As shown in Fig. 5C, reduction of the tactile threshold was just observed for CrEL/EtOH/PTX group and it

was sustained during 14 days of observation. These results strongly suggest that PM formulations could prevent CIPN, one of the major side effects of PTX (KAMEI et al., 2017).

In order to verify whether the incorporation of PTX in PM affect the antitumor activity, 4T1 tumor-bearing mice were treated with repeated doses of PTX formulations. Parameters of antitumor activity and toxicity were evaluated. Regarding antitumor activity, PM/PTX was more effective than CrEL formulation in controlling tumor growth. In previous studies, we have already shown that DSPE-PEG PM has the property to accumulate in tumor site (ODA et al., 2017a). In this way, we believe that due to the superior stability after dilution and higher uptake by 4T1 cells, PM are capable of delivering more PTX inside the tumor than CrEL micelles, resulting in higher effectiveness. Additionally, PM/PTX still seems to be safer than CrEL/EtOH/PTX even when repeated doses are given. Similarly as observed in the acute toxicity, the mice treated with CrEL/EtOH were visible more irritated and the decrease of body weight was also attributed to the toxic effect of the formulation. Even though the hematological and biochemical parameters of PTX- treated groups did not differ from the saline 0.9% (w/w) group, especially the WBC count considerably differ from healthy mice (Table 3.2). These alterations might be attributed to the mammary 4T1 tumor experimental model. Some studies show that tumors from the 4T1 cells are associated with an increased level of granulocytes in the bloodstream, characterizing a leukemoid reaction due to the progression tumor (DUPRE; REDELMAN; HUNTER, 2007; HEPPNER; MILLER; SHEKHAR, 2000) .

Again, neuropathic pain was evaluated in this study, to verify whether blank formulations or the tumor (evaluated by the saline group) has some contribution in the mice sensitization. It was observed that all control groups were not able to induce a decrease in the tactile threshold, while this effect was clearly observed in the CrEL/EtOH/PTX group, suggesting that PTX is responsible for causing the neuropathic pain. On the other hand, the absence of this effect in PM/PTX group corroborates the hypothesis that PM acts as a carrier for the PTX, preventing non-specific action that results in less occurrence of side effects. As described before, the peripheral neurotoxicity is currently one of the main drawbacks of the PTX formulations. In spite of the advantages reported by using of PTX nanoformulation, such as Abraxane™, this side effect still limits the therapy (BLAIR; DEEKS, 2017; SOFIAS et al., 2017; TSUBAKI; TAKEDA; MATSUMOTO, 2018). Therefore, PM/PTX prepared in this study showed better performance than CrEL/EtOH, which was evidenced by the high effectiveness associated with the complete absence of peripheral neuropathy which could result in a better therapeutic response for antitumor therapy approaches.

5. Conclusion

Our results showed that PM/PTX were more efficacious and less toxic than the conventional formulation. Physically it proves itself more stable than CrEL/EtOH/PTX after diluting, indicating that PM will not disassemble immediately once in the bloodstream, and so increasing probability of drug delivery in tumor site by EPR effect. Since it is more stable, PTX will be less available to unspecific effects, which was reflected in less toxicity when PM/PTX was used, including in preventing peripheral neurotoxicity. Besides that, PM/PTX also presented a better antitumor activity than CrEL/EtOH/PTX. In this way, we can infer that this kind of nanocarrier has great potential to be clinically used as a way to reduce PTX toxicity.

ACKNOWLEDGEMENTS

The authors thank Conselho Nacional de Desenvolvimento Científico e Tecnológico (CNPq-Brazil), Fundação de Amparo à Pesquisa do Estado de Minas Gerais (FAPEMIG-Brazil), and Coordenação de Aperfeiçoamento de Pessoal de Nível Superior (CAPES) for their financial support and fellowships.

CONFLICTS OF INTEREST

There are no conflicts of interest.

5 DISCUSSÃO GERAL

O PTX é um dos agentes antitumorais mais utilizados na prática clínica uma vez que ele apresenta eficácia no tratamento de diversos tipos de câncer, inclusive em casos metastáticos de câncer de mama. A importância do PTX é tamanha que a busca por preparações menos tóxicas e, por conseguinte, mais efetivas é muito grande. No entanto, o PTX apresenta um log P próximo a 3,9, o que dificulta a sua solubilização e, somente uma mistura de Cremophor EL e etanol anidro foi capaz de permitir inicialmente sua veiculação para administração por via endovenosa. A formulação mais comercializada mundialmente, na qual o PTX é dissolvido nessa mistura, é o Taxol®. Contudo inúmeros relatos de toxicidade decorrente tanto do fármaco quanto do veículo têm sido reportados limitando, muitas vezes, sua aplicação clínica. Diante disso, existe uma evidente importância da aplicação da nanotecnologia como um recurso para viabilizar a veiculação desse fármaco de maneira eficaz e mais segura. Pensando nesse recurso como uma estratégia para o PTX, preparações farmacêuticas inovadoras estão disponíveis no mercado, dentre elas Abraxane®, Lipusu® e Genexol-PM®. No entanto, como mencionado anteriormente nesse documento, esses sistemas ainda carecem de melhorias principalmente em relação à segurança do paciente.

Entretanto, sabe-se que muitas etapas estão envolvidas no desenvolvimento de um novo medicamento até chegar efetivamente no seu uso clínico. E quando se trata da aplicação de um nanocarreador, o número de etapas é ainda maior, devido à natureza coloidal e à complexidade de constituintes que compõem as formulações.

Baseando-se no exposto acima, nosso grupo de pesquisa desenvolveu micelas lipídico-poliméricas de DSPE-PEG funcionalizadas (DSPE-PEG/DSPE-PEG-DTPA) como um sistema versátil que possibilitasse entregar fármacos antitumorais como o PTX na região tumoral e/ou também agentes de imagem como o ^{99m}Tc (ODA et al., 2017). A proposta foi delinear um sistema e investigar sua utilização como uma nanoplataforma para terapia e diagnóstico de tumores sólidos. Do ponto de vista biológico, esse sistema apresentou propriedades promissoras de acumular na região tumoral e tempo de circulação prolongado. Todavia, durante as etapas de desenvolvimento, observou-se uma instabilidade do sistema, principalmente quando concentrações próximas a 1,0 mg/mL de PTX foram utilizadas, demonstrando uma limitação em se encapsular grandes quantidades desse fármaco. Além disso, embora tenha sido observado acúmulo na região tumoral, o potencial terapêutico desse novo sistema no tratamento de câncer

de mama bem como a sua influência na redução da toxicidade, frequentemente observada com o tratamento com o PTX, ainda eram pontos a serem explorados.

Dessa maneira, esse trabalho de tese de doutorado foi delineado no intuito de responder os seguintes questionamentos:

1. Como ocorre a organização da ultraestrutura das micelas de DSPE-PEG após a encapsulação do PTX e como essa influencia na estabilidade do sistema?
2. Existe alguma correlação entre a organização estrutural e o comportamento biológico desse sistema?
3. Como melhorar a estabilidade de encapsulação do PTX?
4. Esse sistema micelar apresenta vantagens quanto a efetividade antitumoral em comparação à formulação contendo Cremophor®?
5. Em relação à toxicidade, o sistema proposto é mais seguro de fato?

As etapas iniciais do estudo foram focadas na obtenção de parâmetros físico-químicos que nos permitissem compreender a organização do sistema, ao nível molecular e supramolecular, uma vez que essa é de extrema importância para a caracterização de sistemas coloidais. No entanto, sabe-se que em função da complexidade de tais sistemas, a caracterização físico-química dessas nanoestruturas é tecnicamente complexa de ser realizada e a associação de diferentes técnicas faz-se necessária. Nesse estudo, alguns questionamentos que não puderam ser esclarecidos a partir de técnicas convencionais, como DLS e técnicas de microscopia, foram melhor compreendidos mediante o uso de técnicas mais complexas como AF4 e SAXS. A análise por DLS permitiu-nos estimar o diâmetro das partículas, porém, não foi possível verificar mudanças nesse parâmetro quando as formulações avaliadas continham PTX. Alguns estudos demonstram claramente que a presença de um fármaco no núcleo hidrofóbico de DSPE resulta em um aumento do diâmetro médio da micela (AHN et al., 2014; EAWSAKUL et al., 2017; WORAPHATPHADUNG et al., 2018). Ao avaliar os dados de SAXS, nós constamos que o PTX altera a organização do sistema, influenciando as interações entre os componentes da micela, e promove um aumento do núcleo micelar e um "encolhimento" das cadeias de PEG e, por conseguinte, há uma redução da espessura da "casca" micelar. Dessa maneira, o diâmetro das partículas praticamente não foi alterado. Verificou-se ainda que essas mudanças eram proporcionais e dependiam da quantidade de fármaco encapsulado. Quando correlacionado com os dados *in vivo*, essa variação na conformação das cadeias de PEG, forma de escova para micelas brancas e cogumelo para micelas contendo PTX resultou em diferenças no comportamento biológico, especificamente, no tempo de circulação sanguínea das partículas.

Sabe-se que uma maior camada de solvatação é obtida quando o PEG está na conformação de escova, e isso resulta em menor interação das nanopartículas com proteínas plasmáticas dificultando o reconhecimento pelas células do SFM (CHEN et al., 2004; JOKERST et al., 2012).

Com relação à influência da organização micelar na encapsulação e retenção do PTX, os dados claramente mostraram que ocorre uma saturação do núcleo após a concentração de 0,6 mg/mL de PTX uma vez que em concentrações superiores o sistema se desestabiliza. No entanto, mesmo na concentração de 0,6 mg/mL, o tempo que o fármaco permaneceu retido foi relativamente curto (em média 7 dias). Sabe-se que a presença de água tem papel central na instabilidade das preparações farmacêuticas, sendo a liofilização, um processo com elevado potencial para aumentar a estabilidade e o tempo de armazenamento, além de reduzir consideravelmente a probabilidade de crescimento microbiano (FONTE et al., 2014; MIYAJIMA, 1997) Dessa forma, a preparação de um liófilo de micelas de DSPE-PEG/DSPE-PEG-DTPA para reconstituição no momento do uso foi a estratégia adotada. Essa proposta foi elaborada de maneira a manter o PTX no interior das micelas por mais tempo, mas também no intuito de favorecer a rotina de preparação do sistema teranóstico proposto. Isso porque um kit de radiofármaco de preparo simples diminui a probabilidade de erros durante o processo de radiomarcação, assegurando um preparo mais robusto e rápido (DE BARROS et al., 2012b; ZHAO; LI, 2012). Dessa maneira, desenvolvemos um kit que envolve somente duas simples etapas de preparo, sendo a primeira, a reconstituição por meio da adição de água ultrapura, e a segunda, uma purificação do sistema utilizando filtração em filtro de 0,22 μm. Esse kit foi capaz de manter a concentração de PTX por até 180 dias e outras características como tamanho, potencial zeta, radiomarcação eficiente e estável.

Alcançada uma alternativa para os problemas de estabilidade do fármaco encapsulado nas MP e tendo em vista que as principais preocupações e limitações quanto ao uso clínico do PTX, diz respeito aos efeitos tóxicos relacionados a ele próprio e a presença do Cremophor EL na formulação (YANG; HORWITZ, 2017), decidimos conduzir um estudo de avaliação pré-clínica para verificar a toxicidade e a atividade antitumoral da formulação estudada. Este estudo foi realizado utilizando como referência a formulação similar ao Taxol®, preparada com Cremophor EL e etanol desidratado. Os dados de avaliação *in vitro* mostraram que as MP/PTX possuem menor atividade hemolítica e apresentam maior potencial para entregar o fármaco para células de tumor de mama murino triplo negativo comparado com a formulação de Cremophor EL. Além disso, o sistema proposto foi mais estável após diluição liberando o PTX mais lentamente. Nossa hipótese era que essa maior estabilidade possivelmente resultaria em maior

tempo de circulação sanguínea, permitindo um direcionamento passivo das nanoestruturas para a região tumoral e acúmulo das mesmas via efeito EPR. Essa hipótese foi reforçada ao observarmos que realmente o kit desenvolvido foi capaz de acumular mais eficientemente na região tumoral de camundongos BALB/c contendo tumor de mama 4T1. Consequentemente, maior atividade antitumoral foi observada para o sistema proposto comparada à formulação semelhante ao Taxol®.

Por outro lado, por serem mais estáveis após diluição, além de apresentarem uma composição considerada biossegura, as MP de DSPE-PEG evitaram o efeito tóxico de neuropatia periférica causada pelo PTX. Esse achado é de extrema importância, uma vez que este efeito adverso é um dos mais limitantes do uso clínico no PTX (KAMEI et al., 2017; PENG et al., 2017)(KAMEI, J. *et al*., 2017; PENG, L. *et al.*, 2015).

O esquema apresentado na Figura 8 sumariza os principais resultados obtidos nesse estudo:

1) PTX aumenta núcleo hidrofóbico e promove encolhimento das cadeias de PEG.

2) Tamanho das MP não variam com a adição de PTX.

3) Concentração máxima de PTX encapsulada e estável nas micelas foi 0,6mg/mL.

4) MP funcionalizadas com DTPA contendo PTX foram liofilizadas para preparação de um kit com estabilidade quanto as propriedades físico-químicas e de radiomarcação por até 180 dias.

5) MP/PTX do kit liofilizado, após 180 dias de armazenamento, mantiveram as propriedades de acúmulo na região tumoral de camundongos.

6) MP/PTX apresentaram estabilidade após diluição significativamente superior à formulação de Cremophor®.

7) Estudos *in vitro* mostraram que as MP são capazes de entregar mais PTX para células 4T1.

8) Estudos *in vivo* de toxicidade mostraram que as MP/PTX foram seguras para administração intravenosa, inclusive quanto à neurotoxicidade periférica.

9) Estudos de atividade antitumoral *in vivo* indicaram que as MP foram mais eficazes no modelo 4T1.

Sendo assim, o conjunto de dados apresentados no presente estudo, desde a avaliação estrutural até os testes *in vivo*, permite-nos concluir que é grande a potencialidade das MP para aplicação teranóstica no câncer.

Figura 8. Resumo dos principais resultados obtidos nesse estudo.

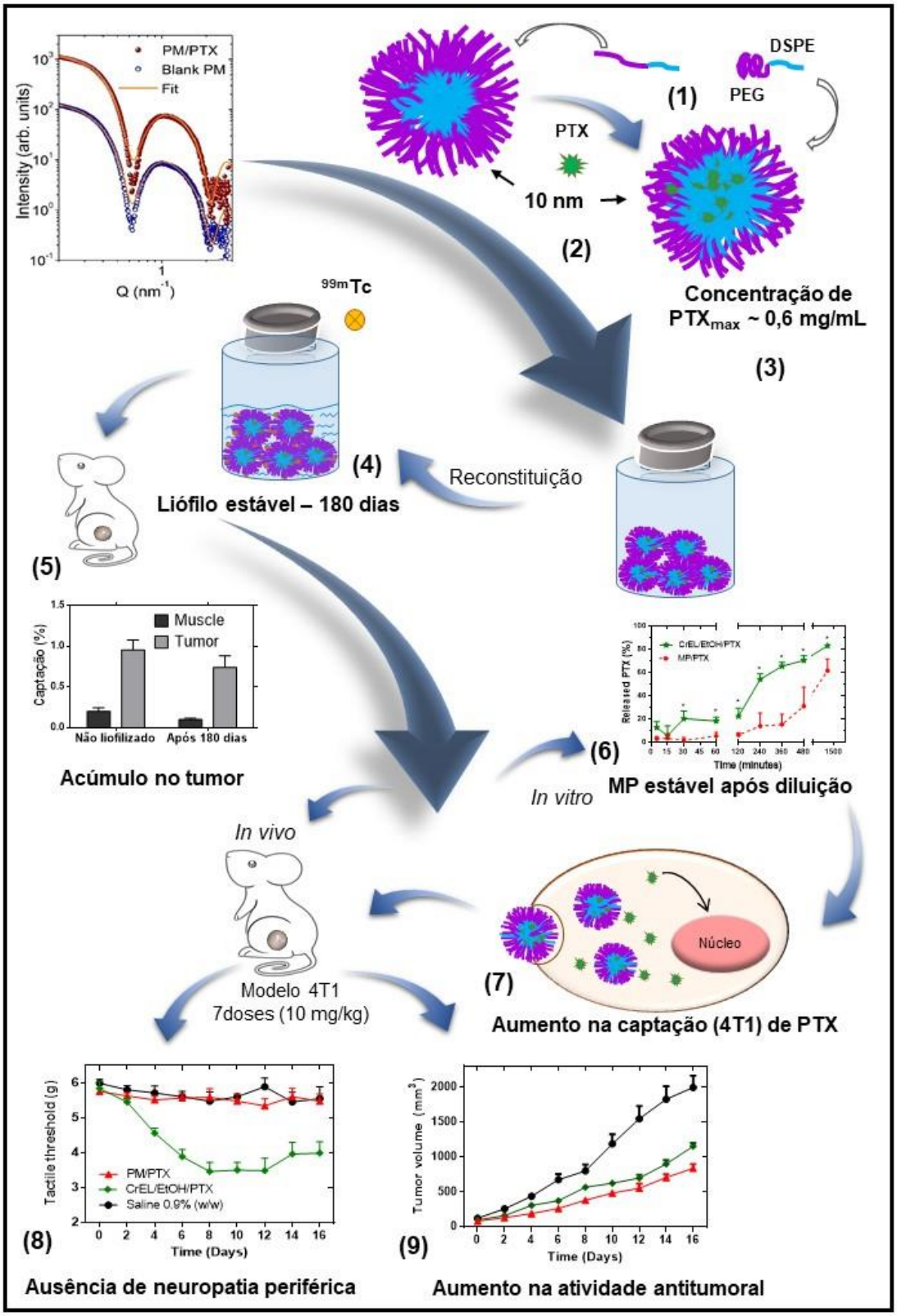

6 CONCLUSÃO GERAL

Esse trabalho representa um estudo aprofundado de uma formulação de PTX baseada em micelas poliméricas, a qual apresentou importantes propriedades biológicas, físicas e químicas vantajosas em relação à formulação de Cremophor e etanol, que é, ainda, a mais comercializada atualmente. Sendo assim, esse estudo apresentou informações de extrema importância para se compreender quais e onde estão as limitações desse sistema, norteando as perspectivas para a otimização das micelas de DSPE-PEG, que se mostraram promissoras como alternativa para a veiculação do PTX. Além disso, vale destacar o papel do sistema desenvolvido como uma potencial plataforma teranóstica, a qual permite carrear agentes de tratamento de tumores sólido e agentes de imagem, se apresentando como um recurso para diagnosticar, acompanhar o progresso do tratamento, e permitir uma terapia mais individualizada para o paciente.

7 PERSPECTIVAS

- Realizar estudos imunohistoquímicos no tecido tumoral para avaliar a atividade antitumoral das MP/PTX;
- Avaliar as vias de internalização das MP/PTX nas células;
- Aumentar a quantidade de PTX encapsulado nas micelas por meio da adição de componentes no núcleo que aumentem a capacidade do mesmo (micelas de composição mista);
- Verificar a estabilidade das micelas modificadas;
- Adicionar um direcionador tumoral na superfície das micelas;
- Avaliar as micelas em um modelo de câncer de mama humano.

REFERÊNCIAS BIBLIOGRÁFICAS

ABDALLA, A. M. E. et al. Current challenges of cancer anti-angiogenic therapy and the promise of nanotherapeutics. **Theranostics**, v. 8, n. 2, p. 533–549, 2018.

ABDELWAHED, W. et al. Freeze-drying of nanoparticles: Formulation, process and storage considerations. **Advanced Drug Delivery Reviews**, v. 58, n. 15, p. 1688–1713, 2006.

AHLGREN, S.; ANDERSSON, K.; TOLMACHEV, V. Kit formulation for 99m Tc-labeling of recombinant anti-HER2 Affibody molecules with a C-terminally engineered cysteine. **Nuclear Medicine and Biology**, v. 37, n. 5, p. 539–546, 2010.

AHMEDIN JEMAL, D. F. B. M. M. C. J. F.; ELIZABETH WARD; DAVID FORMAN. Global cancer statistics. **Ca Cancer J Clin**, v. 61, n. 1, p. 69–90, 2011.

AHN, D. et al. Doxorubicin-Loaded Alginate - g - Poly(N - isopropylacrylamide) Micelles for Cancer Imaging and Therapy. **| ACS Applied Materials & Interfaces**, v. 6, p. 22069−22077, 2014.

AKIBA, I. et al. Encapsulation of a hydrophobic drug into a polymer-micelle core explored with synchrotron SAXS. **Langmuir**, v. 26, n. 10, p. 7544–7551, 2010.

AKIBA, I. et al. Anomalous small-angle X-ray scattering study of structure of polymer micelles having bromines in hydrophobic core. **Macromolecules**, v. 45, n. 15, 2012.

ALEXANDRIDIS, P.; OLSSON, U.; LINDMAN, B. A Record Nine Different Phases (Four Cubic , Two Hexagonal , and One Lamellar Lyotropic Liquid Crystalline and Two Micellar Solutions) in a Ternary Isothermal System of an Amphiphilic Block Copolymer and Selective Solvents (Water and Oil). **Langmuir**, v. 14, n. 10, p. 2627–2638, 1998.

ALLEN, T. M. Drug Delivery Systems: Entering the Mainstream. **Science**, v. 303, n. 5665, p. 1818–1822, 2004.

ARRANJA, A. G. et al. Tumor-targeted nanomedicines for cancer theranostics. **Pharmacological Research**, v. 115, n. 1, p. 87–95, 2017.

BAEK, J. S.; CHO, C. W. Controlled release and reversal of multidrug resistance by co-encapsulation of paclitaxel and verapamil in solid lipid nanoparticles. **International Journal of Pharmaceutics**, v. 478, n. 2, p. 617–624, 2015.

BARBOSA, M. V. et al. Comparative study of first-derivative spectrophotometry and high performance liquid chromatography methods for quantification of paclitaxel in liposomal formulation. **Journal of the Brazilian Chemical Society**, v. 26, n. 7, p. 1338–1343, 2015.

BARBUTI, A. M.; CHEN, Z. Paclitaxel Through the Ages of Anticancer Therapy : Exploring Its Role in Chemoresistance and Radiation Therapy. **Cancers**, v. 7, n. M, p. 2360–2371, 2015.

BELOTTI, D. et al. The Drug Paclitaxel Has Antiangiogenic. **Clinical Cancer Research**, v. 2, n. November, p. 1843–1849, 1996.

BERNABEU, E. et al. Paclitaxel : What has been done and the challenges remain ahead. **International Journal of Pharmaceutics**, v. 526, n. 1–2, p. 474–495, 2017.

BERTRAND, N. et al. Cancer nanotechnology: The impact of passive and active targeting in

the era of modern cancer biology. **Advanced Drug Delivery Reviews**, v. 66, p. 2–25, 2014.

BINDER, S. Evolution of taxanes in the treatment of metastatic breast cancer. **Clin J Oncol Nurs**, v. 17 Suppl, n. 1, p. 9–14, 2013.

BLAIR, H. A.; DEEKS, E. D. Albumin-Bound Paclitaxel : A Review in Non-Small Cell Lung Cancer. **Drugs**, v. 75, n. 17, p. 2017–2024, 2017.

BLANCO, E. et al. Multifunctional Micellar Nanomedicine for Cancer Therapy. **Experimental Biology and Medicine**, v. 234, n. 2, p. 123–131, 2009.

BOCCI, G.; DI PAOLO, A.; DANESI, R. The pharmacological bases of the antiangiogenic activity of paclitaxel. **Angiogenesis**, v. 16, n. 3, p. 481–492, 2013.

CABRAL, H. et al. Accumulation of sub-100 nm polymeric micelles in poorly permeable tumours depends on size. **Nature Nanotechnology**, v. 6, n. 12, p. 815–823, 2011.

CAGEL, M. et al. Polymeric mixed micelles as nanomedicines: Achievements and perspectives. **European Journal of Pharmaceutics and Biopharmaceutics**, v. 113, p. 211–228, 2017.

CHEN, H. et al. DUP1 peptide modified micelle efficiently targeted delivery paclitaxel and enhance mitochondrial apoptosis on PSMA - negative prostate cancer cells. **SpringerPlus**, p. 1–14, 2016.

CHEN, W.-H. et al. Therapeutic nanomedicine based on dual-intelligent functionalized gold nanoparticles for cancer imaging and therapy in vivo. **Biomaterials**, v. 34, n. 34, p. 8798–807, nov. 2013.

CHEN, W. Y. et al. Onset of Tethered Chain Overcrowding. **Physical Review Letters**, v. 8, n. July, p. 7–10, 2004.

CHEN, Y. et al. Pluronic-based functional polymeric mixed micelles for co-delivery of doxorubicin and paclitaxel to multidrug resistant tumor. **International Journal of Pharmaceutics**, v. 488, n. 1–2, p. 44–58, 2015.

CHENG, T. et al. Analytical Measurement of PEGylated Molecules. **Bioconjugate Chemistry**, v. 35, n. 5, p. 881–899, 2011.

CHIRIO, D. et al. Positive-charged solid lipid nanoparticles as paclitaxel drug delivery system in glioblastoma treatment. **European Journal of Pharmaceutics and Biopharmaceutics**, v. 88, n. 3, p. 746–758, 2014.

CHO, H. et al. Polymeric Micelles for Multi-Drug Delivery in Cancer. **AAPS PharmSciTech**, v. 16, n. 1, p. 10–20, 2015.

CRAIEVICH, A. F. Synchrotron SAXS Studies of Nanostructured Materials and Colloidal Solutions: A Review. **Materials Research**, v. 5, n. 1, p. 1–11, 2002.

CROY, S. R.; KWON, G. S. Polymeric micelles for drug delivery. **Current pharmaceutical design**, v. 12, n. 36, p. 4669–4684, 2006.

DABHOLKAR, R. D. et al. Polyethylene glycol-phosphatidylethanolamine conjugate (PEG-PE)-based mixed micelles: Some properties, loading with paclitaxel, and modulation of P-glycoprotein-mediated efflux. **International Journal of Pharmaceutics**, v. 315, n. 1–2, p.

148–157, 2006.

DE BARROS, A. et al. Emerging role of radiolabeled nanoparticles as an effective diagnostic technique. **EJNMMI Research**, v. 2, n. 1, p. 39, 2012a.

DE BARROS, A. L. B. et al. Synthesis and biodistribution studies of carbohydrate derivatives radiolabeled with technetium-99m. **Bioorganic and Medicinal Chemistry Letters**, v. 20, n. 1, p. 315–317, 2010.

DE BARROS, A. L. B. et al. Kit formulation for 99mTc-labeling of HYNIC-BAla-Bombesin (7-14). **Applied Radiation and Isotopes**, v. 70, n. 10, p. 2440–2445, 2012b.

DE BARROS, A. L. B. et al. 99mTc-labeled bombesin analog for breast cancer identification. **Journal of Radioanalytical and Nuclear Chemistry**, v. 295, n. 3, p. 2083–2090, 2013a.

DE BARROS, A. L. B. et al. Long-circulating, pH-sensitive liposomes versus long-circulating, non-pH-sensitive liposomes as a delivery system for tumor identification. **Journal of Biomedical Nanotechnology**, v. 9, n. 9, p. 1636–1643, 2013b.

DESAI, N. et al. Cancer Therapy : Preclinical Increased Antitumor Activity , Intratumor Paclitaxel Concentrations , and Endothelial Cell T ransport of Cremophor-Free , Albumin-Bound. **Clinical Cancer Research**, v. 12, n. 4, p. 1317–1325, 2006.

DESHMUKH, A. S. et al. Polymeric micelles: Basic research to clinical practice. **International Journal of Pharmaceutics**, v. 532, n. 1, p. 249–268, 2017.

DEWANJEE, M. K. The chemistry of 99mTc-labeled radiopharmaceuticals. **Seminars in Nuclear Medicine**, v. 20, n. 1, p. 5–27, 1990.

DI COLA, E.; GRILLO, I.; RISTORI, S. Small angle X-ray and neutron scattering: Powerful tools for studying the structure of drug-loaded liposomes. **Pharmaceutics**, v. 8, n. 2, p. 1–16, 2016.

DISCH, S. et al. Quantitative spatial magnetization distribution in iron oxide nanocubes and nanospheres by polarized small-angle neutron scattering. **New Journal of Physics**, v. 14, 2012.

DOBROVOLSKAIA, M. A.; MCNEIL, S. E. Understanding the correlation between in vitro and in vivo immunotoxicity tests for nanomedicines. **Journal of Controlled Release**, v. 172, n. 2, p. 456–466, 2013.

DOKTOROVOVA, S. et al. Trehalose is not a universal solution for solid lipid nanoparticles freeze-drying. **Pharmaceutical Development and Technology**, v. 19, n. 8, p. 922–929, 2014.

DUPRE, S. A.; REDELMAN, D.; HUNTER, K. W. The mouse mammary carcinoma 4T1 : characterization of the cellular landscape of primary tumours and metastatic tumour foci. **International Journal of Experimental Pathology**, v. 88, p. 351–360, 2007.

EAWSAKUL, K. et al. Preparation and characterizations of rspp050-loaded polymeric micelles using poly(ethylene glycol)-b-poly(ε-caprolactone) and poly(ethylene glycol)-b-poly(d,l-lactide). **Chemical and Pharmaceutical Bulletin**, v. 65, n. 6, p. 530–537, 2017.

EMAMI, J. In vitro-in vivo correlation: From theory to applications. **Journal of Pharmacy and Pharmaceutical Sciences**, v. 9, n. 2, p. 31–51, 2006.

EMAMI, J. et al. Development and in vitro/in vivo evaluation of a novel targeted polymeric micelle for delivery of paclitaxel. **International Journal of Biological Macromolecules**, v. 80, p. 29–40, 2015.

ESKELIN, K. et al. Asymmetric flow field flow fractionation methods for virus purification. **Journal of Chromatography A**, v. 1469, p. 108–119, 2016.

FAN, Z. et al. Adding vitamin E-TPGS to the formulation of genexol-pm: Specially mixed micelles improve drug-loading ability and cytotoxicity against multidrug-resistant tumors significantly. **PLoS ONE**, v. 10, n. 4, p. 1–17, 2015.

FANG, J.; NAKAMURA, H.; MAEDA, H. The EPR effect: Unique features of tumor blood vessels for drug delivery, factors involved, and limitations and augmentation of the effect. **Advanced Drug Delivery Reviews**, v. 63, n. 3, p. 136–151, 2011.

FONTE, P. et al. Stability study perspective of the effect of freeze-drying using cryoprotectants on the structure of insulin loaded into PLGA nanoparticles. **Biomacromolecules**, v. 15, n. 10, p. 3753–3765, 2014.

FRAGUAS-SÁNCHEZ, A. I. et al. Current status of nanomedicine in the chemotherapy of breast cancer. **Cancer Chemotherapy and Pharmacology**, n. 0123456789, 2019.

GALYEAN, A. A. et al. Asymmetric flow field flow fractionation with light scattering detection – an orthogonal sensitivity analysis. **Journal of Chromatography A**, v. 1473, p. 122–132, 2016.

GAO, G. H.; LI, Y.; LEE, D. S. Environmental pH-sensitive polymeric micelles for cancer diagnosis and targeted therapy. **Journal of Controlled Release**, v. 169, n. 3, p. 180–184, 2013.

GELDERBLOM, H. et al. Cremophor EL : the drawbacks and advantages of vehicle selection for drug formulation. **European journal of cancer**, v. 37, p. 1590–1598, 2001.

GIACOMELLI, F. C. et al. pH-triggered block copolymer micelles based on a pH-responsive PDPA (poly[2-(diisopropylamino)ethyl methacrylate]) inner core and a PEO (poly(ethylene oxide)) outer shell as a potential tool for the cancer therapy. **Soft Matter**, v. 7, n. 19, p. 9316, 2011.

GILL, K. K.; KADDOUMI, A.; NAZZAL, S. Mixed micelles of PEG 2000-DSPE and vitamin-E TPGS for concurrent delivery of paclitaxel and parthenolide: Enhanced chemosenstization and antitumor efficacy against non-small cell lung cancer (NSCLC) cell lines. **European Journal of Pharmaceutical Sciences**, v. 46, n. 1–2, p. 64–71, 2012.

GILROY, J. B. et al. Probing the Structure of the Crystalline Core of Field-Aligned, Monodisperse, Cylindrical Polyisoprene- block -Polyferrocenylsilane Micelles in Solution Using Synchrotron Small- and Wide-Angle X-ray Scattering. **Journal of the American Chemical Society**, v. 133, p. 17056–17062, 2011.

GLOBOCAN. **Cancer Fact Sheets**. Disponível em: <https://gco.iarc.fr/today/fact-sheets-cancers>. Acesso em: 2 ago. 2019.

GRADISHAR, W. J. Albumin-bound paclitaxel : a next-generation taxane. **Expert Opinion on Pharmacotherapy**, v. 7, n. 8, p. 1041–1053, 2006.

GRALLERT, S. R. M. et al. Polymeric micelles and molecular modeling applied to the development of radiopharmaceuticals. **Brazilian Journal of Pharmaceutical Sciences (Impresso)**, v. 48, n. 1, p. 1–16, 2012.

GREGORY, A. E.; TITBALL, R.; WILLIAMSON, D. Vaccine delivery using nanoparticles. **Frontiers in Cellular and Infection Microbiology**, v. 3, n. March, p. 1–13, 2013.

GUO, X. et al. Thermo-triggered drug release from actively targeting polymer micelles. **ACS Applied Materials and Interfaces**, v. 6, n. 11, p. 8549–8559, 2014.

HAZARI, P. P. et al. Synthesis of specific SPECT-radiopharmaceutical for tumor imaging based on methionine: 99mTc-DTPA-bis(methionine). **Bioconjugate Chemistry**, v. 21, n. 2, p. 229–239, 2010.

HENNENFENT, K. L.; GOVINDAN, R. Novel formulations of taxanes: A review. Old wine in a new bottle? **Annals of Oncology**, v. 17, n. 5, p. 735–749, 2006.

HEPPNER, G. H.; MILLER, F. R.; SHEKHAR, P. V. M. Nontransgenic models of breast cancer. **Breast Cancer Research**, v. 2, n. 5, p. 331–334, 2000.

HONG, H. et al. Molecular imaging and therapy of cancer with radiolabeled nanoparticles. **Nano Today**, v. 4, n. 5, p. 399–413, 2009.

HUH, K. M. et al. A new hydrotropic block copolymer micelle system for aqueous solubilization of paclitaxel. **Journal of Controlled Release**, v. 126, n. 2, p. 122–129, 2008.

INCA. **Números de câncer**. Disponível em: <https://www.inca.gov.br/numeros-de-cancer>. Acesso em: 2 ago. 2019.

ISRAELACHVILI, J. N.; MITCHELL, JOHN, D.; NINHAM, B. W. Theory of self-assembly of hydrocarbon amphiphiles into micelles and bilayers. **Journal of the Chemical Society, Faraday Transactions 2**, v. 72, p. 1526–1566, 1976.

JAHANSHAHI, M. et al. An Engineered Infected Epidermis Model for In Vitro Study of the Skin ' s Pro-Inflammatory Response. 2020.

JAIN, V. et al. Biomaterials Paclitaxel loaded PEGylated gleceryl monooleate based nanoparticulate carriers in chemotherapy. **Biomaterials**, v. 33, n. 29, p. 7206–7220, 2012.

JIANG, L. et al. Overcoming drug-resistant lung cancer by paclitaxel loaded dual-functional liposomes with mitochondria targeting and. **Biomaterials**, v. 52, p. 126–139, 2015.

JOKERST, J. V et al. Nanoparticle PEGylation for imaging and therapy. **Nanomedicine**, v. 6, n. 4, p. 715–728, 2012.

JONES, A. G. Technetium in nuclear medicine. **Aalam Al-Zarra**, n. 52, p. 119–129, 1997.

JONES, M. C.; LEROUX, J. C. Polymeric micelles - A new generation of colloidal drug carriers. **European Journal of Pharmaceutics and Biopharmaceutics**, v. 48, n. 2, p. 101–111, 1999.

JORDAN, M. A.; WILSON, L. Microtubules as a target for anticancer drugs. **Nat. Rev. Cancer**, v. 4, n. 4, p. 253–265, 2004.

KAIDA, S. et al. Visible drug delivery by supramolecular nanocarriers directing to single-

platformed diagnosis and therapy of pancreatic tumor model. **Cancer Research**, v. 70, n. 18, p. 7031–7041, 2010.

KAMEI, J. et al. Rikkunshito prevents paclitaxel-induced peripheral neuropathy through the suppression of the nuclear factor kappa B (NF κ B) phosphorylation in spinal cord of mice. **PLoS ONE**, p. 1–18, 2017.

KAMIYA, S.; NAKASHIMA, K. Physicochemical interaction mechanism between nanoparticles and tetrasaccharides (stachyose) during freeze-drying. **Drug Development and Industrial Pharmacy**, v. 43, n. 12, p. 2026–2031, 2017.

KAN, P. et al. A Liposomal Formulation Able to Incorporate a High Content of Paclitaxel and Exert Promising Anticancer Effect. **Journal of Drug Delivery**, v. 2011, p. 1–9, 2010.

KATRAGADDA, U. et al. Combined Delivery of Paclitaxel and Tanespimycin via Micellar Nanocarriers: Pharmacokinetics, Efficacy and Metabolomic Analysis. **PLoS ONE**, v. 8, n. 3, 2013.

KAZUNORI, K. et al. Block copolymer micelles as vehicles for drug delivery. **Journal of Controlled Release**, v. 24, n. 1–3, p. 119–132, 1993.

KE, X.-Y. et al. Co-delivery of thioridazine and doxorubicin using polymeric micelles for targeting both cancer cells and cancer stem cells. **Biomaterials**, v. 35, n. 3, p. 1096–1108, 2014.

KIESSLING, F. et al. Nanoparticles for Imaging: Top or Flop? **Radiology**, v. 273, n. 1, p. 10–28, 2014.

KIM, J. H. et al. Tumor-targeted delivery of paclitaxel using low density lipoprotein-mimetic solid lipid nanoparticles. **Molecular Pharmaceutics**, v. 12, n. 4, p. 1230–1241, 2015.

KIM, K. et al. PEGylation of bacteriophages increases blood circulation time and reduces T-helper type 1 immune response. **Microbial Biotechnology**, v. 1, n. 3, p. 247–257, 2008.

KOLATE, A. et al. PEG-A versatile conjugating ligand for drugs and drug delivery systems. **Journal of Controlled Release**, v. 192, p. 67–81, 2014.

KUMAR, P. et al. Development of a single vial kit formulation of [99mTc]-labeled doxorubicin for tumor imaging and treatment response assessment-preclinical evaluation and preliminary human results. **Journal of Labelled Compounds and Radiopharmaceuticals**, v. 58, n. 6, p. 242–249, 2015.

KUMAR, R. et al. In vitro evaluation of theranostic polymeric micelles for imaging and drug delivery in cancer. **Theranostics**, v. 2, n. 7, p. 714–722, 2012.

KWON, G. S.; KATAOKA, K. Block copolymer micelles as long-circulating drug vehicles. **Advanced Drug Delivery Reviews**, v. 16, p. 295–309, 1995.

LANG, I. et al. A comparative analysis on the efficacy and safety of intaxelspi® and taxolspi® in advanced metastatic breast cancer. **Journal of Clinical and Diagnostic Research**, v. 7, n. 6, p. 1120–1124, 2013.

LEE, MIN KYUNG; KIM, MIN YOUNG; KIM, SUJUNG; LEE, J. Cryoprotectants for Freeze Drying of Drug Nano-Suspensions: Effect of Freezing Rate. **JOURNAL OF**

PHARMACEUTICAL SCIENCES, v. 98, n. 12, p. 4808–4817, 2009.

LEE, Y. S. et al. Development of acetylated HDD kit for preparation of 188Re-HDD/lipiodol. **Applied Radiation and Isotopes**, v. 65, n. 1, p. 64–69, 2007.

LEITE, E. A. et al. Acute Toxicity Study of Cisplatin Loaded Long-Circulating and pH-Sensitive Liposomes Administered in Mice. **Journal of Biomedical Nanotechnology**, v. 8, n. 2, p. 1–11, 2011.

LEITE, E. A. et al. Encapsulation of cisplatin in long-circulating and pH-sensitive liposomes improves its antitumor effect and reduces acute toxicity. **International Journal of Nanomedicine**, v. 7, p. 5259–5269, 2012.

LI, Z. et al. Proinflammatory Factors Mediate Paclitaxel-Induced Impairment of Learning and Memory. **Mediators of Inflammation**, v. 2018, p. 1–9, 2018.

LU, J. et al. PEG-derivatized embelin as a nanomicellar carrier for delivery of paclitaxel to breast and prostate cancers. **Biomaterials**, v. 34, n. 5, p. 1591–1600, 2013a.

LU, R. M. et al. Targeted Drug Delivery Systems Mediated by a Novel Peptide in Breast Cancer Therapy and Imaging. **PLoS ONE**, v. 8, n. 6, 2013b.

LUCA, R. DE; PROFITA, G.; CICERO, G. Nab-paclitaxel in pretreated metastatic breast cancer : evaluation of activity , safety , and quality of life. **Oncotargets and therapy**, v. 12, p. 1621–1627, 2019.

LUKYANOV, A. N.; TORCHILIN, V. P. Micelles from lipid derivatives of water-soluble polymers as delivery systems for poorly soluble drugs. **Advanced Drug Delivery Reviews**, v. 56, n. 9, p. 1273–1289, 2004.

LV, L. et al. Novel 4-Arm Poly (Ethylene Glycol) -Block- Poly (Anhydride-Esters) Amphiphilic Copolymer Micelles Loading Curcumin : Preparation , Characterization , and In Vitro Evaluation. v. 2013, 2013.

MA, Z. et al. TCR Triggering by pMHC Ligands Tethered on Surfaces via Poly (Ethylene Glycol) Depends on Polymer Length. v. 9, n. 11, p. 1–10, 2014.

MAEDA, H. Tumor-selective delivery of macromolecular drugs via the EPR effect: Background and future prospects. **Bioconjugate Chemistry**, v. 21, n. 5, p. 797–802, 2010.

MI, P. et al. Molecular Cancer Imaging with Polymeric Nanoassemblies: From Tumor Detection to Theranostics. **Macromolecular Bioscience**, v. 17, n. 1, p. 1–12, 2017.

MIAO, J. et al. Biointerfaces Drug resistance reversal activity of anticancer drug loaded solid lipid nanoparticles in multi-drug resistant cancer cells. **Colloids and Surfaces B: Biointerfaces**, v. 110, p. 74–80, 2013.

MILLER, T. et al. Comparative investigations on in vitro serum stability of polymeric micelle formulations. **Pharmaceutical Research**, v. 29, n. 2, p. 448–459, 2012.

MIYAJIMA, K. Role of saccharides for the freeze-thawing and freeze drying of liposome. **Advanced Drug Delivery Reviews**, v. 24, n. 2–3, p. 151–159, 1997.

MOHAMED, S. et al. Polymeric nano-micelles: versatile platform for targeted delivery in cancer. **Therapeutic Delivery**, v. 5, n. 10, p. 1101–1121, 2014.

MONTEIRO, L. O. F. et al. Phase behavior of dioleyphosphatidylethanolamine molecules in the presence of components of pH-sensitive liposomes and paclitaxel. **Colloids and Surfaces B: Biointerfaces**, v. 144, p. 276–283, 2016.

MONTEIRO, L. O. F. et al. Technetium-99 m radiolabeled paclitaxel as an imaging probe for breast cancer in vivo. **Biomedicine et Pharmacotherapy**, v. 89, p. 146–151, 2017.

MONTEIRO, L. O. F. et al. Paclitaxel-Loaded pH-Sensitive Liposome: New Insights on Structural and Physicochemical Characterization. **Langmuir**, v. 34, n. 20, p. 5728–5737, 2018a.

MONTEIRO, L. O. F. et al. Paclitaxel-loaded folate-coated long circulating and pH-sensitive liposomes as a potential drug delivery system: A biodistribution study. **Biomedicine and Pharmacotherapy**, v. 97, 2018b.

MONTEIRO, L. O. F. et al. Paclitaxel-Loaded Folate-Coated pH-Sensitive Liposomes Enhance Cellular Uptake and Antitumor Activity. **Molecular Pharmaceutics**, 2019.

MORAIS, M. I. et al. Nicorandil inhibits mechanical allodynia induced by paclitaxel by activating opioidergic and serotonergic mechanisms. **European journal of pharmacology**, v. 824, p. 108–114, 2018.

MUTHU, M. S. et al. Nanotheranostics - application and further development of nanomedicine strategies for advanced theranostics. **Theranostics**, v. 4, n. 6, p. 660–677, 2014.

NARAYANAN, T. High brilliance small-angle X-ray scattering applied to soft matter. **Current Opinion in Colloid and Interface Science**, v. 14, n. 6, p. 409–415, 2009.

NIE, S. et al. Thermoreversible Pluronic F127-based hydrogel containing liposomes for the controlled delivery of paclitaxel: In vitro drug release, cell cytotoxicity, and uptake studies. **International Journal of Nanomedicine**, v. 6, n. 1, p. 151–166, 2011.

NIH. **About cancer: diagnosis**. Disponível em: <National Cancer Institute>. Acesso em: 13 ago. 2019.

NILSSON, L. Separation and characterization of food macromolecules using field-flow fractionation: A review. **Food Hydrocolloids**, v. 30, n. 1, p. 1–11, 2013.

NISHIYAMA, N.; MATSUMURA, Y.; KATAOKA, K. Development of polymeric micelles for targeting intractable cancers. **Cancer Science**, v. 107, n. 7, p. 867–874, 2016.

ODA, C. M. R. **Desenvolvimento de micelas poliméricas carreadoras de paclitaxel radiomarcadas com tecnécio-99m para aplicação no tratamento e diagnóstico de câncer.** Belo Horizonte, MG: Universidade Federal de Minas Gerais, 2015.

ODA, C. M. R. et al. Synthesis, characterization and radiolabeling of polymeric nano-micelles as a platform for tumor delivering. **Biomedicine and Pharmacotherapy**, v. 89, 2017a.

ODA, C. M. R. et al. Synthesis, characterization and radiolabeling of polymeric nano-micelles as a platform for tumor delivering. **Biomedicine and Pharmacotherapy**, v. 89, p. 268–275, 2017b.

ODA, C. M. R. et al. Freeze-dried diethylenetriaminepentaacetic acid-functionalized

polymeric micelles containing paclitaxel: A kit formulation for theranostic application in cancer. **Journal of Drug Delivery Science and Technology**, v. 46, 2018.

OERLEMANS, C. et al. Polymeric micelles in anticancer therapy: Targeting, imaging and triggered release. **Pharmaceutical Research**, v. 27, n. 12, p. 2569–2589, 2010.

OLIVEIRA, J. DE et al. Toxicological study of a new doxorubicin-loaded pH-sensitive liposome : A preclinical approach. **Toxicology and Applied Pharmacology**, v. 352, n. February, p. 162–169, 2018.

OOSTENDORP, R. L.; BUCKLE, T.; LAMBERT, G. Paclitaxel in self-micro emulsifying formulations : oral bioavailability study in mice. **Investigational New Drugs**, v. 29, p. 768–776, 2011.

PEARSON, R. M.; JUETTNER, V. V; HONG, S. Biomolecular corona on nanoparticles : a survey of recent literature and its implications in targeted drug delivery. **Frontiers in chemisty**, v. 2, n. November, p. 1–7, 2014.

PEDERSEN, J. S. et al. Article A Small-Angle Neutron and X-ray Contrast Variation Scattering Study of the Structure of Block Copolymer Micelles : Corona Shape and Excluded Volume Interactions Excluded Volume Interactions. **Macromolecules**, v. 36, p. 416–433, 2003.

PEDERSEN, J. S.; GERSTENBERG, M. C. Scattering Form Factor of Block Copolymer Micelles. **Macromolecules**, v. 29, n. 4, p. 1363–1365, 1996.

PEER, D. et al. Nanocarriers as an emerging platform for cancer therapy. **Nature Nanotechnology**, v. 2, p. 751–760, 2007.

PENG, L. et al. Incidence and risk of peripheral neuropathy with nab-paclitaxel in patients with cancer : a meta-analysis. **European journal of cancer care**, v. 26, p. 1–11, 2017.

PERSSON, G.; EDLUND, H.; LINDBLOM, G. Thermal behaviour of cubic phases rich in 1-monooleoyl-rac-glycerol in the ternary system 1-monooleoyl-rac-glycerol/n-octyl-b-D-glucoside/water. **European Journal of Biochemistry**, v. 65, p. 56–65, 2003.

PHILLIPS, W. T. Delivery of gamma-imaging agents by liposomes. **Advanced Drug Delivery Reviews**, v. 37, n. 1–3, p. 13–32, 1999.

PILLAI, G. Nanomedicines for Cancer Therapy: An Update of FDA Approved and Those under Various Stages of Development. **SOJ Pharmacy & Pharmaceutical Sciences**, v. 1, 1 jan. 2014.

RABAH, S. O. Acute Taxol nephrotoxicity : Histological and ultrastructural studies of mice kidney parenchyma. **Saudi Journal of Biological Sciences**, v. 17, n. 2, p. 105–114, 2010.

RAMOS-CABRER, P.; CAMPOS, F. Liposomes and nanotechnology in drug development : Focus on ocular targets. **International Journal of Nanomedicine**, v. 8, n. February, p. 951–960, 2013.

RASSI FERNANDES, M.; RIBEIRO PEDROSO, A. Animal experimentation: A look into ethics, welfare and alternative methods experiMentaÇÃo aniMal: uM olhar soBre Ética, BeM-estar e MÉtodos alternativos. **Rev Assoc Med Bras**, v. 63, n. 11, p. 923–928, 2017.

RYVOLOVA, M. et al. Modern micro and nanoparticle-based imaging techniques. **Sensors (Switzerland)**, v. 12, n. 11, p. 14792–14820, 2012.

SAHA, G. B. Radiopharmaceuticals and methods of radiolabeling. In: **Fundamentals of Nuclear Pharmacy**. 6. ed. New York: Springer, New York, NY, 2010. p. 83–113.

SANADA, Y. et al. Hydrophobic molecules infiltrating into the poly(ethylene glycol) domain of the core/shell interface of a polymeric micelle: Evidence obtained with anomalous small-angle X-ray scattering. **Journal of the American Chemical Society**, v. 135, n. 7, p. 2574–2582, 2013.

SARISOZEN, C. et al. PEG-PE-based micelles co-loaded with paclitaxel and cyclosporine A or loaded with paclitaxel and targeted by anticancer antibody overcome drug resistance in cancer cells. **Drug Delivery**, v. 19, n. 4, p. 169–176, 2012.

SATO, T. et al. Poly(ethylene glycol)-conjugated phospholipids in aqueous micellar solutions: hydration, static structure, and interparticle interactions. **Journal of Physical Chemistry B**, v. 111, n. 6, p. 1393–1401, 2007.

SAWANT, R. R.; TORCHILIN, V. P. Multifunctionality of lipid-core micelles for drug delivery and tumour targeting. **Molecular Membrane Biology**, v. 27, n. 7, p. 232–246, 2010.

SCHWOCHAU, K. **Technetium: chemistry and radiopharmaceutical applications.** Weinheim, Alemanha: Wiley-VCH, 2000.

SERRANO, D. R. et al. Hemolytic and pharmacokinetic studies of liposomal and particulate amphotericin B formulations. **International Journal of Pharmaceutics**, v. 447, n. 1–2, p. 38–46, 2013.

SHARMA, A.; JAIN, N.; SAREEN, R. Nanocarriers for diagnosis and targeting of breast cancer. **BioMed Research International**, v. 2013, 2013.

SHI, X. et al. **Acid-Activatable Theranostic Unimolecular Micelles Composed of Amphiphilic Star-like Polymeric Prodrug with High Drug Loading for Enhanced Cancer Therapy**. [s.l: s.n.]. v. 14

SHIRAISHI, K. et al. Determination of polymeric micelles' structural characteristics, and effect of the characteristics on pharmacokinetic behaviors. **Journal of Controlled Release**, v. 203, p. 77–84, 2015.

SILVA, J. DE O. et al. Folate-coated, long-circulating and pH-sensitive liposomes enhance doxorubicin antitumor effect in a breast cancer animal model. **Biomedicine & Pharmacotherapy**, v. 118, p. 109323, out. 2019.

SOFIAS, A. M. et al. The battle of " nano " paclitaxel. **Advanced Drug Delivery Reviews**, v. 122, p. 20–30, 2017.

STACY, M. R.; MAXFIELD, M. W.; SINUSAS, A. J. Targeted molecular imaging of angiogenesis in PET and SPECT: A review. **Yale Journal of Biology and Medicine**, v. 85, n. 1, p. 75–86, 2012.

STIRLAND, D. L. et al. Mind the gap: A survey of how cancer drug carriers are susceptible to the gap between research and practice. **Journal of Controlled Release**, v. 172, n. 3, p. 1045–1064, 2013.

SURAPANENI, M. S.; DAS, S. K.; DAS, N. G. Designing Paclitaxel Drug Delivery Systems Aimed at Improved Patient Outcomes: Current Status and Challenges. **ISRN Pharmacology**, v. 2012, p. 1–15, 2012.

SVENSON, S. Clinical translation of nanomedicines. **Current Opinion in Solid State and Materials Science**, v. 16, n. 6, p. 287–294, 2012.

SVENSON, S. What nanomedicine in the clinic right now really forms nanoparticles? **Wiley Interdisciplinary Reviews: Nanomedicine and Nanobiotechnology**, v. 6, n. 2, p. 125–135, 2014.

THRALL, J. H.; ZIESSMAN, H. A. **Medicina Nuclear**. 2. ed. Rio de Janeiro,: Guanabara Koogan, 2003.

TORCHILIN, V. P. Recent Approaches To Intracellular Delivery of Drugs and Dna and Organelle Targeting. **Annual Review of Biomedical Engineering**, v. 8, n. 1, p. 343–375, 2006.

TORCHILIN, V. P. Targeted Pharmaceutical Nanocarriers for Cancer Therapy and Imaging. **The AAPS Journal**, v. 9, n. 2, p. 128–147, 2007a.

TORCHILIN, V. P. Micellar nanocarriers: Pharmaceutical perspectives. **Pharmaceutical Research**, v. 24, n. 1, p. 1–16, 2007b.

TRIVEDI, R.; KOMPELLA, U. B. Nanomicellar formulations for sustained drug delivery: strategies and underlying principles. **Nanomedicine (London, England)**, v. 5, n. 3, p. 485–505, 2010.

TSUBAKI, M.; TAKEDA, T.; MATSUMOTO, M. Tamoxifen suppresses paclitaxel- , neuropathy via inhibition of the protein kinase C / extracellular signal-regulated kinase pathway. **Tumor Biology**, n. October, p. 1–13, 2018.

VAN ZUYLEN, L.; VERWEIJ, J.; SPARREBOOM, A. Role of formulation vehicles in taxane pharmacology. **Investigational New Drugs**, v. 19, n. 2, p. 125–141, 2001.

VARSHNEY, R. et al. Synthesis of [DTPA-bis(D-ser)] Chelate (DBDSC): An Approach for the Design of SPECT Radiopharmaceuticals Based on Technetium. **Current Radiopharmaceuticals**, v. 5, n. 4, p. 348–355, 2012.

VIDAL, A. et al. Development of a freeze-dried kit formulation for the preparation of99mTc-NTP 15-5, a radiotracer for scintigraphic imaging of proteoglycans. **Applied Radiation and Isotopes**, v. 101, p. 1–9, 2015.

VOLPE, D. A.; VOLPE, D. A. Expert Opinion on Drug Discovery Advances in cell-based permeability assays to screen drugs for intestinal absorption Advances in cell-based permeability assays to screen drugs for intestinal absorption. **Expert Opinion on Drug Discovery**, v. 00, n. 00, p. 1–11, 2020.

WAGNER, M. et al. Asymmetric flow field-flow fractionation in the field of nanomedicine. **Analytical Chemistry**, v. 86, n. 11, p. 5201–5210, 2014.

WAN, C. P. L. et al. The combined use of paclitaxel-loaded nanoparticles with a low-molecular-weight copolymer inhibitor of P-glycoprotein to overcome drug resistance. **International Journal of Nanomedicine**, v. 8, p. 379–391, 2013.

WANG, S. et al. Nanoscale drug delivery for taxanes based on the mechanism of multidrug resistance of cancer. **Biotechnology Advances**, v. 33, n. 1, p. 224–241, 2015.

WANG, T. et al. Paclitaxel-loaded PEG-PE-based micellar nanopreparations targeted with tumor-specific landscape phage fusion protein enhance apoptosis and efficiently reduce tumors. **Molecular Cancer Therapeutics**, v. 13, n. 12, p. 2864–2875, 2014.

WANG, T.; PETRENKO, V. A.; TORCHILIN, V. P. Paclitaxel-loaded polymeric micelles modified with MCF-7 cell-specific phage protein: Enhanced binding to target cancer cells and increased cytotoxicity. **Molecular Pharmaceutics**, v. 7, n. 4, p. 1007–1014, 2010.

WANG, Z. et al. Reduction responsive liposomes based on paclitaxel-ss-lysophospholipid with high drug loading for intracellular delivery. **International Journal of Pharmaceutics**, v. 564, n. April, p. 244–255, 2019.

WEAVER, B. A.; BEMENT, W. How Taxol / paclitaxel kills cancer cells. **Molecular biology of the Cell**, v. 25, p. 2677–2681, 2014.

WHO. **Monographs: Radiopharmaceuticals: Specific monographs: Technetium (99mTc) pentetate complex injection (Technetii (99mTc) pentetatis multiplex injectio)**. Disponível em: <http://apps.who.int/phint/en/p/docf/>. Acesso em: 14 ago. 2019.

WHO. **Cancer**. Disponível em: <https://www.who.int/cancer/en/>. Acesso em: 2 ago. 2019.

WORAPHATPHADUNG, T. et al. Development of Chitosan-Based pH-Sensitive Polymeric Micelles Containing Curcumin for Colon-Targeted Drug Delivery. **AAPS PharmSciTech**, v. 19, n. 3, p. 991–1000, 2018.

WU, H.; ZHU, L.; TORCHILIN, V. P. PH-sensitive poly(histidine)-PEG/DSPE-PEG co-polymer micelles for cytosolic drug delivery. **Biomaterials**, v. 34, n. 4, p. 1213–1222, 2013.

XU, X. et al. Clinical comparison between paclitaxel liposome (Lipusu®) and paclitaxel for treatment of patients with metastatic gastric cancer. **Asian Pacific Journal of Cancer Prevention**, v. 14, n. 4, p. 2591–2594, 2013.

YANG, C.-P. H.; HORWITZ, S. B. Taxol® : The First Microtubule Stabilizing Agent. **International Journal of Molecular Sciences**, v. 18, p. 11, 2017.

YANG, Z. L. et al. Amphotericin B-loaded poly(ethylene glycol)-poly(lactide) micelles: Preparation, freeze-drying, and in vitro release. **Journal of Biomedical Materials Research - Part A**, v. 85, n. 2, p. 539–546, 2008.

YOKOYAMA, M. Polymeric micelles as a new drug carrier system and their required considerations for clinical trials. **Expert Opinion on Drug Delivery**, v. 7, n. 2, p. 145–158, 2010.

YOKOYAMA, M. Polymeric micelles as drug carriers: their lights and shadows. **Journal of Drug Targeting**, v. 22, n. 7, p. 576–583, 2014.

YOU, J. et al. Pharmacokinetics, clearance, and biosafety of polyethylene glycol-coated hollow gold nanospheres. **Particle and Fibre Toxicology**, v. 11, n. 1, p. 1–14, 2014.

ZHANG, D. et al. Paclitaxel: New uses for an old drug. **Drug Design, Development and Therapy**, v. 8, p. 279–284, 2014.

ZHANG, L. et al. High tumor penetration of paclitaxel loaded pH sensitive cleavable liposomes by depletion of tumor collagen i in breast cancer. **ACS Applied Materials and Interfaces**, v. 7, n. 18, p. 9691–9701, 2015a.

ZHANG, L.; ZHANG, N. How nanotechnology can enhance docetaxel therapy. **International Journal of Nanomedicine**, p. 2927–2941, 2013.

ZHANG, X. et al. PEG-Farnesyl Thiosalicylic Acid Telodendrimer Micelles as an Improved Formulation for Targeted Delivery of Paclitaxel. **Molecular Pharmaceutics**, 2015b.

ZHANG, Z.; MEI, L.; FENG, S.-S. Paclitaxel drug delivery systems. **Expert opinion on drug delivery**, v. 10, n. 3, p. 325–40, 2013.

ZHAO, M.; LI, Z. A single-step kit formulation for the 99mTc-labeling of HYNIC-Duramycin. **Nuclear Medicine and Biology**, v. 39, n. 7, p. 1006–1011, 2012.

ZHOU, J. et al. The anticancer efficacy of paclitaxel liposomes modified with mitochondrial targeting conjugate in resistant lung cancer. **Biomaterials**, v. 34, n. 14, p. 3626–3638, 2013.

ZHU, X. et al. 99mTc-Labeled Cystine Knot Peptide Targeting Integrin αvβ6 for Tumor SPECT Imaging. **Molecular Pharmaceutics**, v. 11, p. 1208–1217, 2014.